crystals

MDPI

Article

Physical and Mathematical Models of Quantum Dielectric Relaxation in Electrical and Optoelectric Elements Based on Hydrogen-Bonded Crystals

Valeriy Kalytka [1,*], Ali Mekhtiyev [2,3,*], Yelena Neshina [1,3,*], Aliya Alkina [1,3], Raushan Aimagambetova [3], Gabit Mukhambetov [3], Aleksandr Bashirov [4], Dmitriy Afanasyev [5], Arkadiy Bilichenko [1,3], Dinara Zhumagulova [1], Zukhra Ismailova [6] and Yelena Senina [1,*]

1 Faculty of Energy, Automation and Telecommunications, Abylkas Saginov Karaganda Technical University, Karaganda 100027, Kazakhstan; alika_1308@mail.ru (A.A.); arkan80@list.ru (A.B.); appdinara@mail.ru (D.Z.)
2 Energy Faculty, S. Seifullin Kazakh AgroTechnical Research University, Astana 010011, Kazakhstan
3 Department of Production, Science and Conformity Assessment, RSE "Kazakhstan Institute of Standardization and Metrology", Astana 010000, Kazakhstan; rauwan2012@mail.ru (R.A.); ceo@ksm.kz (G.M.)
4 Scientific Research Institute Economic and Legal Researches, Karaganda University of Kazpotrebsoyuz, Karaganda 100000, Kazakhstan; bashirov_av@mail.ru
5 Faculty of Physics and Technology, Buketov Karaganda University, Karaganda 100028, Kazakhstan; a.d.afanasyev2@gmail.com
6 Faculty of Hydromelioration, Tashkent Institute of Irrigation and Agricultural Mechanization, Tashkent 100000, Uzbekistan; z.ismailova@tiiame.uz
* Correspondence: valerii.kalytka@gmail.com (V.K.); barton.kz@mail.ru (A.M.); 1_neg@mail.ru (Y.N.); komir-kuat_senina@mail.ru (Y.S.); Tel.: +7-(72)-1256-4422 (V.K.)

Abstract: The quantum statistical properties of the proton subsystem in hydrogen-bonded crystals (HBC) are investigated. Based on the non-stationary Liouville operator equation (taking into account a number of assumptions established in the experiment), a quantum kinetic equation is constructed for the ensemble of non-interacting protons (an ideal proton gas) moving in the crystal potential image perturbed by the external electric field. The balanced density matrix for the unperturbed proton subsystem is constructed using the quantum canonical Gibbs distribution, and the non-balanced density matrix is calculated from the solutions of the nonlinear quantum kinetic equation by methods in linear approximation of perturbation theory for the blocking electrode model. Full quantum mechanical averaging of the polarization operator makes it possible to study the theoretical frequency-temperature spectra of the complex dielectric permittivity (CDP) calculated using quantum relaxation parameters that differ significantly from their semiclassical counterparts. A scheme is presented for an analytical study of the dielectric loss tangent in the region of quantum nonlinear relaxation in HBC. The results obtained in the given paper are of scientific interest in developing the theoretical foundations of proton conduction processes in energy-independent memory elements (with anomalously high residual polarization) based on thin films of ferroelectric materials in the ultralow temperature range (1–10 K). The theoretical results obtained have a direct application to the study of the tunneling mechanisms of spontaneous polarization in ferroelectric HBC with a rectangular hysteresis loop, in particular in crystals of potassium dideutrophosphate (KDP), widely used in nonlinear optics and laser technology. The quantum properties of proton relaxation in HBC can be applied in the future to the study of solid-state electrolytes with high proton conductivity for hydrogen energy, capacitor technology (superionics, varicodes), and elements of MIS and MSM structures in the development of resonant tunnel diodes for microelectronics and computer technology.

Keywords: hydrogen-bonded crystals (HBC); proton semiconductors and dielectrics (PSD); quantum diffusion polarization; quantum transparency; potential barrier; Gibbs's quantum canonical distribution; nonlinear quantum kinetic equation; proton relaxation; dielectric loss tangent

Citation: Kalytka, V.; Mekhtiyev, A.; Neshina, Y.; Alkina, A.; Aimagambetova, R.; Mukhambetov, G.; Bashirov, A.; Afanasyev, D.; Bilichenko, A.; Zhumagulova, D.; et al. Physical and Mathematical Models of Quantum Dielectric Relaxation in Electrical and Optoelectric Elements Based on Hydrogen-Bonded Crystals. *Crystals* **2023**, *13*, 1353. https://doi.org/10.3390/cryst13091353

Academic Editor: Peng Shi

Received: 25 July 2023
Revised: 18 August 2023
Accepted: 23 August 2023
Published: 6 September 2023

1. Introduction

In the last two decades, composite materials based on layered dielectrics with ion-molecular chemical bonding, which are capable of exhibiting high ionic conductivity in certain ranges of field parameters and temperatures, have played a significant role in various branches of modern industry [1–5].

A separate category of ion-molecular dielectrics is represented by hydrogen-bonded crystals (HBC) used in radio electronics (elements of electronically controlled systems of microwave, ultra-high frequency [6]); optoelectronics and nonlinear optics (nonlinear optical signal converters; high-precision long-mode fiber optic strain gauges in solid-state elements of structures and structures in mining and construction technologies); laser technology (regulators of radiation parameters and electric shutters (KDP (potassium dihydrogenphosphate)) [7–9]; microelectronics (field effect transistors, resonant tunnel diodes, MIS, MSM structures); electrochemical technologies (solid-state fuel cells based on dielectrics with high ionic conductivity) [10–14].

According to the results of a number of studies, the mechanism of spontaneous polarization in ferroelectrics of the HBC class (triglycinesulfate, Rochelle salt [15–23], KDP, DKDP (deuterated potassium dihydrogen phosphate) [24–28], etc.) is due to quantum tunneling transitions (displacements) of hydrogen ions (protons) inside the hydrogen sublattice near the second-order phase transition point [25,26,28].

The manifestation of a rectangular hysteresis loop with an anomalously long residual polarization relaxation time (up to 10 years) in ferroelectrics of HBC-class makes it possible to use these materials in capacitors of non-volatile high-speed memory devices (memory cells such as DRAM, FeRAM, etc.) of electronic computing devices [29–71].

Theoretical studies of nonlinear kinetic phenomena during polarization of layered dielectrics of the HBC-class (crystal hydrates; layered silicates) were carried out in a wide range of field parameters and temperatures and indicate the manifestation of an anomalously high dielectric constant ((1.5–2.5) million) in the region of ultralow temperatures (1–10 K) in weak fields (100–1000 kV/m) and in the region of ultra-high temperatures (550–1500 K) in strong fields (10–100 MV/m) [72–78].

In HBC, over a wide range of field parameters (0.1–100 MV/m) and temperatures (1–1500 K), tunneling transitions of protons in the anionic sublattice play a significant role in the formation of volume-charge polarization. In the range of low temperatures (50–100 K) and, moreover, ultra-low temperatures (4–25 K), proton relaxation polarization is determined only by quantum effects in the hydrogen sublattice [79,80].

2. Models and Methods

2.1. Dielectric Relaxation Mechanism in HBC, Comparative Analysis of Different Models

Studies of the electrophysical properties of HBC-class crystals are based on precision measurements of the temperature spectra of thermally stimulated depolarization currents (TSDC) and the frequency-temperature spectra of the dielectric loss angle tangent $\mathrm{tg}\delta_{exp}(\omega, T)$ [75,78,81–89]. In [90], the methodologies of experimental studies and semi-empirical estimates of the characteristic parameters of crystals under various external conditions of the experiment (polarization temperature; polarizing field strength; external mechanical stresses) and methods of processing samples (doping, calcination, etc.) are described. In [90], experimental patterns of behavior of TSDC density spectra in a model Ih-ice crystal and complex HBC crystal lattice structure (layered silicates; crystalline hydrates) on the example of the crystals of natural phlogopite $KMg_3(AlSi_3O_{10})(OH)_2$, muscovite $KAl_2(AlSi_3O_{10})(OH)_2$, onot talc $Mg_3(Si_4O_{10})(OH)_2$ chemically pure chalcanthite $CuSO_4 \cdot 5H_2O$ at temperatures above 50–550 K and at polarizing field strengths of 0.1–1 MV/m with a frequency of the polarizing field in the range of 1 kHz–10 of MHz. At the same time, in natural samples of layered minerals and crystalline hydrates, as a rule, 6–7 monorelaxation maxima [78,90] are found, caused by relaxation of the corresponding types of structure defects: Bjerrum ionization defects and complexes of the "vacation + L-defect" (VL) or "vacation + D-defect" (VD) type [1] are dipole molecules of

crystallization (structural) and adsorbed (interlayer) water. A significant role in relaxation processes in HBC-type dielectrics is acquired by volume-charge polarization associated with relaxation of a mixed type (when defects of a structure of different nature are activated in an electric hollow), manifested in a region of sufficiently high temperatures (250–550 K) and characterized by high polarization nonlinearities (associated with the influence of electric field parameters on the amplitudes of TSDC density maxima and relaxation times of structure defects) [78,90].

In the field of low temperatures (50–100 K), the main contribution to a dielectric relaxation of HBC is made by the quantum microscopic effects connected with tunnel transitions of ions of hydrogen (protons) inside and between ions of an anion sublattice [78,90]. The structure of an anion sublattice is formed in a certain way by the type of anions connected among themselves at the corresponding geometry of a crystal lattice: SiO_4^{4-}—silicate-anions in layered silicates (micas, minerals of group of talc-pyrophyllite, clay minerals, vermiculites, allophanes, halloysites, etc. (Figure A1 in Appendix A)); SO_4^{2-}—sulfate-anions in crystalline hydrates on the basis of the hydrated salts of sulfuric acid (chalcanthite, epsomite, melanterite, morenozite, ertgertsit, plaster, etc.); PO_4^{3-}—anions in crystalline hydrates on the basis of salts of orthophosphoric acid; CO_3^{2-}—carbonate anions, etc. Community of the chemical structure of crystalline hydrates will allow to assume for crystals of this group the universal scheme of migration of ionization defect H_3O^+ due to the stage-by-stage movement of a proton, under the influence of the external electric field, between layers of anions and layers of molecules of water, as it is described on the example of chemically pure chalcanthite $CuSO_4 \cdot 5H_2O$ in Figure 5 in [78] (or in Figure A2 in Appendix A). In [78] the chemical equations describing this movement of a proton are given. Similar schemes of migration of a proton and the chemical equations of his movement, but only between layers SiO_4^{4-} and layers of molecules of water, are reported for layered silicates, on the example of the natural phlogopite $KMg_3(AlSi_3O_{10})(OH)_2$ [78]. It agrees [78,90], at the microscopic level, relaxation process at low-temperature polarization in HBC is implemented, including, due to the tunnel movement of protons in the protonated anions $HSiO_4^{3-}$, SiO_4H^{3-} in layered silicates and, in the protonated anions HSO_4^-, SO_4H^- in the chalcanthite, with the energy of activation $U_0 = (0.01 \div 0.1)$ eV small against the background of energy of activation of high-temperature relaxers $U_0 = (0.1 \div 1)$ eV. In the field of low temperatures, at the movement of a molecule of the next layers significantly approach, the potential barrier is narrowed, and for a proton, the tunneling probability increases, which causes quantum microscopic effects. At the experimental level, it is revealed that in TSDC ranges in HBC, when calcinating crystals, the low-temperature maximum doesn't change on amplitude (at the same time, other maxima disappeared at calcination temperatures 573–1073 K), and only at a calcinating temperature higher than 1200 K (natural phlogopite), when not only all water but also a part of protons [90] is emitted, the low-temperature maximum decreases on amplitude practically to zero. Besides, when alloying crystals in HCl solutions, HF, this maximum also does not change the temperature situation (unlike high-temperature "sands" of TSDC) but increases in amplitude with the increase in concentration of the alloying impurity [78,90]. On this basis, it is possible to claim that in the field of temperatures of T = 50–100 K of the highest density of thermally stimulated current of depolarization in HBC (including ice) it is caused by a relaxation of protons in an anion sublattice. Thus, the tunneling of protons is the dominating mechanism, and the ion of hydrogen (proton) is the main carrier of a charge (relaxers) when forming polarization in class HBC crystals in the field of low temperatures. The phenomenon of diffusive (including tunnel) transfer of protons in an electric field can be determined by hydrogen communications, *proton conductivity*, and the related polarization of dielectrics as *proton and relaxation polarization*. At the same time, the movement of a proton is implemented in the direction of crystal axis C (perpendicular to the cleavage planes). In this connection, when studying proton relaxation and the related polarizing effects in HBC, the external electric field of **E** needs to be focused parallel to a crystal axis. At the orientation of the **E**⊥**C** field in HBC the polarizing effects connected with the movement of carriers of a charge (various types of ions) in the

direction of lines of the chemical bonds localized in the cleavage planes will be observed, but, the proton conductivity and proton and relaxation polarization will practically not be shown at the same time. In this regard, in [78,90] for the mathematical description of the kinetic phenomena connected with proton conductivity in solid dielectrics, the model of the one-dimensional crystal field (or fields of hydrogen communication) is accepted in which the proton moves in an anion sublattice. Movements of a proton in the field of the chemical bonds caused by electrostatic interaction with the ions and ionic groups that are not entering an anion sublattice need to be described by certain potential fields that influence proton conductivity (taking into account effects of quantization of energy of a proton in these fields), which will be reflected in the form of additional quantum numbers in the Schrödinger equation and in the expression for the density matrix for a proton and in the expression for the density matrix for a proton moving in the HBC. In previously developed models of quantum tunnel proton-relaxation polarization [81,82], additional quantum numbers for the proton were not taken into account, and the mathematical description of the kinetics of quantum proton motion was limited to solving the Liouville equation for a one-dimensional model of an external field perturbed one-dimensional crystalline field. This approach is not rigorous in terms of the completeness of the physical description of proton conduction mechanisms in structurally complex HBC crystal lattice in which the effect on the relaxing proton by subsystems other than the anion subsystem, although it is additional to the basic proton-anion interaction, but with certain variations in geometric (crystal sizes), field parameters and temperature, cause corrections to the basic density matrix for the proton subsystem, which can be very significant in value not only in the region of low but higher temperatures ($T > 100$ K). The solution to this issue, in general, is devoted to this article.

The physical mechanisms of dielectric relaxation in HBC in the region of high-temperature maxima (100–550 K) of TSDC density have been investigated and described in [78] on the example of a number of layered dielectrics (phlogopite, muscovite, chalcanthite, talc). Theoretical TSDC density spectra in [78] were investigated in terms of the effects of crystal lattice parameters and temperature on the molecular parameters of relaxers (activation energy; the width of the potential barrier; equilibrium concentration of relaxers; natural frequency of oscillations of relaxers) and parameters of theoretical maxima of thermally stimulated current (amplitude and temperature position) in a wide temperature range (50–550 K). In [78], it was found that theoretical and experimental results are in good agreement when calculating the molecular parameters of relaxers, taking into account the possibility of proton tunneling in HBC in the region of high temperature.

In [78], proton tunneling at the mathematical level was laid down in the structure of kinetic coefficients of the quasi-classical kinetic equation of proton relaxation, which was solved in a generalized nonlinear approximation by dimensionless parameters of perturbation theory. In [75], methods for constructing and analyzing solutions of the Fokker-Planck nonlinear kinetic equation were developed, which is more stringent than the kinetic equation in [78], in terms of taking into account the effects of nonlinear effects (caused by the interaction of spatial relaxation modes of the volume charge density at the main frequency of the variable field) on the kinetics of dielectric relaxation and, accordingly, on the parameters of relaxers in the regions of manifestations of abnormally high polarization nonlinearities. However, the methodology in [75], as in [78], is based on the quasi-classical kinetic theory of proton relaxation and considers quantum tunneling of protons not only in terms of its influence on kinetic coefficients but also on the macroscopic process in dielectrics in general. Since the methods in [75,78] are not strictly quantum-to-mechanical, it is almost impossible to study with their help the dimensional effects associated with the tun-non-plating of protons. A more stringent approach to solving this question, based on the calculations of the density matrix for the proton subsystem, was taken in [81,82], but these works did not disclose the influence of additional quantum numbers for the proton when describing its tunneling in the anion subsystem of HBC.

2.2. Statement of the Quantum Mechanical Problem

The physical and mathematical model of the quantum motion of a proton in the potential field of a crystal lattice in a HBC should be built taking into account all types of chemical bonds that exist in crystals of the HBC class [81,82], including the interaction potentials of the proton and ion-molecular subsystems. View of the totality of the anionic subsystem (consisting of anions of acidic residues of inorganic salts, connected to the proton subsystem by hydrogen bonds) and the ionic subsystem (consisting of heavier (than anions) ions, polar groups, molecules (including molecules of structural and adsorbed water), and molecular clusters), which also interact with the proton subsystem due to various types of electrostatic forces (proton-dipole, proton-quadrupole, etc.) under the ion-molecular subsystem is meant. The geometric model of the problem is taken to be three-dimensional, where the potential field of the proton-anion interaction is taken to be one-dimensional and oriented along the line of hydrogen bonds (along the crystal axis), and the potential field of the proton-ion interaction is taken to be two-dimensional and oriented along the lines of bonds of the proton with ionic groups and molecules [83,84].

The purpose of the given paper is to develop a more rigorous, in comparison with [79–82,85–87] (in terms of the structure of the Hamiltonian and its properties), quantum mechanical model in the form of solutions of a nonlinear quantum kinetic equation that describes, together with the Poisson equation, the motion of the main relaxers (protons) against the background of anionic and ionic-molecular subsystems (accepted as static) in HBC in an electric field. On this basis, the effects of proton tunneling transitions on the temperature and frequency spectra of the complex dielectric permittivity in a wide range of field parameters (100 kV/m–100 MV/m) and temperatures (0–1500 K) have been identified.

In the equations of the mathematical model, the theoretical dependences of the dielectric loss tangent $\mathrm{tg}\delta_{\mathrm{th}}^{(\omega)}(\mathrm{T};\zeta_0)$, $\mathrm{tg}\delta_{\mathrm{th}}^{(\mathrm{T})}(\omega;\zeta_0)$ will be investigated taking into account the properties and ranges of changes in the numerical values of the parameters ζ_0, forming a set on the set of points of the continuum measure (in infinitesimal neighborhoods) near the corresponding points of experimental maxima $\left\{\mathrm{tg}\delta_{\mathrm{max,exp}}^{(\omega)};\mathrm{T}_{\mathrm{max,exp}}\right\}$, $\left\{\mathrm{tg}\delta_{\mathrm{max,exp}}^{(\mathrm{T})};\omega_{\mathrm{max,exp}}\right\}$. Numerical modeling of dependences $\mathrm{tg}\delta_{\mathrm{th}}(\omega;\mathrm{T};\zeta_0)$ is convenient to build by regression analysis methods, in particular, by minimizing the function of comparison of the results of theory and experiment [80], when calculating the characteristic parameters for a proton $\zeta_0 = \{a;\delta_0;\mathrm{U}_0;\nu_0;n_0\}$, where a—is the lattice constant, δ_0—potential barrier width, U_0—potential barrier height (activation energy of the proton in a hydrogen link), ν_0—the natural frequency of proton oscillations in the potential well, n_0—the balanced concentration of relaxers (protons) [81,84,85,87].

The calculation of the unperturbed discrete energy spectrum of protons $E_{\overline{\mathrm{n}}}^{(0)}$ in HBC has been carried out. The calculation of the Hamiltonian of the system (crystal) was carried out by the secondary quantization methods without taking into account the influence of the proton-phonon interaction $\hat{\mathrm{H}}_{\mathrm{pr,ph}} \to 0$, according to the accepted for HBC to the experimental assumptions [79,81]. The Hamiltonian of the phonon subsystem was taken as a constant numeric operator $\hat{\mathrm{H}}_{\mathrm{ph}} \to \mathrm{const}$. The calculation was limited to the ideal model proton gas due to low equilibrium concentration of relaxing protons $n_0 \approx \left(10^{16} \div 10^{18}\right)\ \mathrm{m}^{-3}$. The following will give the rationale for these model simplifications in coordinate representation [81,82].

2.3. Study of the Hamiltonian of the System

The complete Hamiltonian of crystal, unperturbed by an external field, taking into account the types of interactions indicated in Sections 2.1 and 2.2 in the crystal lattice of the dielectric of HBC class, can be represented in the form of the following equation:

$$\hat{\mathrm{H}}_{\mathrm{C}}^{(0)} = \hat{\mathrm{H}}_{\mathrm{pr,C}}^{(0)} + \hat{\mathrm{H}}_{\mathrm{A,C}}^{(0)} + \hat{\mathrm{H}}_{\mathrm{S,C}}^{(0)} + \hat{\mathrm{H}}_{\mathrm{pr,A}} + \hat{\mathrm{H}}_{\mathrm{pr,S}} + \hat{\mathrm{H}}_{\mathrm{A,S}}.$$

Here $\hat{\mathrm{H}}_{\mathrm{pr,C}}^{(0)} = -\frac{\hbar^2}{2\mathrm{m_p}}\sum_{\mathrm{i}=1}^{\mathrm{N_{pr,F}}}\hat{\nabla}_{\mathrm{i}}^2 + \sum_{(\mathrm{i}\neq\mathrm{k})=1}^{\mathrm{N_{pr,F}}}\mathrm{W}_{\mathrm{pr,ik}}(|\mathbf{r}_{\mathrm{i,k}}|)$—Hamiltonian of proton subsystem, $\mathrm{W}_{\mathrm{pr,ik}}(|\mathbf{r}_{\mathrm{i,k}}|)$—potential energy of the interaction of the i-th and k-th protons,

m_p—proton mass, $N_{pr,F}$—the full number (quantity) of relaxers (protons) in the model. In this expression the symbol "pr" stands for the abbreviation of the term "proton".

During the constructing a mathematical model of quantum relaxation processes in the model HBC crystal, we assume that the dielectric has a strictly specified chemical formula and, accordingly, the anionic sublattice is formed by interacting anions of the given type. Then, we construct the Hamiltonian of the anionic subsystem as follows:

$$\hat{H}_{A,C}^{(0)} = -\frac{\hbar^2}{2m_A}\sum_{j=1}^{N_{A,F}}\hat{\nabla}_j^2 + \sum_{(j\neq p)=1}^{N_{A,F}}\hat{W}_{(j,p)}.$$

Here $\hat{W}_{(j,p)}$—potential energy of the interaction of the j-th and p-th anions, m_A—anion mass, $N_{A,F}$—the full number (quantity) of anions in the model.

Similarly, we construct Hamiltonian the ionic subsystem, according to Sections 2.1 and 2.2, including ions (or ionic complexes of a given species, with masses much larger than those of the anions in this model, and affecting in a certain way the proton subsystem and mechanism of proton relaxation.

Similarly, we construct Hamiltonian the ionic subsystem, according to Sections 2.1 and 2.2, including ions (or ionic complexes of a given species, with masses much larger than those of the anions in this model, and affecting in a certain way the proton subsystem and mechanism of proton relaxation:

$$\hat{H}_{S,C}^{(0)} = -\frac{\hbar^2}{2m_S}\sum_{s=1}^{N_{S,F}}\hat{\nabla}_s^2 + \sum_{(s\neq q)=1}^{N_{S,F}}\hat{W}_{(s,q)}.$$

Here $\hat{W}_{(s,q)}$—is the potential energy of interaction between the s-th and q-th ions, m_S—mass of the ion, $N_{S,F}$—the full number (quantity) of ions in the model.

The Hamiltonians of the anionic and ionic subsystems should be based on studies of the phonon subsystems (their energy spectra) corresponding to the anionic and ionic subsystems. In this case, the problem acquires a rigorous theoretical character and is solved by rigorous methods based on the apparatus of statistical solid-state theory. Rigorous analytical studies of phonon subsystems would require the study, at the numerical level, of the structure and parameters of all branches of the energy spectrum of particles (ions; in particular, anions) making complex mechanical motions of vibrational character, interpreted in equations for the displacements of ions relative to equilibrium positions localized in the nodes of the crystal lattice or its sublattices (anionic and ionic). However, in general this paper is semi-theoretical, semi-experimental in nature and, to a large extent, is based on a number of assumptions derived from experimental results [83]. Thus, the Hamiltonian of the anionic subsystem transformed by methods of secondary quantization to the Hamiltonian of the one phonon subsystem $\hat{H}_{A,C}^{(0)} \to \hat{H}_{A,ph} = \hbar\sum_{\mathbf{k}\alpha}\Omega_{\mathbf{k}\alpha}\left(\hat{c}_{\mathbf{k}\alpha}^{+}\hat{c}_{\mathbf{k}\alpha} + \frac{1}{2}\right)$, is characterized by the energy spectrum $E_{A,\mathbf{k}\alpha} = \hbar\Omega_{\mathbf{k}\alpha}\left(n_{A,\mathbf{k}\alpha} + \frac{1}{2}\right)$, determined by the frequency spectrum of anion vibrations. Frequency spectrum phonons of this type consists of $3N_A$ branches of the form $\Omega_{\mathbf{k}\alpha} = \Omega_{\alpha}(\mathbf{k})$ in functions of the wave vector anions, where $\alpha = 1, 2, 3, \ldots, 3N_A, N_A$—total number of anions in one unit cell, spectrum of anion vibration frequencies $\Omega_{\mathbf{k}\alpha}$ is calculated from the solutions of the known system of algebraic equations. Particle vibrations in the ionic sublattice in HBC give rise to another phonon subsystem with Hamiltonian $\hat{H}_{S,C}^{(0)} \to \hat{H}_{S,ph} = \sum_{\mathbf{k}\alpha}\hbar\omega_{\mathbf{k}\alpha}\left(\hat{d}_{\mathbf{k}\alpha}^{+}\hat{d}_{\mathbf{k}\alpha} + \frac{1}{2}\right)$, characterized by energy spectrum $E_{S,\mathbf{k}\alpha} = \hbar\omega_{\mathbf{k}\alpha}\left(n_{S,\mathbf{k}\alpha} + \frac{1}{2}\right)$ and frequency spectrum of ion vibrations $\omega_{\mathbf{k}\alpha} = \omega_{\alpha}(\mathbf{k})$, where $\alpha = 1, 2, 3, \ldots, 3N_S, N_S$—total number of ions in one unit cell. In view of the fact that this paper relies heavily on the experimental results [83], we take into account that the experimentally measured vibrational frequencies of anions in HBC are $\nu_{A,\mathbf{k}\alpha} \cong \nu_{A,0} \approx \left(10^{10} \div 10^{11}\right)s^{-1}$, which is substantially lower than the natural frequencies of proton vibrations in the potential well in HBC $\nu_0 \approx \left(10^{12} \div 10^{13}\right)s^{-1}$ [81,83]. Under

such conditions, at the formal level, in order to simplify the mathematical model, we shall restrict ourselves at this stage of research, albeit roughly but experimentally justified approximation, assuming that the perturbations caused by the phonon subsystem of anions are insignificant against the background of proton fluctuations in the HBC. At transition to the initial form of the Hamiltonian of the anion subsystem, we take for HBC some model constant $\hat{H}^{(0)}_{A,C} \to H^{(0)}_{A,0}$, reflecting at the formal level the degree of manifestations of the parameters of the phonon subsystem generated by anion vibrations in HBC. For similar Hamiltonian simplification of the ionic subsystem $\hat{H}^{(0)}_{S,C}$ there are, according to experimental data, better evidence $\nu_{S,\mathbf{k}\alpha} \cong \nu_{S,0} \approx \left(10^9 \div 10^{10}\right)s^{-1}$ [81,83], whence we introduce one more model constant $\hat{H}^{(0)}_{S,C} \to H^{(0)}_{S,0}$. At further investigation of the Hamiltonian of the whole system $\hat{H}^{(0)}_{C}$ these constants are reduced in the Schrödinger equation and do not take participation in the description of proton motions in HBC. Such an approach, at this stage of research, is forced due to the cumbersome nature of the problem of calculating the vibration spectra of heavy ions in the crystal structure of HBC and will be performed within the framework of another mathematically more rigorous work.

Concerning the influence of the anionic and ionic subsystems on the vibrations and relaxation of protons in HBC, this question is unambiguously considered and is one of the fundamental principles of this model. Without solving the question of proton-anion and proton-ion interactions, within the framework of the developed methods, in principle, it is impossible to do without, since the unperturbed crystal potential for a proton, even if the proton-ion operators are neglected, sums up from the potential energies of the proton in the field of anionic and ion subsystems. The simplification consists only in the calculation of the data operators $\hat{H}_{pr,A}, \hat{H}_{pr,S}$ interactions, we restrict ourselves to the zero approximation for the displacements of ions A and S relative to their equilibrium positions in the crystal lattice $\mathbf{r}_{j0}$, $\mathbf{r}_{s0}$. By unfolding potential interaction energies of i-th proton and j-th anion and i-th proton and s-th ion in series by displacements of anions $\mathbf{u}_j = \mathbf{r}_j - \mathbf{r}_{j0}$ in the anion sublattice and ions $\mathbf{u_s} = \mathbf{r}_s - \mathbf{r}_{s0}$ in the ion sublattice, with accuracy to the linear approximation as follows:

$$W_{pr,A}\left(\left|\mathbf{r}_{ij}\right|\right) \approx W_{pr,A}\left(\left|\mathbf{r}_{i,j0}\right|\right) + \frac{\partial W_{pr,A}\left(\left|\mathbf{r}_{i,j0}\right|\right)}{\partial \mathbf{r}_j}\mathbf{u}_j,$$

$$W_{pr,S}(|\mathbf{r}_{is}|) \approx W_{pr,S}(|\mathbf{r}_{i,s0}|) + \frac{\partial W_{pr,S}(|\mathbf{r}_{i,s0}|)}{\partial \mathbf{r}_s}\mathbf{u}_s.$$

Additionally, restricting by virtue of $\left|\mathbf{u}_j\right| \ll \left|\mathbf{r}_{j0}\right|$, $|\mathbf{u}_s| \ll |\mathbf{r}_{s0}|$ only by zero corrections $W_{pr,A}\left(\left|\mathbf{r}_{i,j0}\right|\right)$, $W_{pr,S}(|\mathbf{r}_{i,s0}|)$, we take the operators of the proton-anion and proton-ion interaction in the simplest form from the point of view of the theory:

$$\hat{H}_{pr,A} \to \hat{H}^{(0)}_{pr,A} = W^{(0)}_{pr,A} = \sum_{i=1}^{N_{pr,F}}\left(\sum_{j=1}^{N_{A,F}} W_{pr,A}\left(\left|\mathbf{r}_{i,j0}\right|\right)\right),$$

$$\hat{H}_{pr,S} \to \hat{H}^{(0)}_{pr,S} = W^{(0)}_{pr,S} = \sum_{i=1}^{N_{pr,F}}\left(\sum_{s=1}^{N_{S,F}} W_{pr,S}(|\mathbf{r}_{i,s0}|)\right),$$

where $\mathbf{r}_{i,j0} = \mathbf{r}_i - \mathbf{r}_{i,j0}$, $\mathbf{r}_{i,s0} = \mathbf{r}_i - \mathbf{r}_{s0}$.

The calculation of secondary quantized displacement operators $\hat{\mathbf{u}}_j$, $\hat{\mathbf{u}}_s$ within the framework of this work is not performed. The solution of the problem of calculating the operators of the proton-phonon interaction will also be carried over to subsequent stages

of research (in other papers). In the linear approximation by displacements $\mathbf{u}_j, \mathbf{u}_s$ these operators have the form:

$$\delta\hat{H}_{pr,A}(\mathbf{n}) = \sum_{i=1}^{N_{pr,F}} \left(\sum_{j=1}^{N_{A,F}} \frac{\partial W_{pr,A}(|\mathbf{r}_{i,j0}|)}{\partial \mathbf{r}_j} \hat{\mathbf{u}}_j(\mathbf{n}) \right),$$
$$\delta\hat{H}_{pr,S}(\mathbf{n}) = \sum_{i=1}^{N_{pr,F}} \left(\sum_{s=1}^{N_{S,F}} \frac{\partial W_{pr,S}(|\mathbf{r}_{i,s0}|)}{\partial \mathbf{r}_s} \hat{\mathbf{u}}_s(\mathbf{n}) \right).$$

Let's note that the application of secondary quantum operators [83] is as follows:

$$\hat{\mathbf{u}}_j(\mathbf{n}) = \sqrt{\frac{\hbar}{2N_1 M_A}} \sum_{\mathbf{k}\alpha} \frac{1}{\sqrt{\Omega_{\mathbf{k}\alpha}}} \left[\hat{c}_{\mathbf{k}\alpha} e_j^{\alpha}(\mathbf{k}) \exp(i\mathbf{k}\mathbf{r}_\mathbf{n}) + \hat{c}^{+}_{\mathbf{k}\alpha} \left(e_j^{\alpha}(\mathbf{k}) \right)^{+} \exp(-i\mathbf{k}\mathbf{r}_\mathbf{n}) \right],$$

$$\hat{\mathbf{u}}_s(\mathbf{n}) = \sqrt{\frac{\hbar}{2N_2 M_S}} \sum_{\mathbf{k}\alpha} \frac{1}{\sqrt{\omega_{\mathbf{k}\alpha}}} \left[\hat{d}_{\mathbf{k}\alpha} e_s^{\alpha}(\mathbf{k}) \exp(i\mathbf{k}\mathbf{r}_\mathbf{n}) + \hat{d}^{+}_{\mathbf{k}\alpha} (e_s^{\alpha}(\mathbf{k}))^{+} \exp(-i\mathbf{k}\mathbf{r}_\mathbf{n}) \right].$$

Here $\mathbf{n}$—characteristic vector of an elementary cell drawn to its arbitrary vertex; N_1, N_2—respectively, the total number of unit cells in the anionic and ionic sublattices; $M_A = m_A N_A$, $M_S = m_S N_S$—masses of anionic and ionic components in unit cells of anionic and ionic sublattices, respectively.

To the calculation of operators $\delta\hat{H}_{pr,A}$, $\delta\hat{H}_{pr,S}$ should be carried out taking into account the summation of displacements $\hat{\mathbf{u}}_j(\mathbf{n})$, $\hat{\mathbf{u}}_s(\mathbf{n})$ by unit cells in crystalline structure of anionic and ionic sublattices, which, in fact, is a separate rather complex problem, reduced to the transformation of expressions of the following form

$$\delta\hat{H}_{pr,A} = \sum_{\mathbf{n}} \sum_{i=1}^{N_{pr,F}} \left(\sum_{j=1}^{N_{A,F}} \frac{\partial W_{pr,A}(|\mathbf{r}_{i,j0}|)}{\partial \mathbf{r}_j} \hat{\mathbf{u}}_j(\mathbf{n}) \right),$$
$$\delta\hat{H}_{pr,S} = \sum_{\mathbf{n}} \sum_{i=1}^{N_{pr,F}} \left(\sum_{s=1}^{N_{S,F}} \frac{\partial W_{pr,S}(|\mathbf{r}_{i,s0}|)}{\partial \mathbf{r}_s} \hat{\mathbf{u}}_s(\mathbf{n}) \right).$$

Thus, the total Hamiltonian of HBC class crystals (belonging to layered dielectrics) can be seen as the sum of the individual Hamiltonians of the proton subsystem (which, due to the low equilibrium concentration of relaxing protons $n_0 \approx (10^{16} \div 10^{17})$ m^{-3} [83], can be defined as a system consisting of non-interacting protons (ideal proton gas: $W_{pr,ik}(|\mathbf{r}_{i,k}|) \to 0$) $\hat{H}^{(0)}_{pr,C} = \sum_{i=1}^{N_{pr,F}} \hat{H}^{(0)}_{(pr,i);C}$, anionic subsystem (consisting of different types of anions (depending on the chemical structure of the particular material) to which the proton is bonded by hydrogen bonds oriented along of the crystal C-axis perpendicular to the cleavage planes) $\hat{H}^{(0)}_{A,C} \to \hat{H}_{A,ph} \to H^{(0)}_{A,0}$ and the ionic subsystem consisting of different types of ions, polar groups and molecules to which the proton is bonded electrostatically and molecularly, oriented within the planes $\hat{H}^{(0)}_{S,C} \to \hat{H}_{S,ph} \to H^{(0)}_{S,0}$. The following designations have been adopted: $\hat{H}^{(0)}_{(pr,i);C} = -\frac{\hbar^2}{2m_p}\hat{\nabla}^2_i$—Hamiltonian of the i-th proton; $N_{pr,F}$—total number of protons moving with a given activation energy U_0, determined by the interaction mechanisms of the proton with the anionic and ionic subsystems (it is obvious from experimental evaluations that the proton-anion interaction makes the main contribution to the numerical value of this parameter; m_p—mass of the proton. The symbol C signifies "crystal".

By virtue of the adiabatic approximation when frequencies of vibrations of ions are taken negligibly small in comparison with frequencies of vibrations of protons (because of a large mass of an ion in comparison with a proton) and ions (including anions) can be considered as motionless against protons moving inside and between the massive ions. Therefore, the Hamiltonians of the *anion* and *ion* subsystems can be simplified to a form of functions in space of time-varying coordinates of single ions (for anions also),

i.e., in this model can be considered numerical constants $\hat{H}^{(0)}_{A,C} \to H^{(0)}_{A,0} = U_{A,C} = const_A$, $\hat{H}^{(0)}_{S,C} \to H^{(0)}_{S,0} = U_{S,C} = const_S$ and interactionoperators of the anionic and ionic subsystems takes the form $\hat{H}_{A,S} \to H_{A,S} = U_{A,S} = const_{A,S}$ which is consistent with the condition superimposed on the Hamiltonian of the phonon subsystem $\hat{H}_{ph} = \hat{H}_{A,ph} + \hat{H}_{S,ph} \to H^{(0)}_{A,0} + H^{(0)}_{S,0} = const$.

The interaction operators of the proton subsystem with the anion and ion subsystems in this model will be constructed in the zero approximation, using the particle displacements of the anion and ion subsystems

$$\hat{H}^{(0)}_{pr,A} = \sum_{i=1}^{N_{pr,F}} \hat{H}^{(0)}_{(pr,i);A} = \sum_{i=1}^{N_{pr,F}} W^{(0)}_{(pr,i);A}, \quad \hat{H}^{(0)}_{pr,S} = \sum_{i=1}^{N_{pr,F}} \hat{H}^{(0)}_{(pr,i);S} = \sum_{i=1}^{N_{pr,F}} W^{(0)}_{(pr,i);S},$$

where $\hat{W}^{(0)}_{(pr;A);i}$, $\hat{H}^{(0)}_{(pr;i);S}$—respectively the potential interaction energy of the i-th proton with anionic and ionic subsystems.

The Hamiltonian of the crystal $\hat{H}^{(0)}_C = \hat{H}^{(0)}_{pr,C} + U_{A,C} + U_{S,C} + \hat{H}^{(0)}_{pr,A} + \hat{H}^{(0)}_{pr,S} + U_{A,S}$ takes the form:

$$\hat{H}^{(0)}_C = \sum_{i=1}^{N_{pr,F}} \hat{H}^{(0)}_{pr,i} + E_{(A;S)}, \tag{1}$$

where:

$$\hat{H}^{(0)}_{pr,i} = -\frac{\hbar^2}{2m_p}\hat{\nabla}^2_i + \hat{W}_{(pr;C);i}, \; \hat{W}_{(pr;C);i} = \hat{W}_{(pr;A);i} + \hat{W}_{(pr;S);i},$$
$$E_{(A;S)} = U_{A,C} + U_{S,C} + U_{A,S} = const.$$

Expression (2) allows us to go to a one-particle three-dimensional problem about the proton motion in potential field of the crystal lattice $\hat{W}_{(pr;C)}(\vec{r}) = \hat{W}_{(pr;A)}(x) + \hat{W}_{(pr;S)}(\vec{r}_\perp)$. Hamiltonianof the individual proton in this model takes the form $\hat{H}^{(0)}_{pr} = -\frac{\hbar^2}{2m_p}\hat{\nabla}^2 + \hat{W}_{(pr;C)}(\vec{r})$.

When studying the electrophysical processes, it is reasonable to direct the external electric field in the direction of the C-axis because in HBC the proton motion in the direction of hydrogen bonds (caused by the proton interaction with anions) oriented along the crystal C-axis (perpendicular to the cleavage planes). It is most likely. It is more convenient to consider the effects of stronger chemical bonds (than hydrogen bonds) caused by the interactions of the proton with heavy (in comparison with anions) ionic groups, clusters and molecules in the planes of cleavage. In this case it is convenient represent the unperturbed external field Hamiltonian of the proton as $\hat{H}^{(0)}_{pr} = \hat{H}^{(0)}_{pr;\parallel} + \hat{H}^{(0)}_{pr;\perp}$, where the longitudinal Hamiltonian of the proton $\hat{H}^{(0)}_{pr;\parallel} = -\frac{\hbar^2}{2m_p}\frac{\partial^2}{\partial x^2} + \hat{W}_{(pr;A)}(x)$ describes the movement proton in the one-dimensional potential field of hydrogen bonds (with the proton radius vector $\vec{r}_\parallel = \vec{i}\,x$ and the transverse Hamiltonian $\hat{H}^{(0)}_{pr;\perp} = -\frac{\hbar^2}{2m_p}\left(\frac{\partial^2}{\partial y^2} + \frac{\partial^2}{\partial z^2}\right) + \hat{W}_{(pr;S)}(\vec{r}_\perp)$ describes the motion the proton in the two-dimensional potential field of stronger (than hydrogen bonds) ionic molecular chemical bonds (with proton radius vector $\vec{r}_\perp = \{y; z\}$, where $\vec{r} = \vec{r}_\parallel + \vec{r}_\perp$. Stationary Schrödinger equation for the proton in the HBC $\hat{H}^{(0)}_{pr}\psi_{n,f_1,f_2}\left(\vec{r}\right) = E^{(0)}_{n,f_1,f_2}\psi_{n,f_1,f_2}\left(\vec{r}\right)$ is characterized by an unperturbed energy spectrum $E^{(0)}_{n,f_1,f_2} = E^{(0)}_n + E^{(0)}_{f_1,f_2}$ and the wave function $\psi_{n,f_1,f_2}\left(\vec{r}\right) = \psi_n(x)\psi_{f_1,f_2}\left(\vec{r}_\perp\right)$. Moreover, stationary Schrödinger equation is divided by into two equations $\hat{H}^{(0)}_{pr;\parallel}\psi_n = E^{(0)}_n\psi_n$, $\hat{H}^{(0)}_{pr;\perp}\psi_{f_1,f_2} = E^{(0)}_{f_1,f_2}\psi_{f_1,f_2}$. The energy levels $E^{(0)}_n$ the undisturbed spectrum are calculated for the model one-dimensional periodic potential field in [80] and for a parabolic model potential field $\hat{W}_{(pr;A)}(x)$ in [81]. Calculation of the energy spectrum of the transverse

proton motions in the cleavage planes $E^{(0)}_{f_1,f_2} = E^{(0)}_{f_1} + E^{(0)}_{f_2}$ with potential $\hat{W}_{(pr;S)}(y;z)$ will is carried out by the method of separation of variables in the rectangular XOY coordinate system by analyzing the individual energy spectra corresponding to its quantum motion in the direction of the bonding action lines along the OX, OY axes with one-dimensional periodic potentials $\hat{W}_{(pr;S_2)}(y)$, $\hat{W}_{(pr;S_2)}(z)$. By quantization of the proton energy spectrum for the transverse of motion is constructed from the solution to the wave equation $\hat{H}^{(0)}_{pr;\perp}\psi_{n_p,m_z} = E^{(0)}_{n_p,m_z}\psi_{n_p,m_z}$ when choosing cylindrical coordinate system (in the case of circular electrodes).

Proton wave function in a three-dimensional steady-state motion model with energy $E^{(0)}_{\bar{n}} \equiv E^{(0)}_{n,f_1,f_2} = E^{(0)}_{n} + E^{(0)}_{f_1,f_2}$, where $\bar{n} = \{n, f_1, f_2\}$, rationed $\int_V \psi^*_{n,f_1,f_2}\left(\vec{r}\right)\psi_{n,f_1,f_2}\left(\vec{r}\right)dV = 1$ in this way, which, given the type of symmetry of the electrodes $\iint_S \psi^*_{f_1,f_2}\left(\vec{r}_\perp\right)\psi_{f_1,f_2}\left(\vec{r}_\perp\right)dS = 1$. The surface integral is calculated over the cross-sectional area S of the sample (comparable to the surface area of the covers of a flat capacitor) for two-dimensional transverse motion of the proton with energy $E^{(0)}_{f_1,f_2}$. The one-dimensional wave function of the proton transfer motion in the direction of the crystal **C** axis along the hydrogen bond line is normalized as $\int_0^d \psi^*_n(x)\psi_n(x)dx = 1$. The proton coordinate varies in the range $0 \le x \le d$ in the one-dimensional mathematical model, where d—dielectric thickness.

The statistical operator of the unperturbed system (crystal) is calculated from solutions to the stationary Liouville equation $\frac{\partial\hat{\rho}^{(0)}_c}{\partial t} + \frac{1}{i\hbar}\left[\hat{\rho}^{(0)}_c, \hat{H}^{(0)}_c\right] = 0$, subject to (1), methods quantum Gibbs statistics. Then, taking into account the accepted model assumptions $E_{(A;S)} = \text{const}$, $\hat{\rho}^{(0)}_C \to B_{(A;S)} \times \exp\left(-\frac{\hat{H}^{(0)}_{pr}}{k_B T}\right) = \hat{\rho}^{(0)}_{pr}$, where is applied rationingconstant $B_{(A;S)} \to B_{pr;(A;S)} \times \exp\left(-\frac{E_{(A;S)}}{k_B T}\right)$ from the stationary equation $\frac{\partial\hat{\rho}^{(0)}_{pr}}{\partial t} + \frac{1}{i\hbar}\left[\hat{\rho}^{(0)}_{pr}, \hat{H}^{(0)}_{pr}\right] = 0$, according to the quantum canonical Gibbs distribution [79,85] for an ideal proton gas. We have the following:

$$\hat{\rho}^{(0)}_{pr} = N_{pr,F}\left[Z^{(0)}_{pr}\right]^{-1} \times \exp\left(-\frac{\hat{H}^{(0)}_{pr}}{k_B T}\right). \quad (2)$$

In (2) $Z^{(0)}_{pr} = \sum_{n=0}^{\infty}\sum_{(f_1,f_2)=0}^{\infty}\exp\left(-\frac{E^{(0)}_{n,f_1,f_2}}{k_B T}\right)$—the statistical sum of the proton subsystem, $N_{pr,F}$—total number of protons moving with a given activation energy U_0.

Elements equilibrium matrix densities $\hat{\rho}^{(0)}_{pr,\bar{n}} = \int_V \psi^*_{n,f_1,f_2}\left(\vec{r}\right)\hat{\rho}^{(0)}_{pr}\psi_{n,f_1,f_2}\left(\vec{r}\right)dV$ are calculated at according to quantum Boltzmann distribution [79,85] as follows:

$$\rho^{(0)}_{pr,\bar{n}} = N_{pr,F}\left[Z^{(0)}_{pr}\right]^{-1} \times \exp\left(-\frac{E^{(0)}_{n,f_1,f_2}}{k_B T}\right). \quad (3)$$

2.4. Quantum Kinetic Equation for Proton Relaxation

Statistical operator of the proton subsystem in the presence of an external homogeneous in time perturbing electric field (applied along the direction of crystal axis) $\hat{W}_{el}(x;t) = -qE_0\hat{x}\exp(i\omega t)$. It was calculate per field perturbed Hamiltonian of a single proton $\hat{H}_{pr} = \hat{H}^{(0)}_{pr} + \hat{W}_{el}(x;t)$ from the solution of the unsteady Liouville equation for proton subsystem $\frac{\partial\hat{\rho}_{pr}}{\partial t} + \frac{1}{i\hbar}\left[\hat{\rho}_{pr}, \hat{H}_{pr}\right] = 0$. By adopting this solution equation in the form $\hat{\rho}_{pr}\left(\vec{r};t\right) = \hat{\rho}^{(0)}_{pr}\left(\vec{r}\right) + \delta\hat{\rho}_{pr}(x;t)$, turning to the linearized approximation, when $\left[\delta\hat{\rho}_{pr}(x;t); \hat{W}_{el}(x;t)\right]\psi_{n,f_1,f_2}\left(\vec{r}\right) \to 0$, introducing the scalar function $u_{\bar{n}}\left(\vec{r};t\right) =$

$\delta\hat{\rho}_{pr}(x;t)\psi_n(x)\psi_{f_1,f_2}\left(\vec{r}_\perp\right)$, $u_{\overline{n}}\left(\vec{r};t\right) = u_{\overline{n}}(x;t)\psi_{f_1,f_2}\left(\vec{r}_\perp\right) = u_{n,f_1,f_2}(x;t)\psi_{f_1,f_2}\left(\vec{r}_\perp\right)$ get quantum kinetic equation as follows:

$$\frac{\partial u_{\overline{n}}}{\partial t} + \frac{E_n^{(0)}}{i\hbar}u_{\overline{n}} - \frac{1}{i\hbar}\hat{H}_{pr;\parallel}^{(0)}u_{\overline{n}} - \frac{qE_0\exp(i\omega t)}{i\hbar}N_{pr,F}\left[Z_{pr}^{(0)}\right]^{-1}\rho_{pr,\perp,f_1,f_2}^{(0)}\left[\hat{\rho}_{pr,\parallel}^{(0)};\hat{x}\right]\psi_n(x) = 0. \quad (4)$$

In (4) $\rho_{pr;\perp}^{(0)}\psi_{f_1,f_2}\left(\vec{r}_\perp\right) = \exp\left(-\frac{\hat{H}_{pr,\perp}^{(0)}}{k_BT}\right)\psi_{f_1,f_2}\left(\vec{r}_\perp\right)$, $\hat{\rho}_{pr,\parallel}^{(0)}\psi_n(x) = \exp\left(-\frac{\hat{H}_{pr,\parallel}^{(0)}}{k_BT}\right)\psi_n(x)$.

Introducing dimensionless variables in (4) $\tau = \omega_0^{(0)}t$, $\xi = \frac{x}{a}$, dimensionless small parameter $\varsigma_0 = \frac{qE_0a}{\hbar\omega_0^{(0)}}$ and $\zeta_n = \frac{E_n^{(0)}}{\hbar\omega_0^{(0)}}$, $\phi = \frac{\hbar}{2m_p\omega_0^{(0)}a^2}$, $w_{(pr;A)}(\xi) = \frac{\hat{W}_{(pr;A)}(x)}{U_0}$, $\chi = \frac{U_0}{\hbar\omega_0^{(0)}}$ retrieve

$$\frac{\partial u_{\overline{n}}}{\partial\tau} - i\zeta_n u_{\overline{n}} - i\phi\frac{\partial^2 u_{\overline{n}}}{\partial\xi^2} + i\chi w_{(pr;A)}(\xi)u_{\overline{n}} + i\varsigma_0\exp\left(i\frac{\omega}{\omega_0^{(0)}}\tau\right) \times N_{pr,F}\left[Z_{pr}^{(0)}\right]^{-1}\rho_{pr,\perp,f_1,f_2}^{(0)} \times \left[\hat{\rho}_{pr,\parallel}^{(0)};(\xi);\hat{\xi}\right]\psi_n(\xi) = 0. \quad (5)$$

Here, the frequency parameter $\omega_0^{(0)} = \frac{E_0^{(0)}}{\hbar}$ corresponds to the «zero» energy level in the energy spectrum $E_n^{(0)}$ of the particle (proton) moving in the unperturbed potential field of the crystal lattice (potential image).

For the linear harmonic oscillator model $E_n^{(0)} = \hbar\omega_0\left(n + \frac{1}{2}\right)$ in the expression $\omega_0^{(0)} = \frac{1}{2}\omega_0$ the value ω_0 has the meaning of the circular frequency of proton oscillations in the isolated potential well.

The solution of Equation (5), in the general case, will be constructed by perturbation theory methods by expansion into series on a small parameter ς_0. Then,

$$u_{\overline{n}}(\xi;\tau) = \sum_{s=1}^{\infty}\varsigma_0^s u_{\overline{n},s}(\xi;\tau). \quad (6)$$

Since there is no polarization of the crystal at the initial moment of time, the initial condition for (5) given in the form [81]

$$u_{\overline{n}}(\xi;0) = 0. \quad (7)$$

When calculating the nonequilibrium density matrix for a perturbed variable field $u_{\overline{n}}(\xi;\tau) \approx \varsigma_0 u_{\overline{n},1}(\xi;\tau)$, in (6) and (7):

$$\frac{\partial u_{\overline{n},1}}{\partial\tau} - i\phi\frac{\partial^2 u_{\overline{n},1}}{\partial\xi^2} + i\left(\chi w_{(pr;A)}(\xi) - \zeta_n\right)u_{\overline{n},1} + i\exp\left(i\frac{\omega}{\omega_0^{(0)}}\tau\right) \times N_{pr,F}\left[Z_{pr}^{(0)}\right]^{-1}\rho_{pr,\perp,f_1,f_2}^{(0)} \times \left[\hat{\rho}_{pr,\parallel}^{(0)};(\xi);\hat{\xi}\right]\psi_n(\xi) = 0, \quad (8)$$

$$u_{\overline{n},1}(\xi;0) = 0. \quad (9)$$

We accept the model of blocking contacts at the crystal boundaries (when the work function of a particle (in HBC, proton) outside the crystal boundaries is equal to infinity) [81]. In this case, the wave function of the relaxing particle (proton) is subject to the boundary conditions $\psi_n(0) = 0$, $\psi_n\left(\frac{d}{a}\right) = 0$ [80,81].

Decomposing $u_{\overline{n},1}(\xi;\tau)$ in a Fourier series $u_{\overline{n},1}(\xi;\tau) = \sum_{m=1}^{\infty}U_{\overline{n},1}(m;\tau) \times \cos\left(\frac{\pi m a}{d}\xi\right)$, by orthogonal functions $\cos\left(\frac{\pi m a}{d}\xi\right)$, on the segment $0 \le \xi \le \frac{d}{a}$, with the way $U_{n,1}(m;\tau) = \frac{2a}{d}\int_0^{d/a}u_{\overline{n},1}(\xi;\tau)\cos\left(\frac{\pi m a}{d}\xi\right)d\xi$ subject to change

$$\frac{\partial^2 u_{\overline{n},1}}{\partial\xi^2} \div \frac{2a}{d}\int_0^{d/a}\frac{\partial^2 u_{\overline{n},1}}{\partial\xi^2}\cos\left(\frac{\pi m a}{d}\xi\right)d\xi = \frac{2a}{d}\left(\frac{\partial u_{\overline{n},1}}{d\xi}|_{\xi-\frac{d}{a}}\cdot(-1)^m - \frac{\partial u_{\overline{n},1}}{d\xi}|_{\xi=0}\right) - \left(\frac{\pi m a}{d}\right)^2 U_{\overline{n},1}(m;\tau). \quad (10)$$

and

$$w_{(\mathrm{pr;A})}(\xi) = \Im_{(\mathrm{pr;A}),0} + \sum_{k=1}^{\infty} \Im_{(\mathrm{pr;A}),k} \cos\left(\frac{\pi k a}{\mathrm{d}}\xi\right)\mathrm{d}\xi,$$
$$\Im_{(\mathrm{pr;A}),k} = \frac{2a}{\mathrm{d}}\int_0^{\mathrm{d}/a} w_{(\mathrm{pr;A})}(\xi)\cos\left(\frac{\pi k a}{\mathrm{d}}\xi\right)\mathrm{d}\xi, \quad (11)$$

leads to

$$\frac{\partial U_{\overline{\mathrm{n}},1}(\mathrm{m};\tau)}{\partial\tau} + \mathrm{i}\left(\phi\left(\frac{\pi \mathrm{m} a}{\mathrm{d}}\right)^2 - \zeta_{\mathrm{n}}\right)U_{\overline{\mathrm{n}},1}(\mathrm{m};\tau) + \mathrm{i}\chi \times \frac{1}{2}\sum_{k=0}^{\infty}\Im_{(\mathrm{pr;A}),k}\times$$
$$(U_{\overline{\mathrm{n}},1}(k+\mathrm{m};\tau) + U_{\overline{\mathrm{n}},1}(k-\mathrm{m};\tau)) - \mathrm{i}\phi \times \mathrm{K}_{\overline{\mathrm{n}},\mathrm{m}}(\tau) + \mathrm{i}\exp\left(\mathrm{i}\frac{\omega}{\omega_0^{(0)}}\tau\right) \times F_{\mathrm{pr;m,n},f_1,f_2} = 0, \quad (12)$$

$$U_{\overline{\mathrm{n}},1}(\mathrm{m};0) = 0. \quad (13)$$

In (12) the notation is adopted:

$$U_{\overline{\mathrm{n}},1}(k \pm \mathrm{m};\tau) = \frac{2a}{\mathrm{d}}\int_0^{\mathrm{d}/a} \mathrm{u}_{\overline{\mathrm{n}},1}(\xi;\tau)\cos\left(\frac{\pi(k\pm\mathrm{m})a}{\mathrm{d}}\xi\right)\mathrm{d}\xi$$
$$\mathrm{K}_{\overline{\mathrm{n}},\mathrm{m}}(\tau) = \frac{2a}{\mathrm{d}}\left(\frac{\partial \mathrm{u}_{\overline{\mathrm{n}},1}}{d\xi}|_{\xi=\frac{\mathrm{d}}{a}}\cdot(-1)^{\mathrm{m}} - \frac{\partial \mathrm{u}_{\overline{\mathrm{n}},1}}{d\xi}|_{\xi=0}\right),$$
$$F_{\mathrm{pr;m,n},f_1,f_2} = \mathrm{N}_{\mathrm{pr,F}}\left[Z_{\mathrm{pr}}^{(0)}\right]^{-1}\rho_{\mathrm{pr},\perp,f_1,f_2}^{(0)} \times \mathrm{G}_{\mathrm{pr;m,n}},$$
$$\mathrm{G}_{\mathrm{pr;m,n}} = \frac{2a}{\mathrm{d}}\int_0^{\mathrm{d}/a}\left[\hat{\rho}_{\mathrm{pr},\parallel}^{(0)}(\xi);\hat{\xi}\right]\psi_{\mathrm{n}}(\xi)\cos\left(\frac{\pi \mathrm{m} a}{\mathrm{d}}\xi\right)d\xi.$$

When calculating the nonequilibrium density matrix for perturbed by an alternating field $\mathrm{E}(\mathrm{t}) = \mathrm{E}_0\exp(\mathrm{i}\omega t)$ proton subsystem, going from the equilibrium density matrix (3) to quote $\rho_{\mathrm{pr},\overline{\mathrm{n}}} = \mathrm{N}_{\mathrm{pr,F}}\left[Z_{\mathrm{pr}}^{(0)}\right]^{-1} \times \exp\left(-\frac{E_{\mathrm{n},f_1,f_2}}{\mathrm{k_B T}}\right)$, for the field frequency range $\nu_{el} = (10^3 \div 10^7)$ Hz, when the period of oscillation of the field is much longer than the relaxation time of the proton subsystem $(T_{\mathrm{el}} \gg T_{\mathrm{rp}})$ [81], correction to unperturbed levels to energy $E_{\mathrm{n}}^{(0)}$ acceptedquasi-stationary (weakly time-dependent) and, in the region of weak fields $\mathrm{E}_0 = (10^5 \div 10^6)$ V/m at ultra-low temperatures T = 1–10 K and in the strong field region $\mathrm{E}_0 = (10^7 \div 10^8)$ V/m, ultra-high temperatures T = 550–1500 K, low in magnitude ultra-high temperatures T = 550–1500 K [83], low in magnitude $E_{\mathrm{n}}^{(0)} \gg \Delta E_{\mathrm{n}}(\mathrm{t})$ [81], in the perturbation theory approximation we write [85] the following:

$$\rho_{\mathrm{pr},\overline{\mathrm{n}}}(\mathrm{t}) \cong \rho_{\mathrm{pr},\overline{\mathrm{n}}}^{(\omega)}(\mathrm{t}) \approx \rho_{\mathrm{pr},\overline{\mathrm{n}}}^{(0)} \times \left(1 - \frac{q\mathrm{E}_0 a}{\mathrm{k_B T}}(\langle\xi_{\mathrm{n}}\rangle_0 - \xi_{\mathrm{n}}) \times \exp(\mathrm{i}\omega\mathrm{t})\right). \quad (14)$$

In (14) $\langle\xi_{\mathrm{n}}\rangle_0 = \left[Z_{\mathrm{pr}}^{(0)}\right]^{-1}\sum_{\mathrm{n}=0}^{\infty}\exp\left(-\frac{E_{\mathrm{n}}^{(0)}}{\mathrm{k_B T}}\right) \times \xi_{\mathrm{n}}$, $\xi_{\mathrm{n}} = a\int_0^{\mathrm{d}/a}\psi_{\mathrm{n}}^*(\xi)\xi\psi_{\mathrm{n}}(\xi)\mathrm{d}\xi$.

Using $\rho_{\mathrm{pr},\overline{\mathrm{n}}}(\mathrm{t})\psi_{\mathrm{n},f_1,f_2}\left(\vec{\mathrm{r}}\right) = \hat{\rho}_{\mathrm{pr}}\left(\vec{\mathrm{r}};\mathrm{t}\right)\psi_{\mathrm{n},f_1,f_2}\left(\vec{\mathrm{r}}\right) = \rho_{\mathrm{pr},\overline{\mathrm{n}}}^{(0)}\psi_{\mathrm{n},f_1,f_2}\left(\vec{\mathrm{r}}\right) + \mathrm{u}_{\overline{\mathrm{n}}}\left(\vec{\mathrm{r}};\mathrm{t}\right)$, from (14) we construct an approximate asymptotic expression for the function sought in (8):

$$\mathrm{u}_{\overline{\mathrm{n}}}(\xi;\tau) = \left(\rho_{\mathrm{pr},\overline{\mathrm{n}}}(\mathrm{t}) - \rho_{\mathrm{pr},\overline{\mathrm{n}}}^{(0)}\right)\psi_{\mathrm{n}}(\xi) = -\frac{q\mathrm{E}_0 a}{\mathrm{k_B T}}\rho_{\mathrm{pr},\overline{\mathrm{n}}}^{(0)}(\langle\xi_{\mathrm{n}}\rangle_0 - \xi_{\mathrm{n}}) \times \mathrm{i}\exp\left(\mathrm{i}\frac{\omega}{\omega_0^{(0)}}\tau\right) \times \psi_{\mathrm{n}}(\xi).$$

Next, we write

$$\mathrm{u}_{\overline{\mathrm{n}},1}(\xi;\tau) = -\frac{\hbar\omega_0}{\mathrm{k_B T}}\rho_{\mathrm{pr},\overline{\mathrm{n}}}^{(0)}(\langle\xi_{\mathrm{n}}\rangle_0 - \xi_{\mathrm{n}}) \times \exp\left(\mathrm{i}\frac{\omega}{\omega_0^{(0)}}\tau\right) \times \psi_{\mathrm{n}}(\xi), \quad (15)$$

where

$$\mathrm{K}_{\overline{\mathrm{n}},\mathrm{m}}(\tau) = L_{\overline{\mathrm{n}},\mathrm{m}} \times \exp\left(\mathrm{i}\frac{\omega}{\omega_0^{(0)}}\tau\right).$$

Here $L_{\overline{\mathrm{n}},\mathrm{m}} = -\frac{2a\hbar\omega_0^{(0)}}{\mathrm{d}\mathrm{k_B T}}\rho_{\mathrm{pr},\overline{\mathrm{n}}}^{(0)}(\langle\xi_{\mathrm{n}}\rangle_0 - \xi_{\mathrm{n}}) \times \left(\frac{\partial\psi_{\mathrm{n}}(\xi)}{d\xi}|_{\xi=\frac{\mathrm{d}}{a}}\cdot(-1)^{\mathrm{m}} - \frac{\partial\psi_{\mathrm{n}}(\xi)}{d\xi}|_{\xi=0}\right)$.

Fourier image of the k-th order for dimensionless crystal potential $\mathfrak{I}_{(\mathrm{pr;A}),k} = \frac{2a}{\mathrm{d}}\int_0^{\mathrm{d}/a} w_{(\mathrm{pr;A})}(\xi)\cos\left(\frac{\pi k a}{\mathrm{d}}\xi\right)\mathrm{d}\xi$, depends on the type off unction $w_{(\mathrm{pr;A})}(\xi)$ and from the type of boundary conditions, superimposed on the movement of charges at the crystal boundaries (depending on the type of contact between the electrode and the polished surface of the sample). In the case of potential relief $\hat{\mathrm{W}}^{(0)}_{\mathrm{C},[\mathrm{H}^+]}(\mathrm{x})$ with potential pits parabolic shape $\breve{w}_{(\mathrm{pr;A}),\mathrm{j}}(\xi) = \frac{\breve{\mathrm{W}}^{(0)}_{(\mathrm{C};[\mathrm{H}^+]),\mathrm{j}}(\mathrm{x})}{\mathrm{U}_0} = \frac{4\left(\mathrm{x}-\breve{\mathrm{x}}_{\mathrm{j},0}\right)^2}{\delta_0^2}$ with blocked electrodes (when output operation relaxants (in HBCs, protons) reach infinitely large values $\mathrm{U}_{\max}\to\infty$. Therefore it is mathematically possible to move to a crystal potential model with infinitely highwalls (external boundaries), in the region of energies $E^{(0)}_{\mathrm{n}} > \mathrm{U}_0$ when $\breve{\mathrm{x}}_{\mathrm{j},0} = \breve{\mathrm{x}}_{1,0} + (\mathrm{j}-1)\delta_0$, $\breve{\mathrm{x}}_{1,0} = \frac{\delta_0}{2}$.

According to the results of the preliminary calculations, in (12) the main contribution to the sum and $\Xi_{(\mathrm{pr;A})}(k\pm\mathrm{m};\tau) = \mathrm{i}\chi\times\frac{1}{2}\sum_{k=0}^{\infty}\mathfrak{I}_{(\mathrm{pr;A}),k}\times\left(U_{\bar{\mathrm{n}},1}(k+\mathrm{m};\tau)+U_{\bar{\mathrm{n}},1}(k-\mathrm{m};\tau)\right)$ meaning parameter Fourier-image interactions $U_{\bar{\mathrm{n}},1}(k\pm\mathrm{m};\tau)$ contribute coefficients $\mathfrak{I}_{(pr;A),k}$ sequential number $k = 0$. For a more rigorous numerical investigation of this question it is clearly necessary, at the formal level, to take into account the Fourier-harmonic effects of $\mathfrak{I}_{(\mathrm{pr;A}),k}$, of all orders on $\Xi_{(\mathrm{pr;A})}(k\pm\mathrm{m};\tau)$. However, such a technique leads to an enormous complication of the mathematical model, which is reduced to the solution of a system of an unlimited number of differential equations of the form (12) and represents a separate problem. The result of solving this problem will have practically no effect on the physical content of the simplified version. In the given work, simplify this element to the form $\mathrm{i}\,\chi\mathfrak{I}_{(\mathrm{pr;A}),k}\times U_{\bar{\mathrm{n}},1}(k+\mathrm{m};\tau)$, where $\mathfrak{I}_{(\mathrm{pr;A}),0} = \frac{2\mathrm{N_W}\delta_0}{\mathrm{d}}$ [83]. Here $\mathrm{N_W}$—full quantity of the potential well in the model [83]. At the same time, Fourier coincidence $\mathfrak{I}_{(\mathrm{pr;A}),k}$ at $k = 0$ in energy regions $E^{(0)}_{\mathrm{n}} < \mathrm{U}_0$ and $\mathrm{U}_0 < E^{(0)}_{\mathrm{n}} < \mathrm{U}_{\max}$ indicates that there is no relation between the configuration of the energy spectrum of a particle and the properties of the potential field at the "zero" spatial Fourier-harmonic level [81].

The most important part of the model under study is to analyze the structure and develop methods for solutions of the quantum kinetic Equation (8) in the Fourier-image (12). In this connection study the properties of the element $F_{\mathrm{pr;m,n},\mathrm{f}_1,\mathrm{f}_2}$ and more specifically the main: $\mathrm{G}_{\mathrm{pr;m,n}} = \frac{2a}{\mathrm{d}}\int_0^{\frac{\mathrm{d}}{a}}\left[\hat{\rho}^{(0)}_{\mathrm{pr},\|}(\xi);\hat{\xi}\right]\psi_{\mathrm{n}}(\xi)\cos\left(\frac{\pi\mathrm{m}a}{\mathrm{d}}\xi\right)d\xi$, where, in order to simplify the calculation procedure commutator $\left[\hat{\rho}^{(0)}_{\mathrm{pr},\|}(\xi);\hat{\xi}\right]\psi_{\mathrm{n}}(\xi) = \hat{\rho}^{(0)}_{\mathrm{pr},\|}\left(\hat{\xi}\psi_{\mathrm{n}}(\xi)\right) - \hat{\xi}\hat{\rho}^{(0)}_{\mathrm{pr},\|,\mathrm{n}}\psi_{\mathrm{n}}(\xi)$ apply decomposition $\hat{\xi}\psi_{\mathrm{n}}(\xi) = \sum_{l\neq\mathrm{n}}a_l(n)\psi_l(\xi)$, where $a_l(\mathrm{n}) = \int_0^{\frac{\mathrm{d}}{a}}\psi_l^*(\xi)\hat{\xi}\psi_{\mathrm{n}}(\xi)\mathrm{d}\xi = \xi_{l\mathrm{n}}$, from the expression $\mathrm{G}_{\mathrm{pr;m,n}} = \mathrm{G}^{(1)}_{\mathrm{pr;m,n}} + \mathrm{G}^{(2)}_{\mathrm{pr;m,n}}$, at the $\mathrm{G}^{(1)}_{\mathrm{pr;m,n}} = \frac{2a}{\mathrm{d}}\sum_{l\neq\mathrm{n}}a_l(\mathrm{n})\hat{\rho}^{(0)}_{\mathrm{pr},\|,l}\int_0^{\frac{\mathrm{d}}{a}}\psi_l(\xi)\times\cos\left(\frac{\pi\mathrm{m}a}{\mathrm{d}}\xi\right)\mathrm{d}\xi$, $\mathrm{G}^{(2)}_{\mathrm{pr;m,n}} = \frac{2a}{\mathrm{d}}\rho^{(0)}_{\mathrm{pr},\|,\mathrm{n}}\int_0^{\frac{\mathrm{d}}{a}}\xi\psi_{\mathrm{n}}(\xi)\cos\left(\frac{\pi\mathrm{m}a}{\mathrm{d}}\xi\right)\mathrm{d}\xi$, where the wave functions $\psi_{\mathrm{n}}(\xi)$ are taken for a model of particle motion in a one-dimensional field a potential pit with spatial-periodic potential relief within the pit and infinitely high edge walls $\mathrm{U}_{\max}\to\infty$. Internal potential barriers and potential pits are taken by parabolic shape, a calculation quasi-discreet the energy spectrum of particles (protons) is performed for the blocking electrode model $\mathrm{U}_{\max}\to\infty$, when $\psi_{\mathrm{n}}(0) = 0$, $\psi_{\mathrm{n}}(0) = 0$, according to the scheme outlined in [8].

Thus, rewriting (12) with respecting the (15), we have

$$\frac{\partial U_{\bar{\mathrm{n}},1}(\mathrm{m};\tau)}{\partial\tau} + \mathrm{i}A_{\mathrm{n,m}}U_{\bar{\mathrm{n}},1}(\mathrm{m};\tau) + \mathrm{i}\left(F_{\mathrm{pr;m,n},\mathrm{f}_1,\mathrm{f}_2} - \phi\times L_{\bar{\mathrm{n}},\mathrm{m}}\right)\exp\left(\mathrm{i}\frac{\omega}{\omega_0^{(0)}}\tau\right) = 0. \qquad (16)$$

Here $A_{\mathrm{n,m}} = \phi\left(\frac{\pi\mathrm{m}a}{\mathrm{d}}\right)^2 - \zeta_{\mathrm{n}} + \frac{2\delta_0\mathrm{N_W}}{3\mathrm{d}}\chi$.

The solution of Equation (16), taking into account (13), gives

$$U_{\overline{n},1}(m;\tau) = \frac{\phi \times L_{\overline{n},m} - F_{pr;m,n,f_1,f_2}}{\frac{\omega}{\omega_0^{(0)}} + A_{n,m}} \left(\exp\left(i\frac{\omega}{\omega_0^{(0)}}\tau \right) - \exp(-iA_{n,m}\tau) \right). \quad (17)$$

Going back to the original $u_{\overline{n},1}(\xi;\tau) = \sum_{m=1}^{\infty} U_{\overline{n},1}(m;\tau) \times \cos\left(\frac{\pi m a}{d}\xi\right)$, assumptions in (5) taking into account and notation, we construct the desired scalar function $u_{\overline{n}}(\xi;\tau) = \varsigma_0 u_{\overline{n},1}(\xi;\tau)$ describing relaxation motion of protons with energies of the unperturbed spectrum $E_n^{(0)}$ [8] in crystal, perturbed by the electric field $E(x;t) = E_0 \exp(i\omega t)$ with blocking electrodes

$$u_{\overline{n}}(x;t) = W_{pol} \sum_{m=1}^{\infty} \frac{D_{\overline{n},m}}{1 + \frac{\omega}{\Omega_{n,m}}} \times \cos\left(\frac{\pi m x}{d}\right) \times (\exp(i\omega t) - \exp(-i\Omega_{n,m} t)). \quad (18)$$

In (18) the notations are taken as follows:

$$W_{pol} = qE_0 a,\ \omega_0^{(0)} = \frac{E_0^{(0)}}{\hbar},\ \Omega_{n,m} = \omega_0^{(0)} A_{n,m},\ A_{n,m} = \frac{\varepsilon_m^{(0)} - E_n^{(0)} + \Im_{(pr;A),0} U_0}{\hbar\omega_0^{(0)}},$$

$$\varepsilon_m^{(0)} = \frac{\hbar^2}{2m_p}\left(\frac{\pi m}{d}\right)^2,$$

$$D_{\overline{n},m} = \frac{\frac{W_{kin.}}{W_{therm}} \times (\langle \xi_n \rangle_0 - \xi_{\overline{n}}) \rho_{pr,\overline{n}}^{(0)} B_{n,m} - N_{pr,F}\left[Z_{pr}^{(0)}\right]^{-1} \rho_{pr,\perp,f_1,f_2}^{(0)} \times G_{pr;m,n}}{\hbar\omega_0^{(0)} A_{n,m}},$$

$$W_{kin.} = \frac{\hbar^2}{2m_p a^2},\ W_{therm.} = k_B T, B_{n,m} = \frac{2a}{d} \times \left(\frac{\partial\psi_n(\xi)}{d\xi}|_{\xi=0} - \frac{\partial\psi_n(\xi)}{d\xi}|_{\xi=\frac{d}{a}} (-1)^m \right).$$

2.5. Quantum Properties of Complex Dielectric Permittivity

Wave functions of mixed energy states of protons will be investigated

$$\Psi\left(\vec{r};t\right) = \sum_{\overline{n}} c_{\overline{n}}(t)\psi_{\overline{n}}(\vec{r}) = \sum_{n}\sum_{f_1,f_2} c_{n,f_1,f_2}(t)\psi_n(x)\psi_{f_1,f_2}(\vec{r}_\perp). \quad (19)$$

Expression (19) satisfies the normalization condition

$$\int_V \Psi^+\left(\vec{r};t\right)\Psi\left(\vec{r};t\right)dV = \sum_{\overline{n}} c_{\overline{n}}^+(t)c_{\overline{n}}(t) = N_{pr,F}.$$

On the basis of (19) the excess over the equilibrium concentration of relaxers (protons) in the crystal is calculated

$$\delta\hat{n}_{pr}\left(\vec{r};t\right) = \sum_{\overline{n}} \psi_{\overline{n}}^*\left(\vec{r}\right)\delta\hat{\rho}_{pr}\psi_{\overline{n}}\left(\vec{r}\right) = \sum_{n}\sum_{f_1,f_2} \psi_n^*(x)\psi_{f_1,f_2}^*(\vec{r}_\perp)u_{\overline{n}}(x;t)\psi_{f_1,f_2}(\vec{r}_\perp). \quad (20)$$

Proton subsystem polarization operator $\hat{P}\left(\vec{r};t\right) = q\vec{r} \times \delta\hat{n}_{pr}\left(\vec{r};t\right)$, subject to (20), takes the form $\hat{P}\left(\vec{r};t\right) = q\vec{r} \times \delta\hat{n}_{pr}\left(\vec{r};t\right) = q\sum_n \sum_{f_1,f_2} \psi_n^*(x)\psi_{f_1,f_2}^*(\vec{r}_\perp)\vec{r}\,u_{\overline{n}}(x;t)\psi_{f_1,f_2}(\vec{r}_\perp)$. Turning to one-dimensional model relaxation polarization in HBC (direction of vector macroscopic value

$$\vec{P}_x\left(\vec{r};t\right) = qx \times \delta\hat{n}_{pr}\left(\vec{r};t\right) = q\sum_{\overline{n}} \psi_{\overline{n}}^*\left(\vec{r}\right)x\delta\hat{\rho}_{pr}\psi_{\mathbf{n}}\left(\vec{r}\right) = q\sum_{n}\sum_{f_1,f_2} \psi_n^*(x)\psi_{f_1,f_2}^*(\vec{r}_\perp)xu_{\overline{n}}(x;t)\psi_{f_1,f_2}(\vec{r}_\perp).$$

Oriented parallel to crystalline axis, taken as axis OX, after complete quantum mechanical averaging $\langle\overline{P}\rangle \equiv Sp\left(\hat{\rho}_{pr} \times \hat{P}\right) = \int_V \Psi^+\left(\vec{r};t\right)\hat{P}_x\left(\vec{r};t\right)\Psi\left(\vec{r};t\right)dV$ [85] gives the expression:

$$\langle \overline{P} \rangle = q \sum_{n'} \sum_{f_1', f_2'} \sum_{n} \sum_{f_1, f_2} \rho_{pr,n',f_1',f_2'}(t)$$
$$\times \int_0^d \iint_S \psi^*_{n'}(x) \psi^*_{f_1',f_2'}\left(\vec{r}_\perp\right) \left(\psi^*_n(x) \psi^*_{f_1,f_2}(\vec{r}_\perp) \hat{x} u_{n,f_1,f_2}(x;t) \psi_{f_1,f_2}(\vec{r}_\perp)\right) \psi_{n'}(x) \psi_{f_1',f_2'}(\vec{r}_\perp) dS dx \quad (21)$$
$$= q \sum_{n'} \sum_{f_1',f_2'} \sum_{n} \sum_{f_1,f_2} \rho_{pr,n',f_1',f_2'}(t) \beta_{f_1,f_2 f_1',f_2'} \int_0^d \psi^*_{n'}(x) \left(\psi^*_n(x) \hat{x} u_{n,f_1,f_2}(x;t)\right) \psi_{n'}(x) dx,$$

where $\beta_{f_1,f_2 f_1',f_2'} = \iint_S \psi^*_{f_1',f_2'}(\vec{r}_\perp) \psi^*_{f_1,f_2}(\vec{r}_\perp) \psi_{f_1,f_2}(\vec{r}_\perp) \psi_{f_1',f_2'}(\vec{r}_\perp) dS$.

In (21) we pass to the quasi-classical formulation [79,81]

$$\Omega_{n,m} \to -i\Omega_{n,m}, \quad \Omega_{n,m} = \left| \frac{\varepsilon^{(0)}_m + \Im_{(pr;A),0} U_0 - E^{(0)}_n}{\hbar} \right|.$$

For times from the start of the polarization process, much longer than the relaxation time proton subsystem $T_{n,m} = \frac{1}{\Omega_{n,m}}$, taking $t \gg T_{n,m}$, from (18) we have

$$u^{(\omega)}_{n,f_1,f_2}(x;t) = E_0 \sum_{m=1}^{\infty} \frac{R_{n,f_1,f_2,m}}{1 + i\frac{\omega}{\Omega_{n,m}}} \times \cos\left(\frac{\pi m x}{d}\right) \times \exp(i\omega t). \quad (22)$$

Here $R_{n,f_1,f_2,m} = qaD_{n,f_1,f_2,m}$.

In (22), we take the unsteady density matrix of the proton subsystem (13) as $\rho_{pr,n',f_1',f_2'}(t) \cong \rho^{(\omega)}_{pr,n',f_1',f_2'}(t) \approx \rho^{(0)}_{pr,n',f_1',f_2'} \times \left(1 - \frac{qE_0 a}{k_B T}(\langle \xi_n \rangle_0 - \xi_n) \times \exp(i\omega t)\right)$.

In (22), transform the relaxation time for the n-th stationary state and the m-th the spatial Fourier-harmonic polarization $T_{n,m} = \frac{\hbar}{\Delta \varepsilon_{n,m}} \hbar \left[\varepsilon^{(0)}_m - E^{(0)}_n + \frac{2\delta_0 N_w U_0}{3d}\right]^{-1}$ like the expression $T_{n,m} = \frac{T_{n,m,spectral}}{\frac{T_{n,m,spectral}}{T_{structure}}+1} \frac{T_{structure}}{\frac{T_{structure}}{T_{n,m,spectral}}+1}$ and further, subject to an additional condition $\frac{\Phi(n)}{m^2} \ll 1$, where $\Phi(n) = \frac{\sqrt{2m_p E^{(0)}_n} d}{\hbar \pi}$, taking $T_{n,m,spectral} \approx \frac{T_{0,spectral}}{m^2}$, go to an approximate (essentially quasi-classical) expression $T_{n,m} \approx T_m = \frac{T_{0,spectral}}{\frac{T_{0,spectral}}{T_{structure}}+m^2}$, where $T_{0,spectral} = \frac{2m_p d^2}{\hbar \pi^2}$, $T_{structure} = \frac{3d\hbar}{2\delta_0 N_w U_0}$.

Restricting ourselves to the linear approximation of perturbation theory by a small parameter $\varsigma_0 = \frac{qE_0 a}{\hbar \omega^{(0)}_0} \ll 1$, Expression (21) transform to a form convenient for comparing the results of theoretical and experimental studies [83,84,86]

$$P^{(\omega)}(t) = \varepsilon_0 \varepsilon_\infty E_0 \times \exp(i\omega t) \times \Xi^{(\omega)}(T) \quad (23)$$

where ε_∞—high-frequency permittivity of the crystal [83,84].

In (23) the dimensionless complex relaxation parameter quantum mechanical model $\Xi^{(\omega)}(T) = \Xi^{(\omega)}_1(T) - i\Xi^{(\omega)}_2(T)$ formally similar related dimensionless complex relaxation parameter of the quasi-classical proton-proton model of relaxation polarization $\Gamma^{(\omega)}(T) = \Gamma^{(\omega)}_1(T) - i\Gamma^{(\omega)}_2(T)$ [87], with the difference that the components of the parameter $\Xi^{(\omega)}(T)$ are somewhat more complex, compared to $\Gamma^{(\omega)}(T)$ [87] in terms of the structure of the common terms of the corresponding power series

$$\Xi^{(\omega)}_1(T) = \frac{8}{\pi^2} \sum_{m=1}^{\infty} \frac{\sin^2\left(\frac{\pi m}{2}\right) \times \frac{T_m}{T_Q}}{m^4(1 + \omega^2 T^2_m)}, \quad \Xi^{(\omega)}_2(T) = \frac{8}{\pi^2} \sum_{m=1}^{\infty} \frac{\sin^2\left(\frac{\pi m}{2}\right) \times \frac{\omega T^2_m}{T_Q}}{m^4(1 + \omega^2 T^2_m)}. \quad (24)$$

In (24) the characteristic for the quantum mechanical model relaxation time is introduced for the proton subsystem in HBC $T_Q(T) = \frac{\pi^2 \varepsilon_0 \varepsilon_\infty \hbar}{d^2 q^2 N^{(0)}_{pr}(T)}$, formally similar to Maxwell's relaxation time in the quasi-classical model [83,84], but, differing from [34] more a sophisti-

cated formula for the quantum concentration of particles (protons) $N_{pr}^{(0)}(T) = \sum_n N(T;n)$, where

$$N(T;n) = N_{pr,F}\left[Z_{pr}^{(0)}\right]^{-1}\psi_n\left(\tfrac{1}{2}\right)\rho_{pr,\|,n}^{(0)}(T) \times \sum_{n'}\sum_{f_1',f_2'}\sum_{f_1,f_2}\rho_{pr,n',f_1',f_2'}^{(0)}(T)\times\left|\alpha_{n,n'}^{(0)}\right|\beta_{f_1,f_2f_1',f_2'} \times \rho_{pr,\perp,f_1,f_2},$$
$$\alpha_{n,n'}^{(0)} = \int_0^d \psi_{n'}^*(x)\psi_n^*(x)x\psi_{n'}(x)dx.$$

A detailed investigation of properties of parameters (24) in terms of the influence of temperature and field frequency on their numerical values should, as in [83,84], be carried out by similar methods of converting power series to analytical form in the form of transcendental expressions [87], convenient for numerical calculations, which is quite an actual applied theoretical problem, the solution of which is a subject of a separate paper.

Based on from equalities $P^{(\omega)}(t) = \varepsilon_0\varepsilon_\infty E(t) \times \Xi^{(\omega)}(T)$, $P^{(\omega)}(t) = \varepsilon_0\left(\hat{\varepsilon}^{(\omega)} - \varepsilon_\infty\right)E(t)$ [83,87], expression can be written for the complex dielectric permittivity (CDP)

$$\hat{\varepsilon}^{(\omega)} = \varepsilon_\infty\left(1 + \Xi^{(\omega)}(T)\right) = \varepsilon_\infty\left(1 + \Xi_1^{(\omega)}(T) - i\Xi_2^{(\omega)}(T)\right). \quad (25)$$

Based on (25), we write the spectral expressions for the CDP components

$$\mathrm{Im}\left[\hat{\varepsilon}^{(\omega)}\right] = \varepsilon_\infty\Xi_2^{(\omega)}(T),\ \mathrm{Re}\left[\hat{\varepsilon}^{(\omega)}\right] = \varepsilon_\infty\left(1 + \Xi_1^{(\omega)}(T)\right). \quad (26)$$

Expression (26) are linear approximations calculated from the small dimensionless parameter external perturbation $\varsigma_0 \approx \frac{qE_0a}{\hbar\nu_0} \ll 1$ from solution of the quantum kinetic equation of the model (5) functional dependence on the circular frequency of the alternating polarizing field and temperature.

The frequency-invariant temperature dependences (26) should be investigated together with (24) according to the schemes outlined in [83,84].

The accuracy of the calculation results of Equation (25) will be assessed by comparing the theoretical values of the dissipation factor calculated without taking into account conduction $tg\delta_{th}(\omega;T;\zeta_0) \approx \frac{\mathrm{Im}\left[\hat{\varepsilon}^{(\omega)}(T;\zeta_{0,th})\right]}{\mathrm{Re}\left[\hat{\varepsilon}^{(\omega)}(T;\zeta_{0,th})\right]}$ [87], taking into account Equation (26):

$$tg\delta_{th}(\omega;T;\zeta_{0,th}) = \frac{\Xi_2^{(\omega)}(T;\zeta_{0,th})}{1 + \Xi_1^{(\omega)}(T;\zeta_{0,th})}. \quad (27)$$

With spectrum measurement data $tg\delta_{exp}(\omega;T;\zeta_{0,exp}) \approx \frac{\mathrm{Im}\left[\hat{C}^{(\omega)}(T;\zeta_{0,exp})\right]}{\mathrm{Re}\left[\hat{C}^{(\omega)}(T;\zeta_{0,exp})\right]}$, in which the complex capacitance of the sample (dielectric) is calculated using the experimental procedure set in [33]. The characteristic parameter sets $\zeta_{0,th} = \{a_{th};\delta_{0,th};U_{0,th};v_{0,th};n_{0,th}\}$ and $\zeta_{0,exp} = \{a_{exp};\delta_{0,exp};U_{0,exp};v_{0,exp};n_{0,exp}\}$ are calculated at the temperatures respectively the calculated maximum $T_{max,th}$ and the maximum $T_{max,exp}$, measured in an experiment using the method, as presented [80]. Similar calculations for the quantum model of proton-relaxation polarization in HBC were performed in [79], but from the numerical solution of the kinetic equation (4), and in the case, a transition to the level of more rigorous analytical solutions (4), performed taking into account statistical corrections reflected in the quantum canonical Gibbs distribution (3) and in the structure of the degenerate discrete energy spectrum of protons in HBC.

3. Results

For modern microelectronics and computer technology, a topical, practically important scientific problem is comprehensive, based on precision measurements and mathematically rigorous calculations, study of the effects of the nanocrystalline state (1–10 nm) of solid-state materials at different values of the parameters of external force fields, mechanical stresses, and temperatures [1,14,81,85].

In this paper, we studied the influence of the thickness of the crystalline layer d on the parameters of the theoretical temperature spectra of the dielectric loss tangent $tg\delta_{th}(T)$ in dielectrics of the HBC class.

Numerical studies of the temperature dependences $tg\delta_{th}(T)$ were carried out using Formulas (26) and (27). The estimation of the numerical values of the parameters of the relaxers was carried out by minimizing the comparison function (MCF-method) [80], by comparing the theoretically calculated graphs $tg\delta_{th}^{(\nu)}(T)$ and the experimentally measured spectra $tg\delta_{exp}^{(\nu)}(T)$ in the vicinity of the temperatures of the experimental maxima $T_{max,exp}$ in onot talc $Mg_3(Si_4O_{10})\cdot(OH)_2$ and gypsumin $CaSO_4\cdot0.5H_2O$ in the temperature range of 50–450 K, at an alternating field frequency of $\nu = 7 \times 10^6$ Hz [82,90].

According to the results presented in [90], in the temperature spectra $tg\delta_{exp}^{(\nu)}(T)$ of onot talc $Mg_3(Si_4O_{10})\cdot(OH)_2$, measured at the calcination temperature $T_{ac} = 1023$ K, at the field frequency $\nu = 7$ MHz, maxima were found at temperatures: 160 K, 220 K, 265 K, 310 K. For gypsum $CaSO_4\cdot0.5H_2O$, at the calcination temperature $T_{ac} = 393$ K and field frequency $\nu = 7$ MHz: 145 K, 210 K, 270 K, 320 K [82,90]. The thickness of the experimental sample in [90] was taken to be 30 μm. The low-temperature maxima in the spectra $tg\delta_{exp}^{(\nu)}(T)$ could not be measured in [90].

Numerical calculation of theoretical graphs of $tg\delta_{th}^{(\nu)}(T))$ was carried out using the Expression (27) in complex with the Expression (24) on a set of points of the continuum measure in the vicinity of the temperatures of the corresponding experimental maxima of the $tg\delta_{exp}^{(\nu)}(T)$ spectrum measured in [90]. The MCF-method [80] was used in the calculation. During the calculation, the activation energies U_0 were calculated for each type of relaxers. The results of the calculations are well consistent with the experiment within the measurement error [82,90]. In terms of visual graphic interpretation of numerical results, there is a small inconvenience connected with small values of amplitudes of theoretical low-temperature maxima $tg\delta_{th}^{(\nu)}(T) \sim (0.2 \div 0.3) \times 10^{-4}$, against the background of amplitudes of high-temperature maxima of $tg\delta_{th}^{(\nu)}(T) \sim (2.0 \div 4.5) \times 10^{-3}$. Note that in [90] in the region of low temperatures (50–100 K), where the measurement error increases sharply due to the low resolution of the measuring circuit, the maximum in the spectra $tg\delta_{exp}^{(\nu)}(T)$ could not be detected.

According to the methodology described in [90], using an improved measuring cell in the experimental installation [91], we measured the experimental spectrum of $tg\delta_{exp}^{(\nu)}(T)$ in gypsum and talc crystals under external conditions coinciding with [90]. Crystal calcination temperatures are taken to be lower than in [90] and equal to $T_{ac} = 923$ for $Mg_3(Si_4O_{10})\cdot(OH)_2$ and $T_{ac} = 293$ for $CaSO_4\cdot0.5H_2O$. Reduction of temperatures of calcination of samples was accepted for the purpose of increase in concentration of molecules of crystallization water and, according to amplitudes of maxima of in the experimental spectra $tg\delta_{exp}^{(\nu)}(T)$, as well as to test the effects of proton concentrations on the amplitude of the low-temperature theoretical maximum $tg\delta_{th}^{(\nu)}(T)$. As a result, the amplitudes of high-temperature experimental maxima are insignificant, but increased for talc crystals, more so for gypsum (this is evident from the comparison of experimental spectra 1 of Figures 1 and 2 of this work and, accordingly, experimental spectra 1 of Figure 28 and Figure 29 in [90]). Theoretical amplitudes of low-temperature maxima (see dashed lines 6 of drawings 1.2 given works), at the same time, increase up to $tg\delta_{th}^{(\nu)}(T) \sim (0.5 \div 0.9) \times 10^{-4}$ (at temperatures of calcination of crystals of $T_{ac} = 923$ K and $T_{ac} = 293$) against $tg\delta_{th}^{(\nu)}(T) \sim (0.2 \div 0.3) \times 10^{-4}$ (at temperatures of calcination of crystals of $T_{ac} = 1023$ K and $T_{ac} = 393$ K). The received regularities indicate increase in concentration of molecules of crystallizational water, as at most at a temperature of 210 K for $CaSO_4\cdot0.5H_2O$ increased from 3.9×10^{-3} at $T_{ac} = 393$ K to 4.3×10^{-3} at $T_{ac} = 293$ K. For $Mg_3(Si_4O_{10})\cdot(OH)_2$ at 220 K temperature, this effect manifests itself to a lesser extent, indicating a weaker sensitivity of talc to calcination than that of gypsum. The physical nature of the maxima at 210 K in gypsum and 220 K in talc

will be justified below in Tables 1 and 2, but the fact that it is bound to the crystallization water molecules is evident already at this stage of the study. The increase in theoretical maximum amplitudes from 0.3 $\times 10^{-4}$ (T_{ac} = 393 K) at 97 K in gypsum and from 0.2 $\times 10^{-4}$ (T_{ac} = 1023 K) to 0.5 $\times$ 10^{-4} (T_{ac} = 923 K) at 105 K in talc clearly indicate an increase in proton concentrations in the crystal as the calcination temperature decreases.

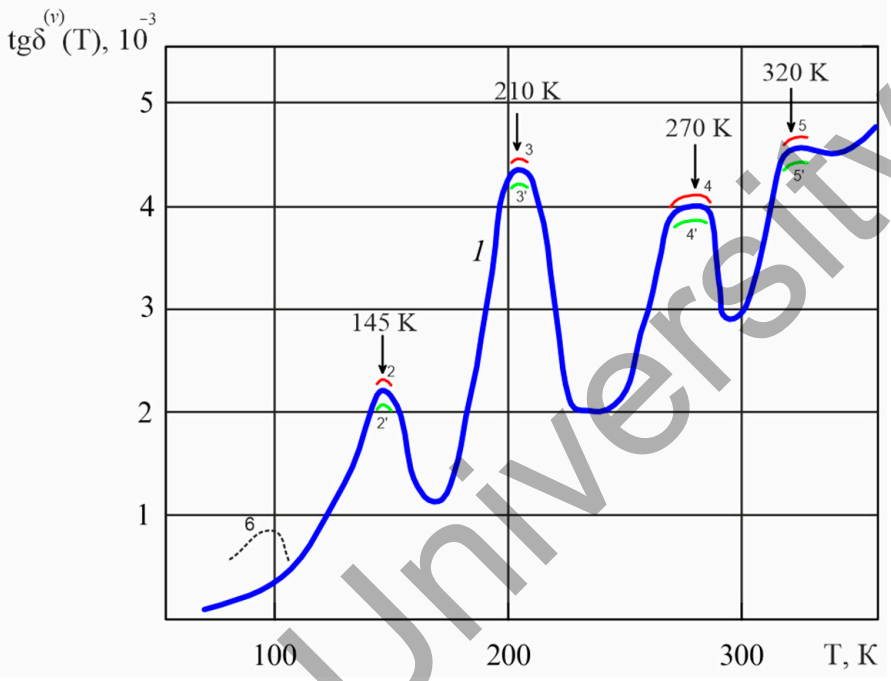

Figure 1. Temperature spectra $tg\delta^{(\nu)}(T)$ in gypsum $CaSO_4 \cdot 0.5H_2O$.

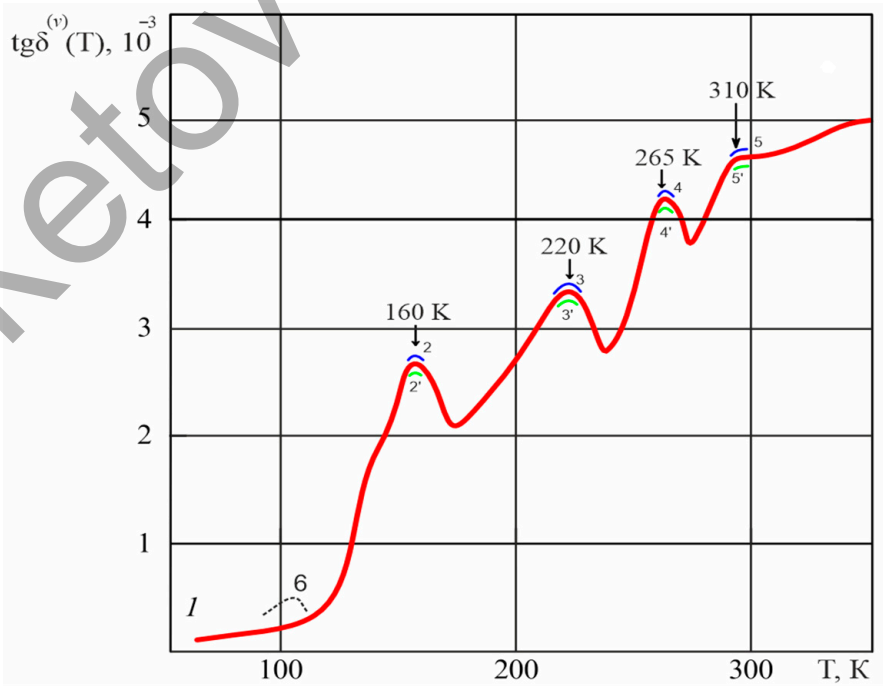

Figure 2. Temperature spectra $tg\delta^{(\nu)}(T)$ of onot talc $Mg_3Si_4O_{10} \cdot (OH)_2$.

Table 1. Energy activation of relaxers in gypsum $CaSO_4 \cdot 0.5H_2O$, calculated using the quasi-classical and quantum-mechanical models of dielectric losses.

Parameters of Experimental Maximum of $tg\delta_{exp}^{(\nu)}(T)$, Measured at Crystal Calcinating Temperature T_{ac}=293 K		Energy Activation U_0, eV		
			Theoretical	
Temperature, K	Amplitude, 10^{-3}	Experimental	Quasi-Classical Model ($tg\delta_{th}^{(\nu)}(T)$ Calculated upon Based the Expressions (38) from [75])	Quantum-Mechanical Model ($tg\delta_{th}^{(\nu)}(T)$ Calculated upon Based the Expression (27))
145	2.2	0.10 ± 0.02	0.13	0.12
210	4.3	0.20 ± 0.05	0.22	0.19
270	4.1	0.45 ± 0.07	0.49	0.45
320	4.5	0.6 ± 0.2	0.8	0.7

Table 2. Energy activation of relaxers in natural mineral of onot talc $Mg_3(Si_4O_{10})(OH)_2$, calculated using the quasi-classical and quantum-mechanical models of dielectric losses.

Parameters of Experimental Maximum of $tg\delta_{exp}^{(\nu)}(T)$, Measured at Crystal Calcinating Temperature T_{ac}=923 K		Energy Activation U_0, eV		
			Theoretical	
Temperature, K	Amplitude, 10^{-3}	Experimental	Quasi-Classical Model ($tg\delta_{th}^{(\nu)}(T)$ Calculated upon Based the Expressions (38) from [75])	Quantum-Mechanical Model ($tg\delta_{th}^{(\nu)}(T)$ Calculated upon Based the Expression (27))
160	2.6	0.09 ± 0.02 (0.09 ± 0.02 in [78])	0.13	0.10
220	3.3	0.2 ± 0.02 (0.19 ± 0.02 in [78])	0.22	0.21
265	4.2	0.33 ± 0.04 (0.32 ± 0.04 in [78])	0.35	0.33
310	4.5	0.43 ± 0.04 (0.41 ± 0.04 in [78])	0.46	0.44

The coincidence of the temperature positions of maxima from experimental spectra 1 of Figures 1 and 2 with the corresponding temperatures of experimental spectra 1 of Figure 28 and Figure 29 of [90] indicates a weak influence of the calcination temperature of the crystal on the structure and properties of the dielectric loss spectrum in it over the entire range of experimental temperatures.

The actual numerical value of the amplitude of the calculated low-temperature "peak" is more than an order of magnitude lower than the following "peak" in the $tg\delta_{th}^{(\nu)}(T)$ spectrum. For the convenience of visual perception, we depicted theoretical maxima in Figures 1 and 2 with dotted lines at their design temperatures with conditional amplitudes an order of magnitude higher than calculated ones.

Based the Expressions (24) and (27), in combination with the MCF method [80], we calculated the activation energy $U_{0,th} = 0.05$ eV for the low-temperature theoretical maxima in gypsum at $T_{max,th} = 97$ K, $tg\delta_{th}^{(\nu)}(T_{max,th}) \approx 0.9 \times 10^{-4}$. For onot talc at $T_{max,th} = 105$ K, $tg\delta(\nu, T_{max}) \approx 0.5 \times 10^{-4}$ we have $U_{0,th} = 0.045$ eV. Small calculated energies of activation

of low-temperature relaxers indicate a quantum mechanism of proton motion in the HBC in the temperature region T < 100 K.

1—the experimental spectrum $tg\delta_{exp}^{(\nu)}(T)$, measured at calcination temperature T_{ac} = 293 K and field frequency $\nu = 7 \times 10^6$ Hz: 145 K, 210 K, 270 K, 320 K; 2-5, 2′-5′—theoretical high-temperature plots of the $tg\delta_{th}^{(\nu)}(T)$, calculated respectively from the quantum mechanical model (Expression (27) in this article) and from the quasi-classical model (using Expressions (38) of [75]) in complex with the MCF method [80] in the vicinity of the temperatures of the corresponding experimental maxima; 6—theoretical low-temperature graph of $tg\delta_{th}^{(\nu)}(T)$ calculated using Expression (27) only in this article.

It should be noted that the calculated theoretical high-temperature graphs made according to the quasi-classical model (using the Expressions (38) of [75]) $tg\delta_{th}^{(\nu)}(T) = \frac{\Gamma_2^{(\omega)}(T;\zeta_{0,th})}{1-\Gamma_1^{(\omega)}(T;\zeta_{0,th})}$ turn out to be slightly lower in amplitude compared to the same graphs calculated according to the quantum-mechanical model (Expression (27) in this article).

The calculated theoretical low-temperature graph from the quasi-classical model cannot be constructed due to insufficient initial data in the Expressions (38) of [75]. The quantum mechanical model, according to Expression (27) in this article, is quite suitable for calculating the theoretical low-temperature graph of the $tg\delta_{th}^{(\nu)}(T)$ shown in Figures 1 and 2 of the dotted lines. Moreover, the range of temperature values permissible in Expression (27) is wider than in the case of high-temperature graphs. All these circumstances again indicate the specific quantum nature of proton relaxation in the HBC in the temperature region T < 100 K.

Experimental spectrum $tg\delta_{exp}^{(\nu)}(T)$ measured at calcination temperature T_{ac} = 923 K and field frequency $\nu = 7 \times 10^6$ Hz: 160 K, 220 K, 265 K, 310 K; 2-5, 2′-5′—theoretical high-temperature plots of $tg\delta_{th}^{(\nu)}(T)$ calculated respectively from the quantum mechanical model (Expression (27) in this article) and from the quasi-classical model (using the Expressions (38) of [75]) in complex with the MCF method [80] in the vicinity of the temperatures of the corresponding experimental maxima; 6—theoretical low-temperature graph $tg\delta_{th}^{(\nu)}(T)$ calculated using Expression (27) only in this article.

Tables 1 and 2, according to Figures 1 and 2, show the results of estimating numerical experimental and theoretical values of activation energies for each type of relaxers in gypsum and Onot talc crystals. Theoretical calculations of activation energies were carried out using the MCF-method [80] according to two schemes: using the quasi-classical model, where $tg\delta_{th}^{(\nu)}(T)$ calculated upon based the Expressions (38) from [75]; using the quantum-mechanical model, where $tg\delta_{th}^{(\nu)}(T)$ calculated upon based the Expressions (24) and (27).

From a comparison of experimental values of U_0 activation energies (Table 2) and temperature positions of maxima in the experimental $tg\delta_{exp}^{(\nu)}(T)$ spectrum (Figure 2) and in the experimental TSDC of onot talc density spectrum (Table 2 on page 13 in [78]; Figure 2 on page 15 in [78] or Table A1 and Figures A3 and A4 in Appendix B) it can be argued that the first maximum (160 K) is due to the movement of ionization defects H_3O^+, the second maximum (220 K) is due to the relaxation of the dipoles of crystallization water, the third maximum (265 K) is due to the relaxation of ionization defects OH^-, and the fourth maximum (310 K) is due to the migration of complexes VL, VD. Activation energies calculated by theoretical methods fall within the confidence interval of measured values (Table 2 in this article). At the same time, it can be seen that the quantum mechanical method (upon based the Expressions (24) and (27)) versus the quasi-classical method (upon based the Expressions (38) from [75]) gives numerical activation energies closer to experimental ones over the entire temperature range of the measured $tg\delta_{exp}^{(\nu)}(T)$ spectrum. Thus, here we confirm, as in [78], the statement that quantum tunneling of protons continues to affect dielectric relaxation in HBC both at the microscopic level (in terms of proton transitions between potential wells [75,78]) and at the macroscopic level (in terms of proton relaxation kinetics in the crystal sample space). In addition, the experimental activation

energies themselves measured from the $tg\delta_{exp}^{(\nu)}(T)$ (Table 2) and TSDC spectra (Table A1 in Appendix B) are practically the same.

The absence on the experimental spectrum of $tg\delta_{exp}^{(\nu)}(T)$ maximum associated with the relaxation of the dipoles of adsorbed water (maximum at 206 K in the TSDC talc spectrum [78]) is due to the fact that before measurement the samples were freed from adsorbed moisture by calcination. The dielectric relaxation of the volume charge did not appear in the $ttg\delta_{exp}^{(\nu)}(T)$ spectra due to significant loss of electrical conductivity.

Similar patterns of dielectric loss processes appear when evaluating and comparing numerical experimental and theoretical values of activation energies for each type of relaxers in gypsum crystals (Table 2). TSDC spectra in gypsum, at this point in time, have not yet been measured.

The parameters of the theoretical spectrum of $tg\delta_{th}^{(\nu)}(T)$ and the quantum properties of dielectric losses in gypsum crystals appear, as in talc.

The processes of proton-relaxation polarization in the region of low temperature (50–100 K) significantly depend on the dimensional characteristics of the crystal (thickness of the experimental sample) [83]. In [83] examined the effects of crystal layer thicknesses on the parameters (temperature positions and amplitudes) of theoretical TSDC density maxima in HBC. It has been found that as the crystal size decreases from 30 μm to 3 nm, the theoretical low-temperature maximum (50–100 K) of the TSDC-density spectrum shifts towards helium temperatures (4–25 K) and increases in amplitude by 3–4 orders of magnitude. The determining role in these effects is given to quantum tunneling of protons inside nanoscale clusters (1–10 nm), acting as centers for localization of the proton-relaxation process, realized as a result of quantum transitions of protons through potential barriers with a height of about 0.01–0.03 eV (versus 0.05–0.1 eV at 1–10 μm) with a quantum distribution of protons over energy levels degenerate energy spectrum [81,85]. Under such conditions, the steady-state statistically averaged probability of proton tunneling inside on-no-clusters reaches 0.3–0.5 even at temperatures of 1–10 K, which is very severe for such a heavy particle as a proton. According to the results of statistical analysis, in the crystal structure of the HBC, the Fermi temperature of the proton ensemble tends to zero (due to low equilibrium concentrations of protons in the HBC and a large proton mass compared to the electron [78]) and the proton gas remains non-degenerate near the absolute zero temperature [78,85]. Then, a non-propagated proton gas is described by the quantum canonical Gibbs distribution for protons with a degenerate (due to the strong interaction of the proton with the environment) discrete energy spectrum [81,85]. This will be discussed in more detail in the Discussion section below.

We have considered transformations of theoretical low-temperature $tg\delta_{th}^{(\nu)}(T)$ plots with variation of theoretical thickness HBC from 30 μm to 3 nm. The calculation was performed using the Expressions (24) and (27) using the MCF-method [80].

According to Tables 3 and 4, a reduction in the crystal thickness from 30 μm to 3 nm leads to a shift in the first theoretical maximum $tg\delta_{th}^{(\nu)}(T)$ in onot talc from low (105 K) to ultra-low temperatures (22 K), while the amplitude of the maximum decreases from 0.5×10^{-4} to 0.39×10^{-8}. In gypsum, the maximum of $tg\delta_{th}^{(\nu)}(T)$ shifts from 97 K to 15 K with a decrease in amplitude from 0.9×10^{-4} to 0.86×10^{-8}. Thus, in HBC, the amplitudes of the low-temperature maxima of the dielectric loss tangent $tg\delta_{th}^{(\nu)}(T)$ decrease by four orders of magnitude with a shift of 80–100 K toward ultra-low temperatures (4–25 K) with a reduction in the thickness of the crystalline layer from 30 μm to 3 nm.

Table 3. Temperature maxima of the dielectric loss tangent in gypsum, calculated at a frequency of the polarizing field $\nu = 7 \times 10^6$ Hz, for different thicknesses of crystalline layers.

Layer Thickness, nm	Amplitudes and Temperature Positions of Theoretical Maxima of $tg\delta_{th}^{(\nu)}(T_{max})$				
30,000	0.9×10^{-4} (97)	2.2×10^{-3} (145)	4.3×10^{-3} (210)	4.1×10^{-3} (270)	4.5×10^{-3} (320)
3000	0.3×10^{-4} (89)	1.3×10^{-3} (142)	3.3×10^{-3} (209)	3.3×10^{-3} (270)	4.1×10^{-3} (320)
300	0.1×10^{-4} (80)	0.4×10^{-3} (138)	2.9×10^{-3} (200)	3.3×10^{-3} (270)	4.1×10^{-3} (320)
30	1.6×10^{-6} (47)	7.4×10^{-6} (130)	1.6×10^{-6} (190)	3.2×10^{-3} (267)	4.1×10^{-3} (320)
3	0.86×10^{-8} (15)	3.4×10^{-7} (102)	5.1×10^{-2} (183)	2.9×10^{-3} (264)	3.5×10^{-3} (317)

Table 4. Temperature maxima of the dielectric loss tangent in onot talc, calculated at a frequency of the polarizing field $\nu = 7 \times 10^6$ Hz, for different thicknesses of the crystalline layers.

Layer Thickness, nm	Amplitudes and Temperature Positions of Theoretical Maxima of $tg\delta_{th}^{(\nu)}(T_{max})$				
30,000	0.5×10^{-4} (105)	2.6×10^{-3} (160)	3.3×10^{-3} (220)	4.2×10^{-3} (265)	4.5×10^{-3} (310)
3000	0.4×10^{-4} (96)	2.2×10^{-3} (157)	2.14×10^{-3} (219)	4.25×10^{-3} (265)	4.5×10^{-3} (310)
300	0.3×10^{-4} (88)	2.4×10^{-3} (146)	1.17×10^{-3} (215)	4.25×10^{-3} (265)	4.5×10^{-3} (310)
30	4.6×10^{-6} (50)	6.8×10^{-6} (127)	1.05×10^{-3} (207)	4.25×10^{-3} (265)	4.5×10^{-3} (310)
3	0.39×10^{-8} (22)	5.8×10^{-7} (103)	0.54×10^{-3} (190)	3.3×10^{-3} (259)	4.4×10^{-3} (308)

The "second" maximum in onot talc $(160\ K;\ 2.6 \times 10^{-3})$ measured at 30 μm shifts to $(103\ K;\ 5.8 \times 10^{-7})$ at 3 nm. In gypsum, respectively, the maximum $(145\ K;\ 2.2 \times 10^{-3})$ measured at 30 μm shifts to $(102\ K;\ 3.4 \times 10^{-7})$ at 3 nm. Thus, in HBC, there is a decrease in the amplitudes of the "second" maxima of the dielectric loss tangent $tg\delta_{th}^{(\nu)}(T)$ by three to four orders of magnitude with a shift of 40–60 K towards low temperatures (70–105 K) with a reduction in the thickness of the crystalline layer from 30 mm to 3 nm.

The third, fourth, and fifth maxima $tg\delta_{th}^{(\nu)}(T)$ exhibit size effects to a lesser extent, with an increase in the temperatures of the experimental maxima $tg\delta_{exp}^{(\nu)}(T)$, so that for the last maximum (in talc 310 K; in gypsum 320 K) this effect is practically absent (Tables 3 and 4).

4. Discussion

For a detailed comparison of the properties of the semiclassical [83,85] more rigorous quantum mechanical (explored in Section 2 of this work) models of tunneling proton relaxation in HBC, we consider important fundamental mathematical expressions that follow from the semiclassical model and, reflecting, onot a sufficiently high analytical level, the value of quantum tunneling during proton relaxation in solid dielectrics.

The quantum-mechanical model of proton relaxation in HBC developed in this article is based on a rigorous solution of the quantum kinetic Equation (8) for theoretical estimates of the influence of quantum effects (proton tunneling) on the values of the dielectric loss tangent (27) in a wide temperature range (1–1500 K) and the thickness of the

crystalline layer (1–10,000 nm). The relaxation coefficients (24) in the formulas for the complex dielectric permittivity (26) do not explicitly contain expressions for the statistically averaged energy levels $E_{\mathrm{n}}^{(0)}$) of relaxers (protons) of the potential barrier transparency, which does not allow, in contrast to from the semiclassical quantum model of proton relaxation [83,86,87], to reveal at the theoretical level, the influence of microscopic mechanisms of quantum transitions of protons on the parameters of the temperature-frequency spectra of dielectric losses. In this case, the characteristic relaxation time of protons calculated above in a rigorous quantum model $T_Q(\mathrm{T}) = \frac{\pi^2 \varepsilon_0 \varepsilon_\infty \hbar}{\mathrm{d}^2 q^2 \mathrm{N}_{\mathrm{pr}}^{(0)}(\mathrm{T})}$ is determined by the equilibrium (notdepending on the parameters of the external perturbation) by the quantum-mechanical proton concentration $\mathrm{N}_{\mathrm{pr}}^{(0)}(\mathrm{T})$, which explicitly depends on the crystal temperature. The statistically averaged quantum transparency of the potential barrier unperturbed by the field is hidden in the formula for energy levels $E_{\mathrm{n}}^{(0)}$, which determines the value $\mathrm{N}_{\mathrm{pr}}^{(0)}(\mathrm{T})$ and, accordingly, the relaxation time $T_Q(\mathrm{T})$, as more stringent, in comparison with semiclassical expressions [83,86,87], functions of the parameters of the potential field of the crystal lattice. This is the advantage of the quantum mechanical model. In the semiclassical model [83,86,87], $T_Q(\mathrm{T})$ is the Maxwellian relaxation time $T_{\mathrm{M}}(\mathrm{T}) = \frac{\varepsilon_0 \varepsilon_\infty}{q n_0 \mu_{mob}^{q.-classic;(1)}(\mathrm{T})}$, in which the equilibrium concentration of protons n_0 is defined as a numerical constant of the model and does not explicitly depend on the crystal temperature. The presence in the function $T_{\mathrm{M}}(\mathrm{T})$ of the proton mobility coefficient $\mu_{mob}^{q.-classic;(1)}(\mathrm{T}) = \frac{qW^{q.-classic;(1)}(\mathrm{T})}{\mathrm{k_B T}}$ calculated in the linear approximation with respect to the small dimensionless perturbation parameter $\zeta_{q.-class.}(t) = \frac{q\mathrm{E}(t)a}{2\mathrm{k_B T}} < 1$), when calculating quasi-classical kinetic coefficients [83,87]:

$$\begin{aligned} W^{q.-classic;(\pm)}(\mathrm{T}) &= \frac{\nu_0}{2} \\ &\times (\exp(-\mathrm{X})\exp\left(\mp\zeta_{q.-class.}(\mathrm{t})\right) \\ &+ \frac{\exp(-\Lambda)\exp\left(\mp\eta_{q.-class.}(\mathrm{t})\right) - \exp(-\mathrm{X})\exp\left(\mp\zeta_{q.-class.}(\mathrm{t})\right)}{1-\frac{\Lambda}{\mathrm{X}}}\Bigg) \\ &= \sum_{l=0}^{\infty} \frac{(\mp 1)^l}{l!} W^{q.-classic;(l)}(\mathrm{T}) \times \zeta_{q.-class.}^{l}(\mathrm{t}), \\ W^{q.-classic;(l)}(\mathrm{T}) &= \frac{\nu_0}{2} \times \left(\exp(-\mathrm{X}) + \frac{\left(\frac{\Lambda}{\mathrm{X}}\right)^l \exp(-\Lambda) - \exp(-\mathrm{X})}{1-\frac{\Lambda}{\mathrm{X}}}\right). \end{aligned}$$

Enhances the effect of temperature on the relaxation time of particles (protons) and, accordingly, on the semiclassical relaxation coefficients calculated from the solution of the nonlinear Fokker-Planck kinetic equation, together with the Poisson equation $\Gamma_1^{(\omega)}(\mathrm{T}) = \frac{8}{\pi^2}\sum_{\mathrm{n}=1}^{\infty} \frac{\sin^2\left(\frac{\pi \mathrm{n}}{2}\right) \times \frac{T_{\mathrm{n}}}{T_{\mathrm{M}}}}{\mathrm{n}^2(1+\omega^2 T_{\mathrm{n}}^2)}$, $\Gamma_2^{(\omega)}(\mathrm{T}) = \frac{8}{\pi^2}\sum_{\mathrm{n}=1}^{\infty} \frac{\sin^2\left(\frac{\pi \mathrm{n}}{2}\right) \times \frac{\omega T_{\mathrm{n}}^2}{T_{\mathrm{M}}}}{\mathrm{n}^2(1+\omega^2 T_{\mathrm{n}}^2)}$ [83,87]. This is the advantage of the semiclassical model. In the semiclassical model of dielectric relaxation [83,86,87], the statistically averaged over energy levels of the continuous spectrum quantum transparency of a one-dimensional parabolic potential barrier for ions (in HBC, protons) is calculated as follows:

$$D_{quant,tunn.}^{q.-classic;(\pm)}(\mathrm{T}) = \sum_{l=0}^{\infty} \frac{(\mp 1)^l}{l!} D_{quant,tunn.}^{q.-classic;(l)} \times \zeta_{q.-class.}^{l}(\mathrm{t}) = \frac{\exp(-\Lambda)\exp\left(\mp\eta_{q.-class.}(\mathrm{t})\right) - \exp(-\mathrm{X})\exp\left(\mp\zeta_{q.-class.}(\mathrm{t})\right)}{1-\frac{\Lambda}{\mathrm{X}}},$$

where $D_{quant,tunn.}^{q.-classic;(l)}(\mathrm{T}) = \frac{\left(\frac{\Lambda}{\mathrm{X}}\right)^l \exp(-\Lambda) - \exp(-\mathrm{X})}{1-\frac{\Lambda}{\mathrm{X}}}$. Parameters $\eta_{\mathrm{q.-class.}}(\mathrm{t}) = \Lambda\frac{\Delta \mathrm{U}(\mathrm{t})}{\mathrm{U}_0}$, $\zeta_{\mathrm{q.-class.}}(\mathrm{t}) = \frac{\Delta \mathrm{U}(\mathrm{t})}{\mathrm{k_B T}}$, $\Delta \mathrm{U}(\mathrm{t}) = \frac{q\mathrm{E}(t)a}{2}$, $\mathrm{X} = \frac{\mathrm{U}_0}{\mathrm{k_B T}}$, $\Lambda = \frac{\pi\delta_0\sqrt{\mathrm{m}}}{\mathrm{k_B T}}\sqrt{\mathrm{U}_0}$ are calculated as functions of the characteristic parameters of the system (crystal structure of a dielectric or semiconductor, etc.), which include the activation energy of an ion on a chemical bond U_0, the width of the potential barrier δ_0, the linear oscillation frequency of the ion (in HBC, protons) on a chemical bond (in a one-dimensional potential well) ν_0, the lattice constant a. Here m is the ion mass (in HBC $\mathrm{m} = \mathrm{m_p}$–proton mass). In the model of quantum tunneling

relaxation (conductivity, polarization) under study, protons moving in the direction of hydrogen bonds (in HBC) under the action of an electric field are taken as conduction ions or relaxers. In this model, the external electric field E(t) is assumed to be non-stationary homogeneous. In this case, the relation $\frac{\eta_{q.-class.}(t)}{\zeta_{q.-class.}(t)} = \frac{\Lambda}{X}$ important for the quasi-classical model is fulfilled. From condition $\frac{\Lambda}{X} = 1$, it is easy to calculate the critical temperature $T_{cr,move} = \frac{U_0}{k_B \Lambda} = \frac{\hbar\sqrt{2U_0}}{\pi\delta_0\sqrt{mk_B}}$ separating the temperature regions (zones) of tunneling or quantum $\Lambda < X$; $T < T_{cr,\ move}$ and thermally activated or classical $\Lambda > X$; $T > T_{cr,\ move}$ (relaxation of ions (in HBC, protons).

For further comparative analysis of quantum-mechanical and quasi-classical models of dielectric relaxation, let us touch upon the question of the relaxation times of a system (respectively, an ion or proton subsystem) in a dielectric in a polarizing electric field in a wide temperature range in more detail. For the n-th spatial mode of the space charge (calculated from the solution of the system of Fokker-Planck and Poisson equations for an arbitrary model of electrodes), the relaxation time of the system is $T_n(T) = \frac{T_{n,D} \cdot T_M}{T_{n,D}+T_M}$ [86,87], where $T_{n,D}(T) = \frac{T_D(T)}{n^2}$—is the diffusion relaxation time of the nth spatial mode, and $T_D(T) = \frac{d^2}{\pi^2 D_{diff}^{q.-classic;(0)}(T)}$ for the 0th spatial mode. The relaxation time is the quantity $T_n(T) = \frac{T_D(T)}{\frac{T_D(T)}{T_M(T)}+n^2} = \frac{T_D(T)}{1+\frac{n^2 T_M(T)}{T_D(T)}}$ significantly dependent on the temperature range in which the relaxation process of a certain type dominates (tunneling, thermally activated relaxation; diffusion, Maxwellian relaxation) [83,87], in view of the explicit effect of temperature on the semiclassical zero-order diffusion coefficient with respect to the small dimensionless parameter $\zeta_{q.-class.}(t)$, we have the following:

$$D_{diff}^{q.-classic;(0)}(T) = a^2 W^{q.-classic;(0)}(T),$$

where $W^{q.-classic;(0)}(T) = \frac{\nu_0}{2} \times \left(D_{term}^{classic}(T) + D_{quant,tunn}^{q.-classic;(0)}(T)\right)$ and $D_{term}^{classic}(T) = \exp(-X), D_{quant,tunn}^{q.-classic;(0)}(T) = \frac{\exp(-\Lambda)-\exp(-X)}{1-\frac{\Lambda}{X}}$ are, respectively, the classical and tunnel (quantum) components of the statistically averaged over energy levels transparency coefficient of the potential barrier (in this model, parabolic [81]). In an arbitrary approximation l with respect to the small parameter $\zeta_{q.-class.}(t)$, the influence of temperature on the semiclassical diffusion coefficient of particles (ions, protons) remains the determining factor:

$$D_{diff}^{q.-classic;(l)}(T) = a^2 W^{q.-classic;(l)}(T),$$

where

$$W^{q.-classic;(l)}(T) = \frac{\nu_0}{2} \times \left(D_{term}^{classic}(T) + D_{quant,tunn}^{q.-classic;(l)}(T)\right),$$

$$D_{term}^{classic}(T) = \exp(-X), D_{quant,tunn.}^{q.-classic;(l)}(T) = \frac{\left(\frac{\eta_{q.-class.}(t)}{\zeta_{q.-class.}(t)}\right)^l \exp(-\Lambda)-\exp(-X)}{1-\frac{\Lambda}{X}}.$$

Note that, according to the results of numerous theoretical studies, for crystals with hydrogen bonds (HBC), in which hydrogen ions (protons) are the main relaxers, quantum tunneling continues to play a significant role in the formation of the crystal polarization not only in the low-temperature region (50–100 K), but also at sufficiently high temperatures (150–550 K) [72–75,78,81,83–87], which requires a detailed study of the temperature dependences for various approximations when calculating the transparency coefficient of a potential barrier. Within the framework of this work, we, in particular, will study the behavior of the classical permeability of a potential barrier (describing thermally activated particle transfers) $D_{term}^{classic}(T) = \exp\left(-\frac{U_0}{k_B T}\right)$ and tunneling quantum permeability (calculated for the model of continuous energy spectrum in the semiclassical approximation

(WKB-method)) $D_{quant,tunn}^{q.-classic;(0)}(\mathrm{T}) = \frac{\exp\left(-\frac{\pi\delta_0\sqrt{\mathrm{m}}}{\mathrm{k_B T}}\sqrt{\mathrm{U_0}}\right)-\exp\left(-\frac{\mathrm{U_0}}{\mathrm{k_B T}}\right)}{1-\frac{T}{\mathrm{T}_{cr,\ move}}}$ in the temperature range T = 0–1500 K at proton activation energies characteristic of HBC $\mathrm{U_0} \approx 0.01 \div 0.1$ eV [81,87]. According to the experimental data, the width of the potential barrier in HBC varies in $\delta_0 \approx 0.085 \div 0.1$ nm [73,83,84,87].

The question of the influence of size effects on quantum transparency at thicknesses of crystalline layers on the order of 1–10 nm remains important [75,77,78,80]. In this case, it is expedient to take into account the influence of the crystal thickness on the structure of the proton energy spectrum, which is typical for the discrete proton energy spectrum in HBC [77,78,83,85]. Let us consider a model of proton oscillations in an isolated one-dimensional parabolic potential well, when protons, under the condition $\left|E_{\mathrm{n}\pm1}^{(0)} - E_{\mathrm{n}}^{(0)}\right| = \hbar\omega_0 \gg \mathrm{k_B T}$, are distributed over unperturbed energy levels $E_{\mathrm{n}}^{(0)} = \hbar\omega_0\left(\mathrm{n}+\frac{1}{2}\right)$, and, taking into account the properties of the crystal lattice, the minimum energy level in the potential well is $E_{\mathrm{n_{min}}}^{(0)} = E_0^{(0)} \equiv \frac{1}{2}\hbar\omega_0$, and the maximum energy level in the potential well must satisfy the condition $E_{\mathrm{n_{max}}}^{(0)} = \hbar\omega_0\left(\mathrm{n_{max}}+\frac{1}{2}\right) \leq \mathrm{U_0}$ [85], when constructed the expression $\mathrm{n_{max}} = \frac{1}{2}\left(\frac{\mathrm{U_0}}{E_0^{(0)}} - 1\right)$. In this case, in the WKB approximation, according to [84,85], the transparency of the potential barrier $D\left(E_{\mathrm{n}}^{(0)}\right) = \exp\left(-\frac{\pi\delta_0\sqrt{\mathrm{m}}\left(\mathrm{U_0}-E_{\mathrm{n}}^{(0)}\right)}{\hbar\sqrt{\mathrm{U_0}}}\right)$.

The influence of the crystal lattice on this potential well generates the effect of splitting energy levels $E_{\mathrm{n}}^{(0)}$ into energy zones, including $\mathrm{N_W}$ energy levels each (with numbers from s = 1 to $\mathrm{s} = \mathrm{N_W}$ energy levels inside the n-th energy zone) and, the spectral equation [81,85]:

$$E_{\mathrm{n,s}}^{(0)} = E_{\mathrm{n}}^{(0)} + \frac{2E_0^{(0)}}{\pi}\sqrt{D\left(E_{\mathrm{n}}^{(0)}\right)} \times \cos\left(\frac{\pi\mathrm{s}}{\mathrm{N_W}+1}\right). \quad (28)$$

The width of the n-th energy band formed as a result of splitting the energy level $E_{\mathrm{n}}^{(0)}$, defined as $\Delta E_{\mathrm{n}} = E_{\mathrm{n,s_{max}}}^{(0)} - E_{\mathrm{n,s_{min}}}^{(0)}$, where $\mathrm{s_{min}} = \mathrm{N_W}$, $\mathrm{s_{max}} = 1$, is calculated from the following expression:

$$\Delta E_{\mathrm{n}} = \frac{4\ E_0^{(0)}}{\pi}\sqrt{D\left(E_{\mathrm{n}}^{(0)}\right)} \times \cos\left(\frac{\pi}{\mathrm{N_W}+1}\right). \quad (29)$$

The total number of potential wells in the $\mathrm{N_W}$ model is taken equal to the integer part of the parameter $\frac{\mathrm{d}-\mathrm{a}}{\mathrm{a}+\delta_0}$, or from the parameter $1 + \frac{\mathrm{d}-\delta_0}{\mathrm{a}+\delta_0}$, where d is the sample thickness, a is the width potential hole (well). In this case, $\mathrm{a} + \delta_0 = a$.

The quantum transparency of the parabolic potential barrier for energy levels $E_{\mathrm{n,s}}^{(0)}$ is calculated in the WKB approximation as follows [81]

$$D\left(E_{\mathrm{n,s}}^{(0)}\right) = \exp\left(-\frac{\pi\delta_0\sqrt{\mathrm{m}}\left(\mathrm{U_0} - E_{\mathrm{n,s}}^{(0)}\right)}{\hbar\sqrt{\mathrm{U_0}}}\right). \quad (30)$$

In (30), the expression $E_{\mathrm{n,s}}^{(0)}$ is taken from (28).

In the presence of an external perturbing field, taking into account a small correction to the height of the potential barrier, we have the following

$$D^{(\pm)}\left(E_{\mathrm{n,s}}^{(0)};\mathrm{t}\right) = \exp\left(-\frac{\pi\delta_0\sqrt{\mathrm{m}}\left(\mathrm{U_0} \pm \Delta\mathrm{U(t)} - E_{\mathrm{n,s}}^{(0)}\right)}{\hbar\sqrt{\mathrm{U_0}}}\right). \quad (31)$$

Since the Fermi energy of an ideal proton gas in HBC tends to zero [81], we can write the solution of the quantum kinetic equation for protons unperturbed by an external field (see Formula (2)) using the quantum canonical Gibbs distribution (statistical matrix) $w^{(0)}_{pr;\mathrm{n,s}}\left(E^{(0)}_{\mathrm{n,s}}\right) = A{\cdot}\exp\left(-\frac{E^{(0)}_{\mathrm{n,s}}}{\mathrm{k_B T}}\right)$, satisfying the normalization condition $\sum_{\mathrm{n}=0}^{\infty}\sum_{S=1}^{N_W} w^{(0)}_{pr;\mathrm{n,s}}\left(E^{(0)}_{\mathrm{n,s}}\right) = 1$, on the set of discrete energy values $E^{(0)}_{\mathrm{n,s}}$.

Statistically averaged using the quantum canonical Gibbs distribution $w^{(0)}_{pr;\mathrm{n,s}}\left(E^{(0)}_{\mathrm{n,s}}\right) = \left(\sum_{\mathrm{n}=0}^{\infty}\sum_{\mathrm{s}=1}^{\mathrm{N_W}}\exp\left(-\frac{E^{(0)}_{\mathrm{n,s}}}{\mathrm{k_B T}}\right)\right)^{-1}\exp\left(-\frac{E^{(0)}_{\mathrm{n,s}}}{\mathrm{k_B T}}\right)$ quantum transparency of potential barrier perturbed by non-stationary (alternating) external (polarizing) electric field:

$$D^{deg.;(\pm)}_{quant,tunn}(\mathrm{T}) = \left\langle D^{(\pm)}\left(E^{(0)}_{\mathrm{n,s}};\mathrm{t}\right)\right\rangle = \frac{\sum_{\mathrm{n}=0}^{\mathrm{n_{max}}}\sum_{\mathrm{s}=1}^{\mathrm{N_W}}\exp\left(-\frac{E^{(0)}_{\mathrm{n,s}}}{\mathrm{k_B T}}\right)\cdot D^{(\pm)}\left(E^{(0)}_{\mathrm{n,s}};\mathrm{t}\right)}{\sum_{\mathrm{n}=0}^{\infty}\sum_{\mathrm{s}=1}^{\mathrm{N_W}}\exp\left(-\frac{E^{(0)}_{\mathrm{n,s}}}{\mathrm{k_B T}}\right)},$$

taking into account (31), takes the form:

$$D^{deg.;(\pm)}_{quant,tunn}(\mathrm{T}) = \exp\left(\mp\Lambda\frac{\Delta\mathrm{U(t)}}{\mathrm{U_0}}\right)\times D^{deg.;(0)}_{quant,tunn}(\mathrm{T}). \tag{32}$$

Quantum transparency of potential barrier unperturbed by an external field:

$$D^{deg.;(0)}_{quant,tunn}(\mathrm{T}) = \left\langle D^{(0)}\left(E^{(0)}_{\mathrm{n,s}}\right)\right\rangle = \frac{\sum_{\mathrm{n}=0}^{\mathrm{n_{max}}}\sum_{\mathrm{s}=1}^{\mathrm{N_W}}\exp\left(-\frac{E^{(0)}_{\mathrm{n,s}}}{\mathrm{k_B T}}\right)\cdot D\left(E^{(0)}_{\mathrm{n,s}}\right)}{\sum_{\mathrm{n}=0}^{\mathrm{n_{max}}}\sum_{\mathrm{s}=1}^{\mathrm{N_W}}\exp\left(-\frac{E^{(0)}_{\mathrm{n,s}}}{\mathrm{k_B T}}\right)} \tag{33}$$

is calculated taking into account the condition obtained from numerical calculations

$$\sum_{\mathrm{n}=0}^{\infty}\sum_{\mathrm{s}=1}^{\mathrm{N_W}}\exp\left(-\frac{E^{(0)}_{\mathrm{n,s}}}{\mathrm{k_B T}}\right) \approx \sum_{\mathrm{n}=0}^{\mathrm{n_{max}}}\sum_{\mathrm{s}=1}^{\mathrm{N_W}}\exp\left(-\frac{E^{(0)}_{\mathrm{n,s}}}{\mathrm{k_B T}}\right),$$

calculated in the range of activation energies of protons $\mathrm{U_0} \approx 0.01 \div 0.1$ eV [81,87].

In (33), the expression $D\left(E^{(0)}_{\mathrm{n,s}}\right)$ is taken from (30).

We write Formula (33), for the case of a non-degenerate energy spectrum $E^{(0)}_{\mathrm{n}}$, as a function of temperature:

$$D^{non.-deg.;(0)}_{quant,tunn}(\mathrm{T}) = \left\langle D^{(0)}\left(E^{(0)}_{\mathrm{n}}\right)\right\rangle = \frac{\sum_{\mathrm{n}=0}^{\mathrm{n_{max}}}\exp\left(-\frac{E^{(0)}_{\mathrm{n}}}{\mathrm{k_B T}}\right)D\left(E^{(0)}_{\mathrm{n}}\right)}{\sum_{\mathrm{n}=0}^{\infty}\exp\left(-\frac{E^{(0)}_{\mathrm{n}}}{\mathrm{k_B T}}\right)}. \tag{34}$$

In (34) $D\left(E^{(0)}_{\mathrm{n}}\right) = \exp\left(-\frac{\pi\delta_0\sqrt{\mathrm{m}}\left(\mathrm{U_0}-E^{(0)}_{\mathrm{n}}\right)}{\hbar\sqrt{\mathrm{U_0}}}\right)$, $E^{(0)}_{\mathrm{n}} = \hbar\omega_0\left(\mathrm{n}+\frac{1}{2}\right)$.

Introducing the notation $\beta = \frac{\hbar\omega_0}{\mathrm{k_B T}}$, $\alpha = \frac{\hbar\omega_0}{\mathrm{k_B T}}\left(1-\frac{\mathrm{T}}{\mathrm{T}_{cr,move}}\right)$, and calculating the sums in (34), we obtain the following:

$$D^{non.-deg.;(0)}_{quant,tunn}(\mathrm{T}) = \exp(-\Lambda)\times\exp\left(\frac{\hbar\omega_0}{2\mathrm{k_B T}_{cr,move}}\right)\frac{\left(1-\xi_2^{\mathrm{n_{max}}+1}\right)(1-\xi_1)}{1-\xi_2}. \tag{35}$$

Here $\xi_1 = \exp(-\beta)$, $\xi_2 = \exp(-\alpha)$.

Note that for arbitrary values of the parameters δ_0, U_0, ν_0, according to the equalities $T_{cr,move} = \frac{U_0}{k_B\Lambda} = \frac{\hbar\sqrt{2U_0}}{\pi\delta_0\sqrt{mk_B}}$, $U_0 = \frac{m\omega_0^2\delta_0^2}{8}$ [81], $\omega_0 = 2\pi\nu_0$, we have $\frac{\hbar\omega_0}{2k_BT_{cr,\ move}} = \pi$. Hence, it is obvious that near the temperature of absolute zero, the formula for quantum transparency (35), which is more rigorous than $D^{q.-classic;(0)}_{quant,tunn}(T)$, gives an increase in this quantity in $\frac{D^{non.-deg.;(0)}_{quant,tunn.}(0)}{D^{q.-classic;(0)}_{quant,tunn}(0)} = \exp(\pi)$ times.

Stationary quantum tunneling coefficient (transparency of potential barrier perturbed by stationary external electric field) will be calculated upon based the generalized expression (for the energy spectrum model of an arbitrary structure $E^{(0)}$), assuming stationarity of external fiel $D_{quant,tunn;stationary}(T) = \frac{\left\langle D^{(-)}\left(E^{(0)}\right)\right\rangle + \left\langle D^{(+)}\left(E^{(0)}\right)\right\rangle}{2}$. Here, the statistically averaged transparencies are functions of temperature at a given external electric field strength $D^{(\pm)}_{quant,tunn;stationary}(T) = \left\langle D^{(\pm)}\left(E^{(0)}\right)\right\rangle$. Thus, for the model of classical (thermally activated) transitions of protons through a potential barrier, with probabilities $D^{classic;(\pm)}_{term;stationary}(T) = \exp(-X)\exp\left(\mp\zeta^{(0)}_{q.-class.}\right)$, where $\zeta^{(0)}_{q.-class.} = \frac{(\Delta U)_0}{k_BT}$, $(\Delta U)_0 = \frac{qE_0a}{2}$, according to $D^{classic}_{term;stationary}(T) = \frac{D^{classic;(-)}_{term;stationary}(T) + D^{classic;(+)}_{term;stationary}(T)}{2}$, we have

$$D^{classic}_{term;stationary}(T) = \exp(-X)ch\left(\zeta^{(0)}_{q.-class.}\right). \quad (36)$$

For the model of the continuous energy spectrum of proton

$$D^{q.-classic;(\pm)}_{quant,tunn;stationary}(T) = \frac{\exp(-\Lambda)\exp\left(\mp\eta^{(0)}_{q.-classic.}\right) - \exp(-X)\exp\left(\mp\zeta^{(0)}_{q.-classic.}\right)}{1-\frac{\Lambda}{X}},$$

where $\eta^{(0)}_{q.-class.} = \Lambda\frac{(\Delta U)_0}{U_0}$, we calculate

$$D^{q.-classic}_{quant,tunn;stationary}(T) = \frac{D^{q.-classic;(-)}_{quant,tunn;stationary}(T) - D^{q.-classic;(+)}_{quant,tunn;stationary}(T)}{1-\frac{\Lambda}{X}} = \frac{\exp(-\Lambda)ch\left(\eta^{(0)}_{q.-class.}\right) - \exp(-X)ch\left(\zeta^{(0)}_{q.-class.}\right)}{1-\frac{\Lambda}{X}}. \quad (37)$$

The critical temperature at an activation energy of $U_0 = 0.01$ eV and a potential barrier width of $\delta_0 \approx 0.085$ nm is $T_{cr,move,1} = 39.5774$ K (much lower than the freezing point of nitrogen (77 K)) with an amplitude of $D^{q.-classic}_{quant,tunn;stationary}(T_{cr,move,1}) \approx 0.1555$. The value of the polarizing field strength was taken as $E_0 = 10^6$ V/m.

At higher activation energies:

$$U_0 = 0.03 \text{ eV},\ T_{cr,move,2} = 68.55 \text{ K},\ D^{q.-classic}_{quant,tunn;stationary}(T_{cr,move,2}) = 0.031;$$

$$U_0 = 0.05 \text{ eV},\ T_{cr,move,3} = 88.4977 \text{ K},\ D^{q.-classic}_{quant,tunn;stationary}(T_{cr,move,3}) = 0.008;$$

$$U_0 = 0.07 \text{ eV},\ T_{cr,move,4} = 104.7119 \text{ K},\ D^{q.-classic}_{quant,tunn;stationary}(T_{cr,move,4}) = 0.0035;$$

$$U_0 = 0.1 \text{ eV},\ T_{cr,move,5} = 125.1546 \text{ K},\ D^{q.-classic}_{quant,tunn;stationary}(T_{cr,move,5}) = 0.00087.$$

Thus, with an increase in the calculated activation energy of protons from 0.01 eV to 0.1 eV, the critical temperature noticeably increases but remains in the range of 50–125 K, and the amplitude of quantum transparency noticeably decreases from 0.05 to 0.001, which is very significant from the point of view of the manifestation of quantum properties for such heavy (in comparison with an electron) charge carriers as protons.

Against the background of small activation energies (0.01.0.03.05, 0.07 eV), critical temperatures (39.57 K, 68.55 K, 88.49 K, 104.71 K) are distributed in the T < 105 K region

with amplitudes of the quantum transparency sufficiently high (0.1555, 0.031, 0.008, 0.0035) for such heavy (in comparison with electrons) charge carriers as protons. With an activation energy of 0.1 eV, the critical temperature shifts already to 125.15 K, and the amplitude of the quantum transparency decreases to 0.00087. This indicates a significant contribution of quantum tunneling to the mechanism of relaxation motion of protons in HBC in the temperature region T = 1–100 K. At temperatures T > 100, quantum tunneling continues to affect the relaxation of protons in HBC to a certain extent.

For the model of degenerate discrete energy spectrum $E_{n,s}^{(0)}$, according the Expression (32), we get the following:

$$D_{quant,tunn;stationary}^{deg.}(T) = \frac{D_{quant,tunn}^{deg.;(-)}(T) + D_{quant,tunn}^{deg.;(+)}(T)}{2} = D_{quant,tunn}^{deg.;(0)}(T) \times ch\left(\eta_{q.-class.}^{(0)}\right). \quad (38)$$

In (38), the expression $D_{quant,tunn}^{deg.;(0)}(T)$ is taken from (33).

For the model of non-degenerate discrete energy spectrum $E_n^{(0)}$, we get the following:

$$D_{quant,tunn;stationary}^{non.-deg.}(T) = D_{quant,tunn}^{non.-deg.;(0)}(T) \times ch\left(\eta_{q.-class.}^{(0.)}\right) \quad (39)$$

In (39), the expression $D_{quant,tunn}^{non.-deg.;(0)}(T)$ is taken from (34) and (35).

The results of numerical calculations according to Formulas (34) and (35) coincide absolutely. Figures 3–7 show the results of numerical calculations of the values of the statistically averaged stationary tunneling coefficient (transparency of potential barrier perturbed by stationary external electric field) $D_{stationary}(T)$ for protons (with barrier height $U_0 = 0.01$ eV, $U_0 = 0.03$ eV, $U_0 = 0.05$ eV, $U_0 = 0.07$ eV, $U_0 = 0.1$ eV, respectively) as a function of temperature for various models of the proton energy spectrum: 1—classical model thermally activation of particles (protons) $D_{term;stationary}^{classic}(T)$ (Expression (36)); 2—quasi-continuous energy spectrum $D_{quant,tunn;stationary}^{q.-classic}(T) = \frac{\exp(-\Lambda)ch\left(\eta_{q.-class.}^{(0)}\right) - \exp(-X)ch\left(\zeta_{q.-class.}^{(0)}\right)}{1-\frac{\Lambda}{X}}$ (quasi-classical quantum model (Expression (37)); 3—non-degenerate discrete energy spectrum $D_{quant,tunn;stationary}^{non.-deg.}(T)$ (Expression (39)); 4—degenerate discrete energy spectrum $D_{quant,tunn;stationary}^{deg.}(T)$ (Expression (38)). The thickness of the crystal is $d = 10^{-9}$ m. The temperature accepted in diapason from 0 to 2500 K. The value of the polarizing field strength is taken as $E_0 = 10^6$ V/m. According to the results of numerical calculations, the value of the polarizing field strength has practically no effect on the values of quantum transparency $D_{stationary}(T)$ in the region of fields $E_0 = (10^6 \div 10^7)$ V/m at widerange of temperatures T = 0–2500 K and only in the region $E_0 = (10^8 \div 10^9)$ V/m the field begins to affect the value of quantum transparency.

The properties of the $D_{term;stationary}^{classic}(T)$ function and its graph (curve 1 in Figures 3–7) are in good agreement with the classical statistical theory.

The ratio of the graphs of the classical probability of proton transfer through the potential barrier (curve 1 in Figures 3–7) and the quasi-classical quantum probability of proton tunneling through the potential barrier (curve 2 in Figures 3–7) with an increase in proton activation energies from 0.01 to 0.1 eV indicates a shift of the intersection point of graphs 1, 2 towards higher temperatures, from T = 68 K at 0.01 eV with the value of functions 1, 2 equal to 0.185 to T = 145 K at 0.1 eV with the value of functions 1, 2 equal to 0.00099, which corresponds to an increase in the effects of thermal activation at high activation energies (0.05; 0.07; 0.1 eV) with low classical proton transition probabilities (0.0009–0.001).

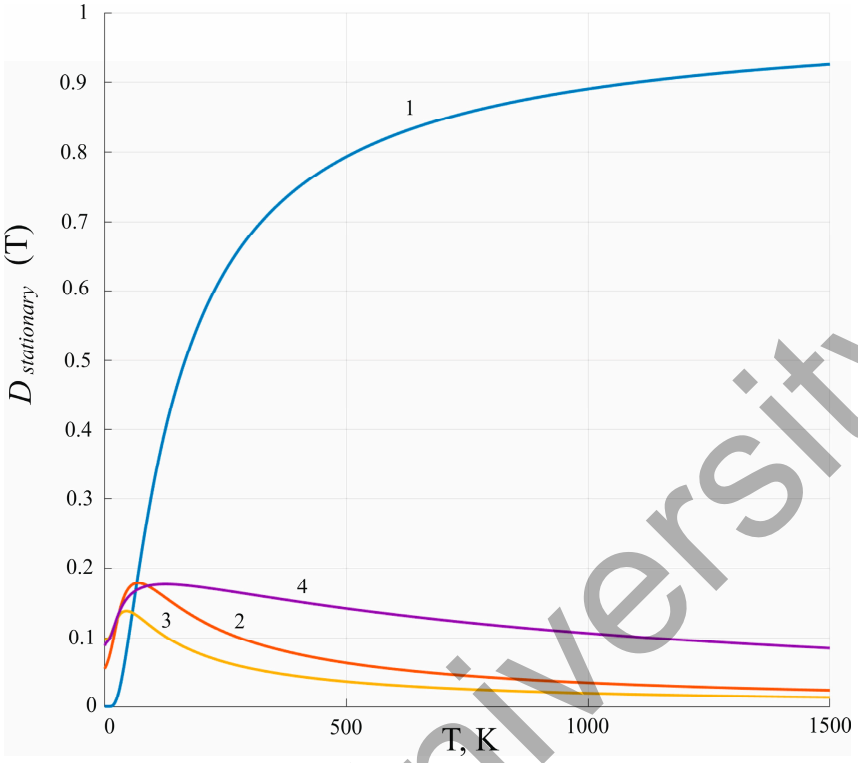

Figure 3. 1—$D^{classic}_{term;stationary}$(T); 2—$D^{q.-classic}_{quant,tunn;stationary}$(T); 3—$D^{non.-deg.}_{quant,tunn;stationary}$(T); 4—$D^{deg.}_{quant,tunn;stationary}$(T) at $U_0 = 0.01$ eV; d $= 10^{-9}$ m.

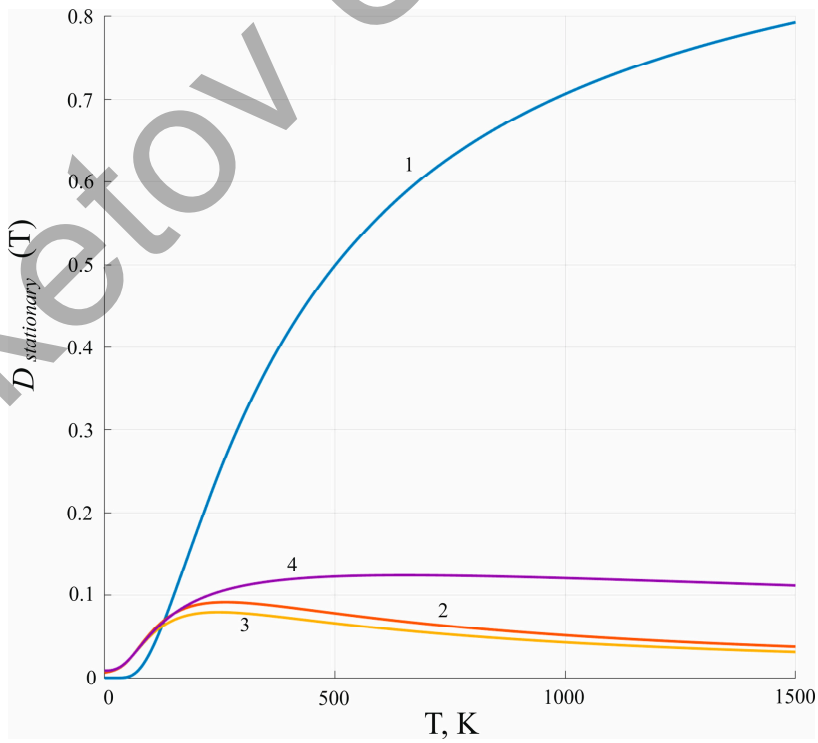

Figure 4. 1—$D^{classic}_{term;stationary}$(T); 2—$D^{q.-classic}_{quant,tunn;stationary}$(T); 3—$D^{non.-deg.}_{quant,tunn;stationary}$(T); 4—$D^{deg.}_{quant,tunn;stationary}$(T) at $U_0 = 0.03$ eV; d $= 10^{-9}$ m.

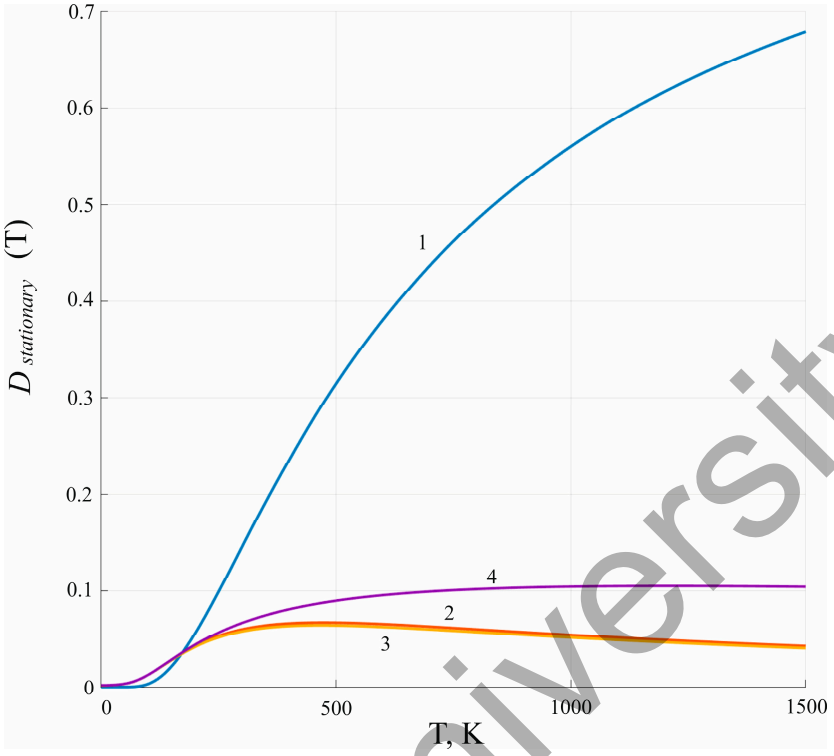

Figure 5. 1—$D^{classic}_{term;stationary}$(T); 2—$D^{q.-classic}_{quant,tunn;stationary}$(T); 3—$D^{non.-deg.}_{quant,tunn;stationary}$(T); 4—$D^{deg.}_{quant,tunn;stationary}$(T) at $U_0 = 0.05$ eV; d $= 10^{-9}$ m.

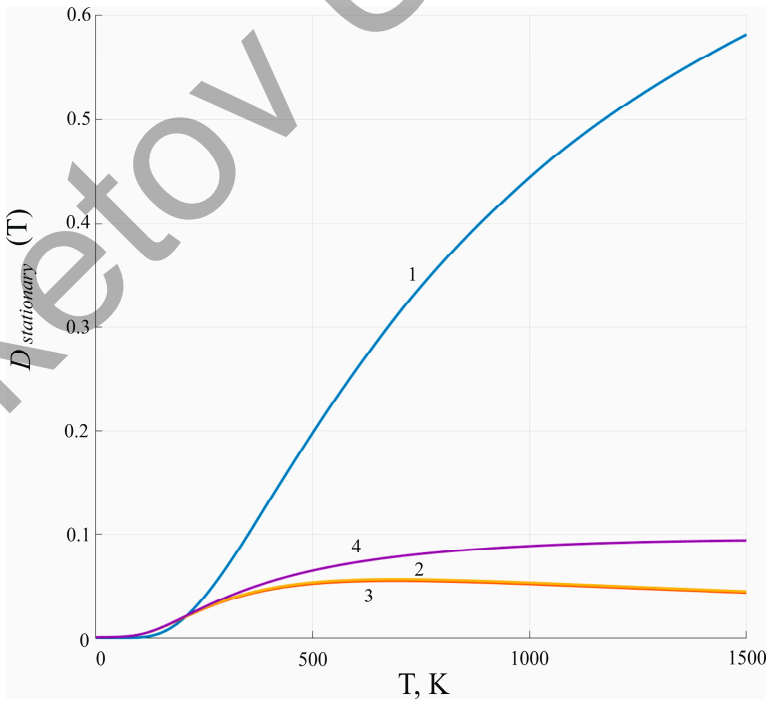

Figure 6. 1—$D^{classic}_{term;stationary}$(T); 2—$D^{q.-classic}_{quant,tunn;stationary}$(T); 3—$D^{non.-deg.}_{quant,tunn;stationary}$(T); 4—$D^{deg.}_{quant,tunn;stationary}$(T) at $U_0 = 0.07$ eV; d $= 10^{-9}$ m.

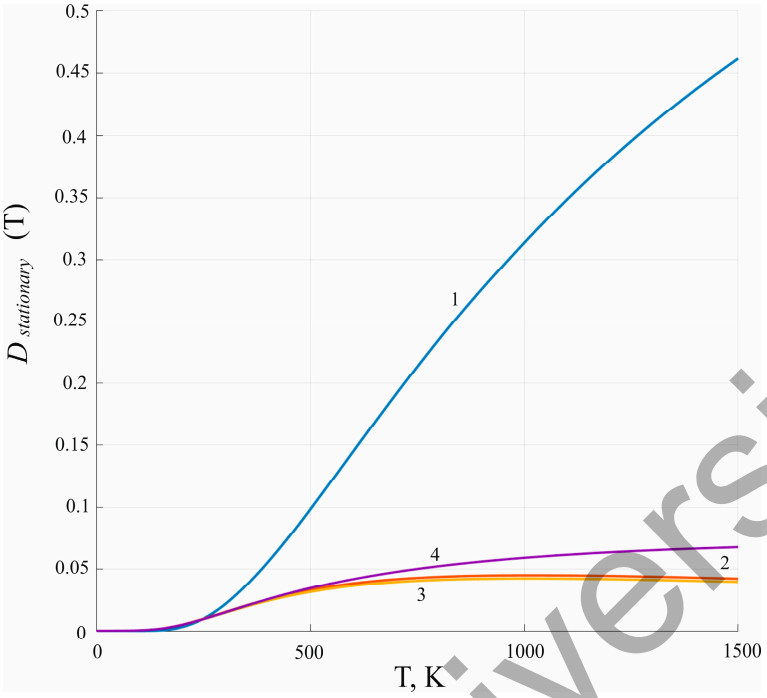

Figure 7. 1—$D^{classic}_{term;stationary}(T)$; 2—$D^{q.-classic}_{quant,tunn;stationary}(T)$; 3—$D^{non.-deg.}_{quant,tunn;stationary}(T)$; 4—$D^{deg.}_{quant,tunn;stationary}(T)$ at $U_0 = 0.1$ eV; $d = 10^{-9}$ m.

At the same time, the graphs of the functions $D^{non.-deg.}_{quant,tunn;stationary}(T)$, $D^{q.-classic}_{quant,tunn;stationary}(T)$ for small activation energies (0.01; 0.03 eV) have the same course of the curve line and differ somewhat at the points of maximum in magnitude (temperature and amplitude), and with increasing activation energy (0.05; 0.07; 0.1 eV) become almost identical, which indicates a higher degree of reliability of quantum transparency calculations using the quantum model of the discrete proton energy spectrum (graph 3) in comparison with the semiclassical quantum model (graph 2) in the region of low activation energies, when quantum effects are most significant, and in the region of higher activation energies, when the role of quantum transitions of protons decreases, the results of both models are practically the same.

As can be seen from Figures A5–A29 presented in Appendix C), the thickness of the crystalline layer has absolutely no effect on the course of the graphs of functions 1, 2, 3 at different activation energies, and graph 4, although it depends on the value of d, remains within the framework of the dependences under study at a fixed thickness d (1 nm). As can be seen from a comparison of Figures 3–7, with an increase in the activation energy, the temperature maxima of the graphs of functions 2–4 shift noticeably to the right, decreasing in amplitude, which indicates the determining factor for tunneling at low activation energies of protons (0.01; 0.03 eV) in Figures A5–A9, Figures A9–A13 (presented in Appendices C.1 and C.2), and at higher activation energies of protons (0.05; 0.07; 0.1 eV) in Figures A14–A19 (Appendix C.3), Figures A20–A24 (Appendix C.4), Figures A25–A29 (Appendix C.5) the influence of quantum transitions of particles noticeably decreases, but continues to influence in a certain way the course of temperature dependences 2–4.

The plot of the function $D^{deg.}_{quant,tunn;stationary}(T)$ for all activation energies (0.01; 0.03 eV; 0.05; 0.07; 0.1 eV) exceeds in amplitude and is shifted towards higher temperatures relative to the graph of the function $D^{non.-deg.}_{quant,tunn;stationary}(T)$, which indicates a significant effect of the crystal thickness d, which is incorporated in Formula (31) for the model of a degenerate discrete energy spectrum, on the quantum permeability (graph 4 in Figure 3), in comparison with the model of a non-degenerate discrete energy spectrum of protons (graph 3 in Figure 3), in which the parameter d is absent by definition. Thus, at $U_0 = 0.01$, the

maximum of graph 3 is realized at a temperature of T = 55 K with an amplitude of 0.12 (Figure 3), and the maximum of graph 4 is calculated at a temperature of T = 150 K with an amplitude of 0.18 (Figure 3),whence it is clear that taking into account the degenerate structure of the energy spectrum of particles (protons) in the quantum model reflects at the theoretical level the significant role of quantum tunneling of protons with low activation energies (0.01; 0.03 eV) in the region of sufficiently high temperatures (T = 150–250 K). At $U_0 = 0.1$ eV, the maximum of graph 4 (Figure 7) is located in the region of anomalously high temperatures (T = 1500 K) with an amplitude of 0.05, and the maximum of graph 3 (Figure 7) is realized at lower temperatures (T = 1050 K) with an amplitude of 0.03, which is a continuation of the regularity indicated at $U_0 = 0.01$ eV, but with smaller amplitudes of the tunneling probability maxima, and, accordingly, with a smaller contribution of tunneling to proton relaxation.

Investigation of the temperature dependence of $D^{deg.}_{quant,tunn;stationary}(T)$ at different thicknesses of the crystalline layer ($d = 10^{-9}$ m; $d = 10^{-8}$ m; $d = 10^{-7}$ m; $d = 10^{-6}$ m; $d = 10^{-5}$ m) at $U_0 = 0.01$ eV (Figures A5–A9 in Appendix C.1) indicates a significant effect of the parameter d on the properties plot of the function $D^{deg.}_{quant,tunn;stationary}(T)$ at the transition between the values d = 1 nm and d = 10 nm and, between the values d = 10 nm and d = 100 nm, when the maximum temperature increases from 150 K with an amplitude of 0.18 (at 1 nm) to 500 K with an amplitude of 0.2 (at 10 nm). Further, the change in the value at d = 100 nm, 1000 nm, and 10,000 nm does not significantly affect the temperature of the maximum, which is approximately 1500 K with an amplitude of 0.21–0.23.

At $U_0 = 0.03$ eV (Figures A10–A14 in Appendix C.2), the influence of the parameter d on the graph of the function $D^{deg.}_{quant,tunn;stationary}(T)$ appears only during the transition between the values d = 1 nm and d = 10 nm, when the temperature of the maximum increases from 850 K with an amplitude of 0.12 (at 1 nm) to 1500 K with an amplitude of 0.15 (at 10 nm).

At $U_0 = 0.05$ eV (Figures A15–A19 in Appendix C.3), variation in the thickness of the crystalline layer leads to a jump in the parameters of the graph of the function $D^{deg.}_{quant,tunn;stationary}(T)$ also during the transition between 1 nm and 10 nm: the temperature of the maximum increases from 1500 K with an amplitude of 0.11 (at 1 nm) up to 2000 K with an amplitude of 0.12 (at 10 nm) and, further, the graph parameters remain practically unchanged at d = 100 nm, 1000 nm, and 10,000 nm. At values $U_0 = 0.07; 0.1$ eV (Figures A20–A24 in Appendix C.4, Figures A25–A29 in Appendix C.5), the trend of shifting the temperatures of the maxima to the zone of anomalously high temperatures (2000–2050 K at 1 nm) continues with a decrease in amplitude to 0.05 (at 1 nm).

As in [80], the size effects found in this work in HBC will be explained by the degenerations of the discrete energy spectrum $E_n^{(0)}$ of low-temperature relaxators (protons) [85] moving in the temperature range T = 50–150 K, in mainly due to tunnel transitions through the potential barrier, and energy spectrum distributed over energy levels $E_{n,s}^{(0)}$ with a band structure (s is the energy level number of the nth energy band) [85] in accordance with Boltzmann's quantum statistics (Expressions (33) and (34)). At activation energies $U_0 = 0.01 \div 0.03$ [81], the statically averaged transparency coefficient for the energy levels of the non-degenerate spectrum $E_n^{(0)}$ is equal to $D^{non.-deg.}_{quant,tunn;stationary}(T) \approx 0.12 \div 0.15$, and for the energy levels of the degenerate spectrum it is equal to $D^{deg.}_{quant,tunn;stationary}(T) \approx 0.18 \div 0.22$, which is a sufficiently large number for such a massive (compared to electrons) particle as a proton and indicates the significant role of the effect of degeneration of energy levels $E_n^{(0)}$ into energy bands $E_{n,s}^{(0)}$ against the background of low activation energies of protons ($0.01 \div 0.03$ eV) moving in nanometer HBC layers due to quantum tunneling, and in a very wide temperature range (0–1550 K).

Let us consider the question of calculating the diffusion coefficients and mobility of protons for the semiclassical and more rigorous quantum model. For the quasi-

classical model, we write a non-stationary expression for the probability rate of proton transfers [81,83,84,86].

$$W^{q.-classic;(\pm)}(\mathrm{T}) = \frac{\nu_0}{2} \times \left(D^{classic}_{term}(\mathrm{T}) \exp\left(\mp \zeta_{\mathrm{q.-class.}}(\mathrm{t}) \right) + D^{q.-classic;(\pm)}_{quant,tunn}(\mathrm{T}) \right), \quad (40)$$

Here

$$D^{classic}_{term}(\mathrm{T}) = \exp(-\mathrm{X}), D^{q.-classic;(\pm)}_{quant,tunn}(\mathrm{T}) = \frac{\exp(-\Lambda)\exp\left(\mp\eta_{q.-class.}(\mathrm{t})\right) - \exp(-\mathrm{X})\exp\left(\mp\zeta_{q.-class.}(\mathrm{t})\right)}{1-\frac{\Lambda}{\mathrm{X}}},$$
$$\eta_{\mathrm{q.-class.}}(\mathrm{t}) = \Lambda\frac{\Delta \mathrm{U}(\mathrm{t})}{\mathrm{U}_0},\ \zeta_{\mathrm{q.-class.}}(\mathrm{t}) = \frac{\Delta \mathrm{U}(\mathrm{t})}{\mathrm{k_B T}}. \quad (41)$$

Nonstationary quasi-classical diffusion coefficient [83]

$$\mathrm{D}^{q.-classic;(\pm)}_{diff}(\mathrm{T}) = a^2 \frac{W^{q.-classic;(-)}(\mathrm{T}) + W^{q.-classic;(+)}(\mathrm{T})}{2}, \quad (42)$$

taking into account (40), takes the form

$$\mathrm{D}^{q.-classic}_{diff}(\mathrm{T}) = \mathrm{D}^{q.-classic}_{diff,classic}(\mathrm{T}) + \mathrm{D}^{q.-classic}_{diff,tunn}(\mathrm{T}). \quad (43)$$

Here

$$\mathrm{D}^{q.-classic}_{diff,classic}(\mathrm{T}) = \mathrm{D}^{q.-classic;(0)}_{diff,classic}(\mathrm{T})\mathrm{ch}\left(\zeta_{q.-class.}(\mathrm{t})\right), \mathrm{D}^{q.-classic;(0)}_{diff,classic}(\mathrm{T}) = \mathrm{D}_0 D^{classic}_{term}(\mathrm{T}) \mathrm{D}^{q.-classic}_{diff,tunn}(\mathrm{T})$$
$$= \mathrm{D}_0 \frac{\exp(-\Lambda)\mathrm{ch}\left(\eta_{q.-class.}(\mathrm{t})\right) - \exp(-\mathrm{X})\mathrm{ch}\left(\zeta_{q.-class.}(\mathrm{t})\right)}{1-\frac{\Lambda}{\mathrm{X}}}, \mathrm{D}_0 = \frac{\nu_0 a^2}{2}.$$

Nonstationary steady semiclassical proton transfer rate in an electric field [83]

$$\mathrm{v}^{q.-classic}_{mob}(\mathrm{T}) = a\left(W^{q.-classic;(-)}(\mathrm{T}) - W^{q.-classic;(+)}(\mathrm{T}) \right), \quad (44)$$

taking into account (40), takes the form

$$\mathrm{v}^{q.-classic}_{mob}(\mathrm{T}) = \mathrm{v}^{q.-classic}_{mob,classic}(\mathrm{T}) + \mathrm{v}^{q.-classic}_{mob,tunn}(\mathrm{T}). \quad (45)$$

Here

$$\mathrm{v}^{q.-classic}_{mob,classic}(\mathrm{T}) = \mathrm{v}^{q.-classic;(0)}_{mob,classic}(\mathrm{T})\mathrm{sh}\left(\zeta_{q.-class.}(\mathrm{t})\right),$$
$$\mathrm{v}^{q.-classic;(0)}_{mob,classic}(\mathrm{T}) = \mathrm{V}_0 D^{classic}_{term}(\mathrm{T})$$
$$\mathrm{v}^{q.-classic}_{mob,tunn}(\mathrm{T}) = \mathrm{V}_0 \frac{\exp(-\Lambda)\mathrm{sh}\left(\eta_{q.-class.}(\mathrm{t})\right) - \exp(-\mathrm{X})\mathrm{sh}\left(\zeta_{q.-class.}(\mathrm{t})\right)}{1-\frac{\Lambda}{\mathrm{X}}},$$
$$\mathrm{V}_0 = \nu_0 a.$$

For the model of a degenerate discrete spectrum of proton energies, the non-stationary quantum-mechanical diffusion coefficient [85]

$$\mathrm{D}^{deg.}_{diff,tunn}(\mathrm{T}) = \frac{\nu_0 a^2}{2} \times \frac{D^{deg.;(-)}_{quant,tunn}(\mathrm{T}) + D^{deg.;(+)}_{quant,tunn}(\mathrm{T})}{2}$$

Taking into account (32), we write

$$\mathrm{D}^{deg.}_{diff,tunn}(\mathrm{T}) = \mathrm{D}_0 D^{deg.;(0)}_{quant,tunn}(\mathrm{T}) \times \mathrm{ch}\left(\eta_{q.-class.}(\mathrm{t})\right). \quad (46)$$

The non-stationary steady-state quantum-mechanical rate of proton transfer in an electric field [85]

$$\mathrm{v}^{deg.}_{mob,tunn}(\mathrm{T}) = \nu_0 a \times \left(D^{deg.;(-)}_{quant,tunn}(\mathrm{T}) - D^{deg.;(+)}_{quant,tunn}(\mathrm{T}) \right)$$

We also write, taking into account (32)

$$v_{mob,tunn}^{deg.}(T) = V_0 \times D_{quant,tunn}^{deg.;(0)}(T) \times sh\left(\eta_{q.-class.}(t)\right). \quad (47)$$

For the model of a non-degenerate discrete spectrum of proton energies, we construct the corresponding non-stationary expressions

$$D_{diff,tunn}^{non.-deg.}(T) = D_0 D_{quant,tunn.}^{non.-deg.;(0)}(T) \times ch\left(\eta_{q.-class.}(t)\right), \quad (48)$$

$$v_{mob,tunn}^{non.-deg.}(T) = V_0 \times D_{quant,tunn.}^{non.-deg.;(0)}(T) \times sh\left(\eta_{q.-class.}(t)\right). \quad (49)$$

Note the equalities important for practical application

$$\frac{v_{mob,tunn}^{deg.}(T)}{D_{diff,tunn}^{deg.}(T)} = \frac{2}{a} \times th\left(\eta_{q.-class.}(t)\right), \quad \frac{v_{mob,tunn}^{non.-deg.}(T)}{D_{diff,tunn}^{non.-deg.}(T)} = \frac{2}{a} \times th\left(\eta_{q.-class.}(t)\right),$$

$$\frac{v_{mob,tunn}^{q.-classic}(T)}{D_{diff,tunn}^{q.-classic}(T)} = \frac{2}{a} \times \frac{\exp(-\Lambda)sh\left(\eta_{q.-class.}(t)\right) - \exp(-X)sh\left(\zeta_{q.-class.}(t)\right)}{\exp(-\Lambda)ch\left(\eta_{q.-class.}(t)\right) - \exp(-X)ch\left(\zeta_{q.-class.}(t)\right)}$$

Further, when varying the theoretical thickness of the crystal from 30 μm to 3 nm, for onot talc and gypsum, as shown in Tables 3 and 4, all the same effects of displacements of low-temperature ($T_{max,1}$ = 50–100 K) theoretical maxima $tg\delta_{th}^{(\nu)}(T_{max,1})$ appear in the direction of ultra-low temperatures ($T_{max,2}$ = 4–25 K) with the maxima $tg\delta_{th}^{(\nu)}(T_{max,2})$. The drop in the amplitudes of the shifted maxima $tg\delta_{th}^{(\nu)}(T_{max,2})$, in comparison with the initial maxima $tg\delta_{th}^{(\nu)}(T_{max,1})$, by 3–4 orders of magnitude (Tables 3 and 4), is explained, according to the results of numerical calculations, primarily by a significant increase in the values of the real component of the complex permittivity (26): $\frac{Re(\hat{\varepsilon}(\nu,T_{max,1}))}{Re(\hat{\varepsilon}(\nu,T_{max,2}))} \approx (0.00008 \div 0.0001)$—by 4 orders. In this case, the changes in the imaginary component turn out to be insignificant $\frac{Im(\hat{\varepsilon}(\nu,T_{max,2}))}{Im(\hat{\varepsilon}(\nu,T_{max,1}))} \approx (0.89 \div 1)$.

Nevertheless, despite the low values of the electrical conductivity of the materials under study (micas, crystalline hydrates) $\frac{\sigma}{2\pi\nu\varepsilon_0} \ll \frac{Im(\hat{\varepsilon}(\nu,T_{max}))}{Re(\hat{\varepsilon}(\nu,T_{max}))}$, the anomalously low values of the converted calculated data in terms of the loss tangent $tg\delta_{th}^{(\nu)}(T_{max,2}) \approx \frac{Im(\hat{\varepsilon}(\nu,T_{max,2}))}{Re(\hat{\varepsilon}(\nu,T_{max,2}))} \cong 10^{-8}$, make it possible to state that a dielectric of nano size has passed (in calculations, the thickness of the dielectric was taken, as in [85], equal to d = 3–30 nm) near the temperature $T_{max,2} \cong$ 4–25 K into the state of the quasi-ferroelectric phase [81, 85], characterized by anomalously high values of the real component $Re(\hat{\varepsilon}(\nu, T_{max,2})) \approx (2 \div 3) \times 10^6$ at $Im(\hat{\varepsilon}(\nu, T_{max,2})) \approx (1.4 \div 2.7) \times 10^{-2}$. For a crystal with a thickness of d = 3–30 μm, near the temperature $T_{max,1}$ = 50–100 K, when $Re(\hat{\varepsilon}(\nu, T_{max,1})) \approx (1.5 \div 2.8) \times 10^2$, $Im(\hat{\varepsilon}(\nu, T_{max,1})) \approx (1.38 \div 2.54) \times 10^{-2}$, this effect is not observed and the dielectric reacts to the electric field in a standard way.

The physical mechanism of the observed regularities can be explained by the rearrangement of the hydrogen sublattice in HBC due to anomalously high values of quantum transparency for protons $\varsigma = \frac{\left\langle D(U_0;E_{nmax,s}^{(0)})\right\rangle|_{T\to T_{max,2}}}{\left\langle D(U_0;E_{0,s}^{(0)})\right\rangle|_{T\to T_{max,1}}} \cong 10^5$, which determines the quantum nonlinear polarization [85].

5. Scientific and Practical Significance of the Research Results

To date, a fairly large amount of experimental data has been accumulated on the use of proton semiconductors and dielectrics (PSD), mainly in the field of electrochemical technologies and physical chemistry in the development of solid electrolytes (perovskites, alkali metal orthoperiodates and biperiodates) [10–12] and hydrogen fuel cells energy [13–19]. At the same time, there are not so many practical applications of proton semiconductors

and dielectrics and their composites (MSM, MIS) in the field of industrial electrical engineering, physical and quantum electronics, optoelectronics and nonlinear optics. Relevant, from the point of view of fundamental science, are theoretical developments aimed at applying the methods of the nonlinear quantum kinetic theory of proton conductivity and relaxation [72–87] to the development of quantum field-effect transistors, tunnel resonant diodes, high-temperature superconductors, etc. [2,9]. The methods of the quantum theory of proton conductivity have a direct application to theoretical and applied studies of quantum transitions of protons in the hydrogen sublattice during the formation of spontaneous polarization in ferroelectric crystals with hydrogen bonds (KDP) near the second-order phase transition point [3–8]. The results of the research, in the future, will find application in the field of laser technology and nonlinear optics, in particular, in studying the effects of quantum proton tunneling on second-order nonlinear optical processes (second harmonic generation, parametric generation and amplification of light, frequency mixing, electro-optical effect)and nonlinearity of a higher order in the frequency of the electromagnetic field (the effect of self-action of laser radiation), which is important for the technique of femtosecond lasers [24–28]. It is promising to use thin films (1 μm–1 nm) of ferroelectric HBCs (triglycine sulfate (TGS), ferroelectric salt, etc.) in the development of high-speed non-volatile memory elements with an anomalously high residual polarization relaxation time (up to 10 years) and ultra-high thermal stability and mechanical strength (for information technology) [15–23].

The semi-empirical studies of the migration of adsorbed protons over the surface of single-walled carbon nanotubes [83] performed to date are not complete, due to the lack of a rigorous theoretical justification: (1) the relationship between the configuration of the tube surface and the dominant physical mechanism of proton transfer (tunneling or thermally activated transferprotons through a potential barrier); (2) the temperature dependence of the probability of tunneling proton transitions; (3) potential relief forms and activation energies for protons. The methods of the quantum kinetic theory of low-temperature proton conductivity, the foundations of which were laid down by the authors [81,85], will make it possible to consider in more detail, at a more rigorous theoretical level, using the density matrix apparatus, the quantum mechanism of tunneling proton transfer in nanosized materials (1–10 nm) with high proton conductivity, which is promising for cryogenic engineering and space technologies.

A promising technical application of polymeric materials with proton conductivity in fiber optic (FO) devices and control and measurement FO systems is characterized by a number of advantages (they are not affected by electromagnetic interference (noise); they have high electrophysical (nonlinear relaxation polarization and conductivity), optical (non-linear electro-optical phenomena) and metrological characteristics; have distributed and quasi-distributed sensitivity; are capable of operating in an explosive environment; at the same time, the measuring channels have a significant length, the cost of fiber-optic conductors is lower than that of copper; annually, the cost of optical fiber decreases, and its properties improve). Another feature of the use of fiber optic sensors is their low power consumption and the ability to work at a considerable distance from the data processing unit, since the light signal is weakly attenuated, unlike the electric one, it can also be added that optical fibers are not subject to oxidation. Optical fibers can be used to build distributed and quasi-distributed measuring systems for monitoring geotechnical parameters and the safety of mining operations in quarries [92] and coal mines [93], as well as other extended objects. On the basis of fiber-optic sensors, security systems for perimeters and borders of various types and purposes have been developed [94]. Fiber-optic sensors are actively used in the aerospace and oil and gas industries [95,96], as they have significant advantages over electrical ones, based on the clarity of the physical principle of operation and their positive properties, which ensures their large-scale implementation.

The scientific and practical significance of the theoretical methods in this article lies in the development of universal algorithms for computer programs based on modern software and hardware, which allow not only to analyze but also to predict, with a high

degree of accuracy, the results of scientific and industrial experiments in the development and application of quantum technologies (tunnel, field, resonant) functional semiconductor and dielectric elements (diodes, triodes, capacitors, regulators, controllers, sensors, etc.) of electrical, electronic and optoelectrical devices and systems [97,98].

6. Conclusions

1. The quantum kinetic equation is constructed that describes the relaxation of the majority charge carriers (protons) in the hydrogen sublattice in PSD in an electric field. In the linear approximation of perturbation theory by the small comparison parameter, with the help of the Fourier series, solutions of quantum kinetics are constructed. The transition to higher orders of perturbation theory requires the construction of more cumbersome analytical schemes.
2. The influence of the nonlinearities of the quantum kinetic equation on the mechanism of migration polarization in the HBC is analyzed. Quantum-mechanical relaxation parameters are obtained, which differ from the same parameters for the semiclassical kinetic model of proton relaxation [33,34] by additional quantum corrections $T_{\mathrm{Q}}(\mathrm{T}) = \frac{\pi^2 \varepsilon_0 \varepsilon_\infty \hbar}{\mathrm{d}^2 q^2 \mathrm{N}_{\mathrm{pr}}^{(0)}(\mathrm{T})}, \mathrm{N}_{\mathrm{pr}}^{(0)}(\mathrm{T})$.
3. At the theoretical level, the quantum-mechanical frequency-temperature dependences for the components of the complex dielectric permittivity (CDP) have been studied. The results of the calculations make it possible to proceed to a comparison of theory and experiment by numerically calculating the tangent of the dielectric loss angle in the HBC.
4. At the theoretical level, size effects were found in HBC, manifested in the shifts of low-temperature (50–100 K) maxima of the dielectric loss tangent towards ultra-low temperatures (4–25 K) with a decrease in the amplitudes of the maxima by 3–4 order in the case of a reduction in the thickness of the crystalline layer from 1–10 μm to 1–10 nm. This effect is explained by changes in the configuration of the discrete energy spectrum of protons when, at an HBC film thickness of 1–10 nm, the activation energy of low-temperature relaxers (protons) decreases to 0.01–0.03 eV (against 0.05–0.1 eV at 1–10 μm) and, for energy levels falling into an isolated potential well, quantum transparencies of the potential barrier (0.2–0.3) are anomalously high for protons. Thus, in HBC nanofilms, near ultra-low temperatures (4–25 K), the dielectric, due to the rearrangement of the hydrogen sublattice structure, passes into a quasi-ferroelectric state, which is also characterized by anomalously high values of the CDP real component (2.5–3.5 million).

7. Patents

Kalytka V.A., Baimukhanov Z.K., Bashirov A.V., Khanov T.A., Isaev V.L. Suleimanov S.R. Patent of the Republic of Kazakhstan for utility model. Universal setup for measuring the parameters of microscopic structural defects. No.5016, 6 May 2020.

Author Contributions: Conceptualization, V.K.; methodology, V.K.; software, V.K., A.B. (Aleksandr Bashirov), A.M., Y.N. and D.A.; validation, V.K., A.M., Y.N., A.A., D.A. and G.M.; formal analysis, V.K., Y.S., Y.N. and D.A.; investigation, V.K., A.M., Y.N., A.B. (Aleksandr Bashirov), G.M., A.A., A.B. (Arkadiy Bilichenko), D.Z., R.A., D.A. and Z.I.; resources, V.K., A.B. (Aleksandr Bashirov), A.M., Y.N., G.M., A.A., A.B. (Arkadiy Bilichenko), D.Z. and R.A.; data curation, V.K., Y.S. and Y.N.; writing—original draft preparation, V.K., Y.S. and Y.N.; writing—review and editing, V.K., Y.S. and Y.N.; visualization, A.A., A.B. (Arkadiy Bilichenko), D.Z. and R.A.; supervision, V.K. and Y.S.; project administration, V.K., A.M., Y.N. and Y.S.; funding acquisition, A.M., Y.N., G.M., A.A. and R.A. All authors have read and agreed to the published version of the manuscript.

Funding: This research was funded by the Ministry of Trade and Integration of the Republic of Kazakhstan (Grant No. BR19980899 "Development of a system for monitoring the geotechnical state of mine workings and quarries based on intelligent fiber-optic sensors").

Data Availability Statement: Not applicable.

Conflicts of Interest: The authors declare no conflict of interest.

Appendix A. Features of the Crystal Lattice (of Layered Crystals) and Mechanism of Proton Conductivity in HBC

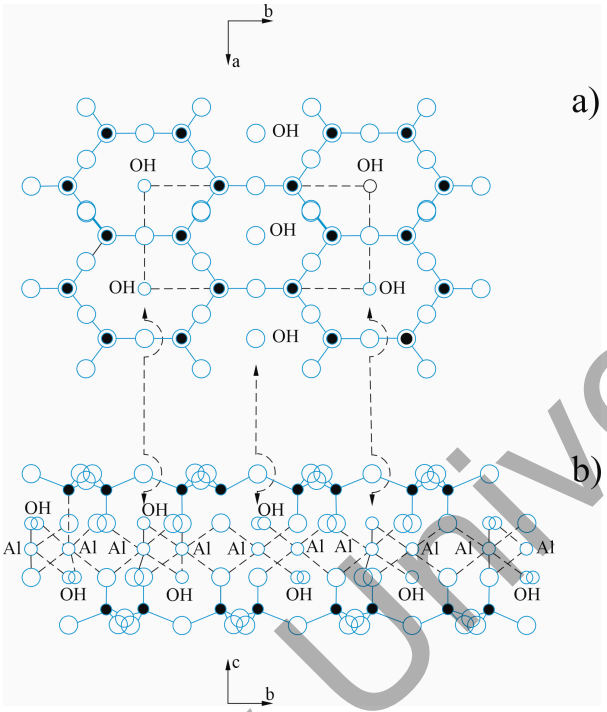

Figure A1. Fragments of the crystal structure of mica (**a**) the separate layer of hexagonal mesh of silica tetrahedra with hydroxyl ions located in the plane of the vertices of tetrahedra in the center of each hexagonal ring; (**b**) the side view of two similar layers with inwardly directed tetrahedron vertices of the formed double silicate layer. The relative orientation of the layers and the location of the A1 atoms (or Mg) between them is shown [83].

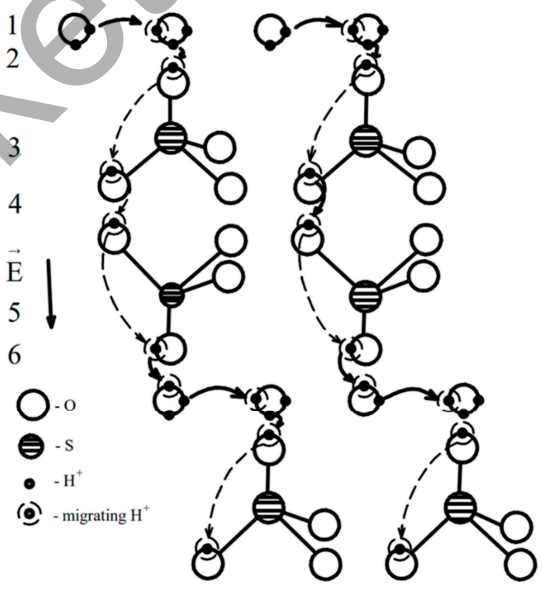

Figure A2. Scheme of the H_3O^+ ion movement due to the gradual transfer of the proton in a chalcanthite crystal $CuSO_4 \cdot 5H_2O$ [78].

The arrows show the movement of the proton, the numbers indicate the stages of its movement [78]:

1. Defect formation H_3O^+ in the water layer or due to the introduction of proton-donor impurities $H_2O + H^+ \rightarrow H_3O^+$.
2. Transition from ion H_3O^+ to anion SO_4^{2-}, the formation of a protonated anion HSO_4^-: $H_3O^+ + SO_4^{2-} \rightarrow H_2O + HSO_4^-$.
3. Reorientation of a protonated anion due to the transition of protons inside it: $HSO_4^- \rightarrow SO_4H^-$.
4. Transition of a proton between cells of the anionic sublattice, and the newly formed protonated anion acquires the opposite orientation: $SO_4H^- \rightarrow HSO_4^-$.
5. Reorientation of the second protonated anion: $HSO_4^- \rightarrow SO_4H^-$.
6. Transition of a proton to a water molecule and the formation of a defect H_3O^+: $SO_4H^- + H_2O \rightarrow SO_4^{2-} + H_3O^+$.

Appendix B. Thermally Stimulated Depolarization Currents Spectrum of Onot Talc

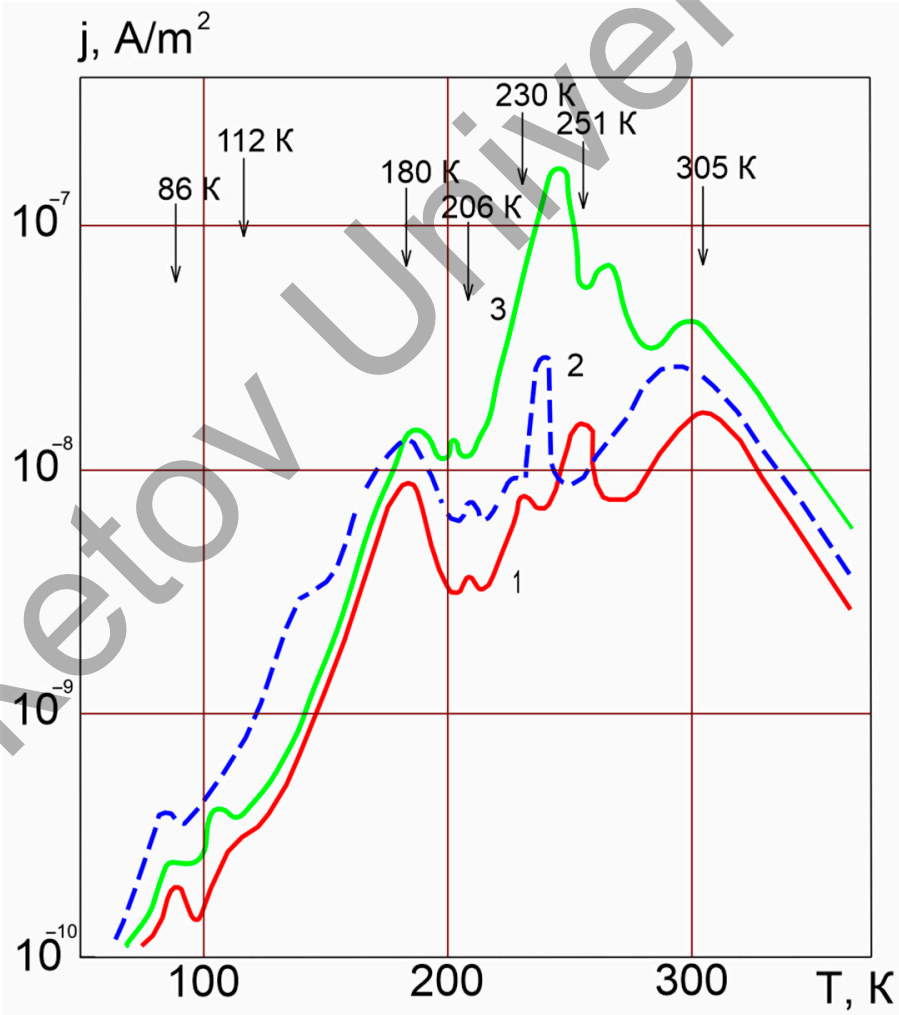

Figure A3. Thermally stimulated depolarization currents (TSDC) density spectrum of onot talc $Mg_3(Si_4O_{10})(OH)_2$ [78]. 1—natural mineral of onot talc $Mg_3(Si_4O_{10})(OH)_2$, 2—talc doped in hydrochloric acid solution ($n_{HCl} = 7.4 \times 10^{-5}$ mol/m^3). 3—talc doped in NH_4OH solution ($n_{NH_4OH} = 9.2 \times 10^{-5}$ mol/m^3). The measurements were carried out at $E_{pol,0} = 2 \times 10^5$ V $\times$ m^{-1}, T_{pol} = 300 K, c = 0.1 K $\times$ s^{-1} [91].

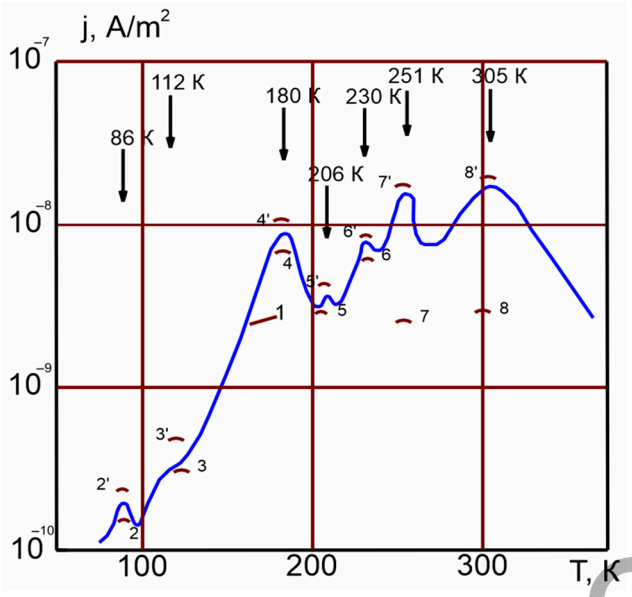

Figure A4. Graphs of TSDC density in onot talc: 1—experimental spectrum (graph 1 in Figure A3); 2–8, 2′–8′-theoretical charts, calculated according to the phenomenological Bucci-Riva theory, respectively, with (2′–8′) and without (2–8) proton tunneling [78].

Table A1. Relaxers parameters in natural mineral of onot talc $Mg_3(Si_4O_{10})(OH)_2$, calculated using the phenomenological theory of thermally stimulated depolarization currents (TSDC) for the parabolic potential barrier model (Graph 1 in Figure A3) [78].

Temperature of Experimental Maximum of TSDC	Type of Relaxer	Energy Activation U_0, eV			Balanced Concentration n_0, 10^{16} m^{-3}		
		Experimental [91]	Theoretical (Calculated upon Based the Expression (22) in [78])		Experimental (Calculating in This Paper)	Theoretical (Calculated upon Based the Expression (22) in [78]), 10^{16}	
			Without Respecting the Quantum Tunneling	With Respecting the Quantum Tunneling		Without Respecting the Quantum Tunneling	With Respecting the Quantum Tunneling
86	$HSiO_4^{3-}$	0.06 ± 0.01	0.12	0.06	1.4	1.5	1.4
112	H_3O^+	0.09 ± 0.02	0.19	0.18	1.3	1.33	1.29
180	H_2O—water molecules of crystallization (structural water)	0.19 ± 0.02	0.27	0.27	200	208	205
206	H_2O—adsorbed water molecules (on bundles)	0.25 ± 0.03	0.32	0.32	30	32	32
230	OH^-	0.32 ± 0.04	0.42	0.41	120	122	120
251	L,D-defects, VL,VD-complexes	0.41 ± 0.04	0.51	0.49	200	207	205
305	H_3O^+, OH^-, H^+	0.40 ± 0.06	0.49	0.43	4600	3900	4610

When calculating the TSDC-density spectrum in [78], the crystal thickness was taken to be 30 μm.

Appendix C. Investigation of the Temperature Dependence of $D_{stationary}(T)$

The results of the function calculations $D_{stationary}(T)$ are presented as graphs calculated at different thicknesses of the crystalline layer ($d = 10^{-9}$ m; $d = 10^{-8}$ m; $d = 10^{-7}$ m; $d = 10^{-6}$ m; $d = 10^{-5}$ m) for fixed values of activation energy: $U_0 = 0.01$ eV, $U_0 = 0.03$ eV, $U_0 = 0.05$ eV, $U_0 = 0.07$; $U_0 = 0.1$ eV. These charts are labeled: $1 - D^{classic}_{term;stationary}(T)$; $2 - D^{q.-classic}_{quant,tunn;stationary}(T)$; $3 - D^{non.-deg.}_{quant,tunn;stationary}(T)$; $4 - D^{deg.}_{quant,tunn;stationary}(T)$.

Appendix C.1. For the Activation Energy $U_0 = 0.01$ eV

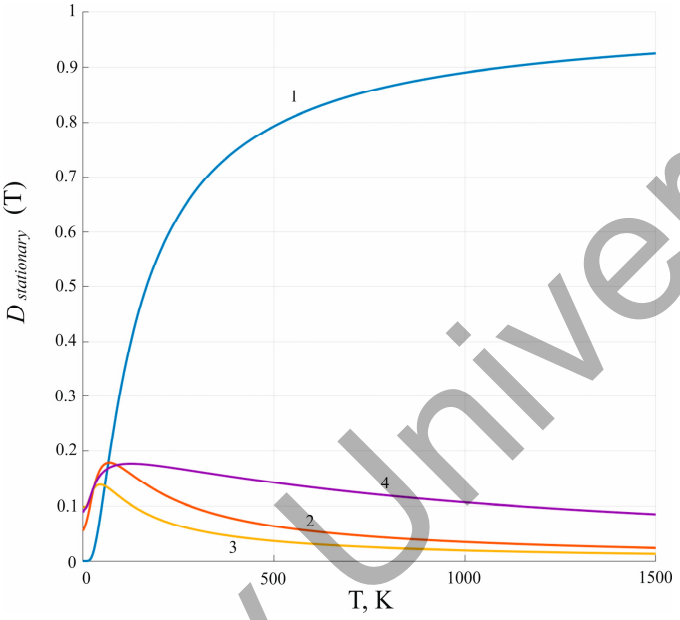

Figure A5. $d = 10^{-9}$ m.

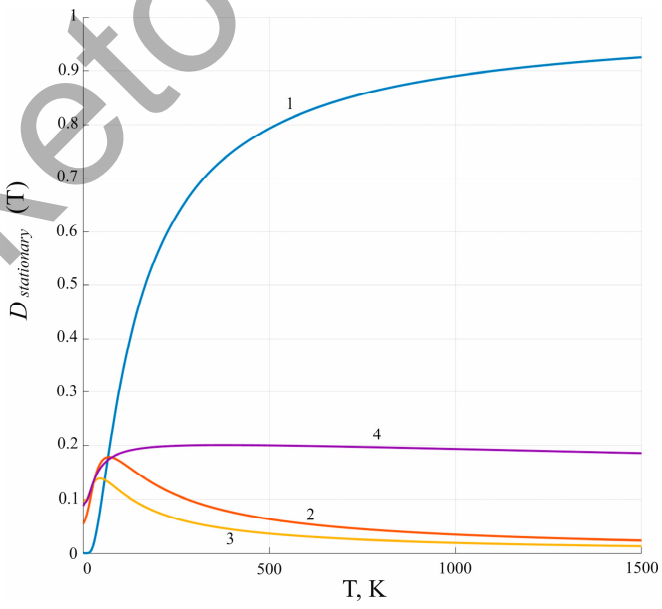

Figure A6. $d = 10^{-8}$ m.

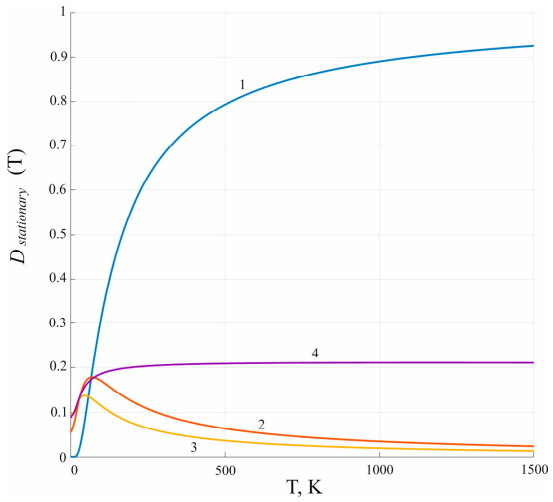

Figure A7. d = 10^{-7} m.

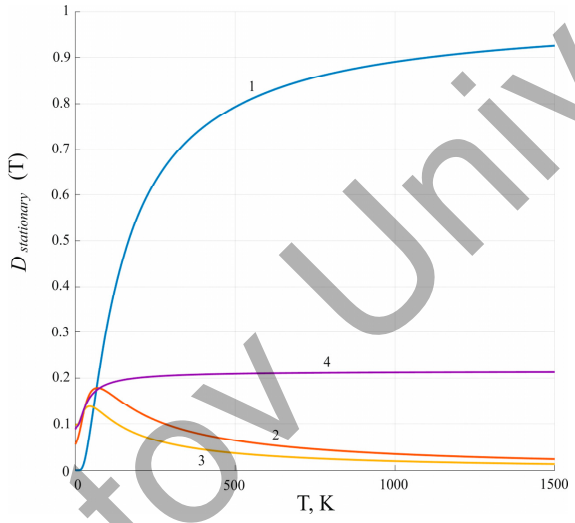

Figure A8. d = 10^{-6} m.

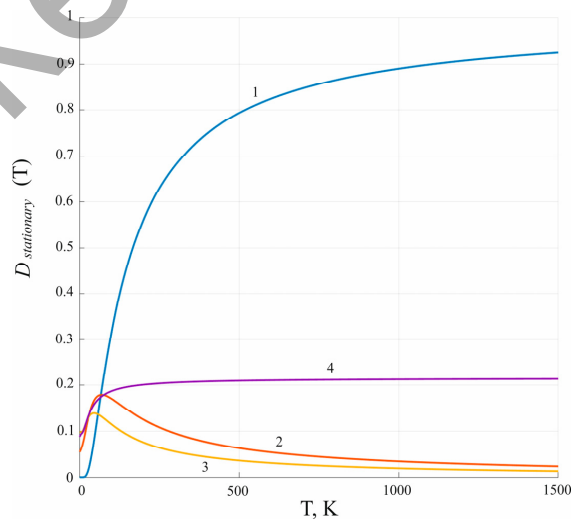

Figure A9. d = 10^{-5} m.

Appendix C.2. For the Activation Energy $U_0 = 0.03\ eV$

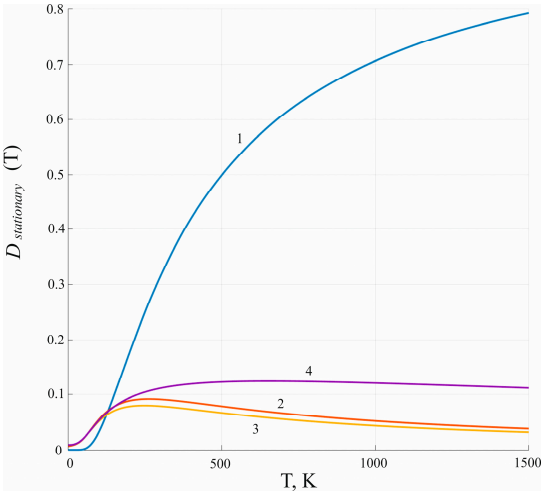

Figure A10. d $= 10^{-9}$ m.

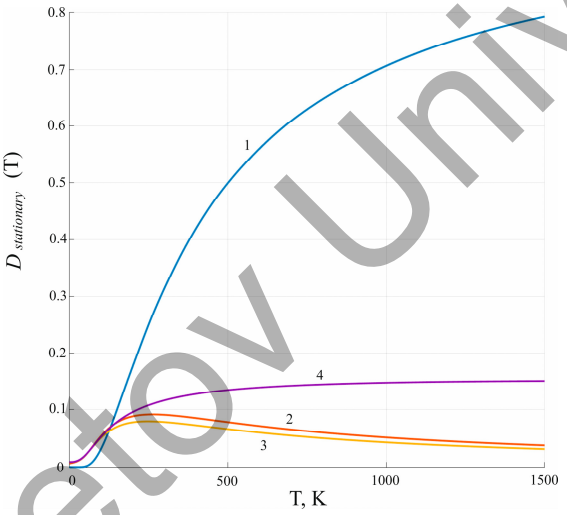

Figure A11. d $= 10^{-8}$ m.

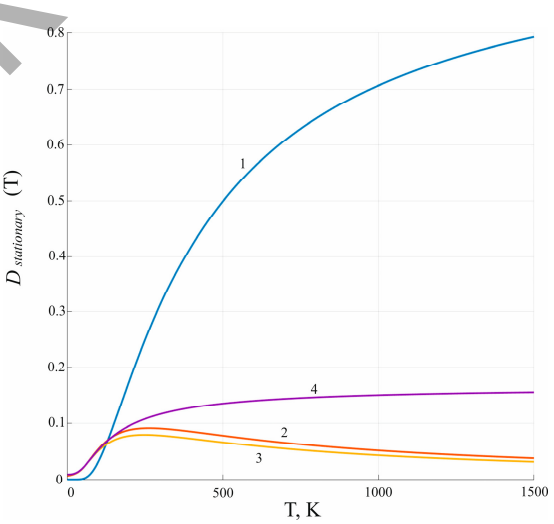

Figure A12. d $= 10^{-7}$ m.

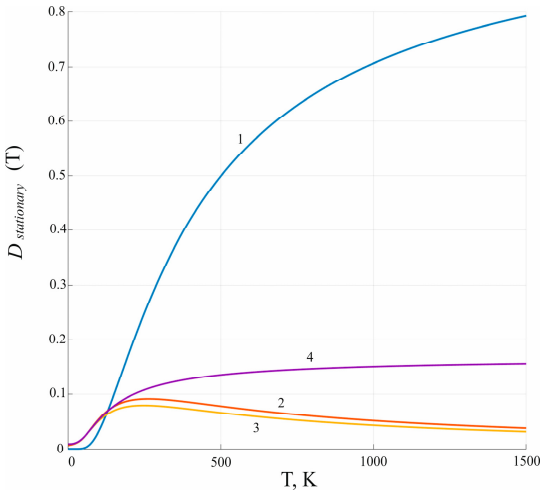

Figure A13. d $= 10^{-6}$ m.

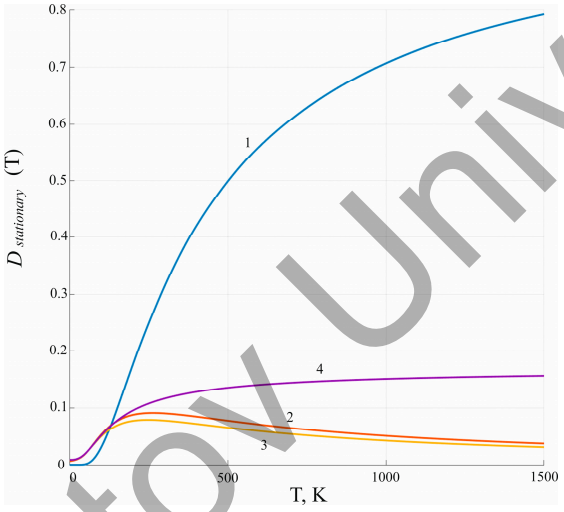

Figure A14. d $= 10^{-5}$ m.

Appendix C.3. For the Activation Energy $U_0 = 0.05\ eV$

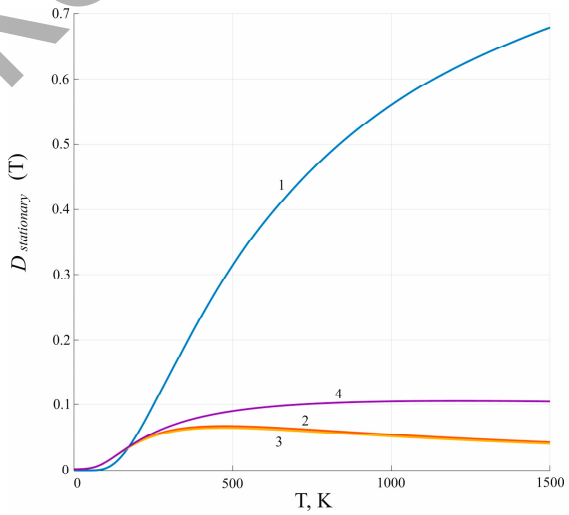

Figure A15. d $= 10^{-9}$ m.

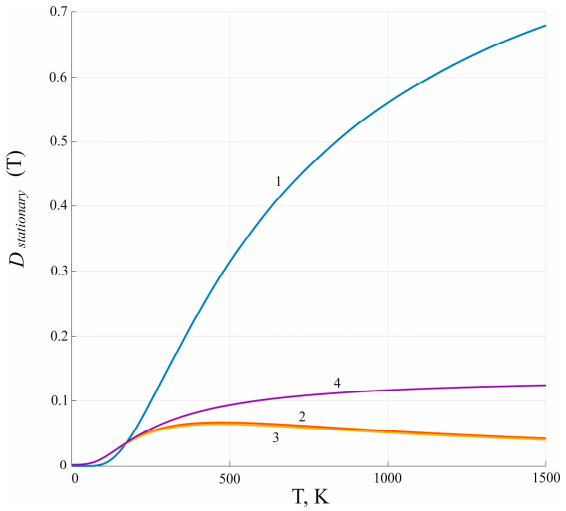

Figure A16. d = 10^{-8} m.

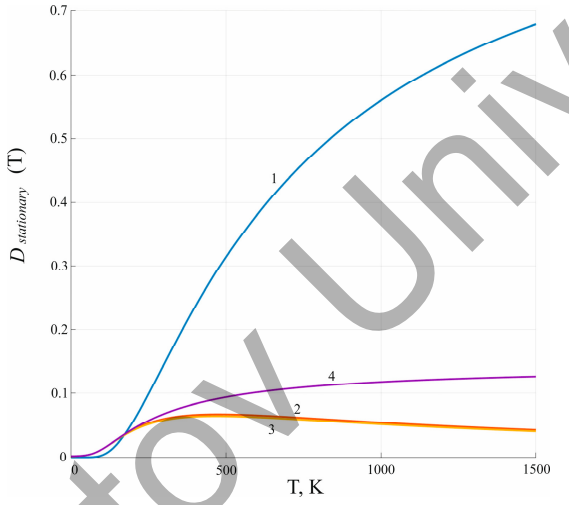

Figure A17. d = 10^{-7} m.

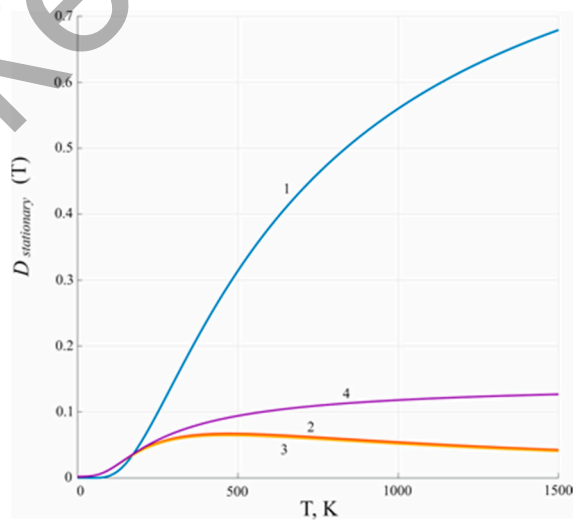

Figure A18. d = 10^{-6} m.

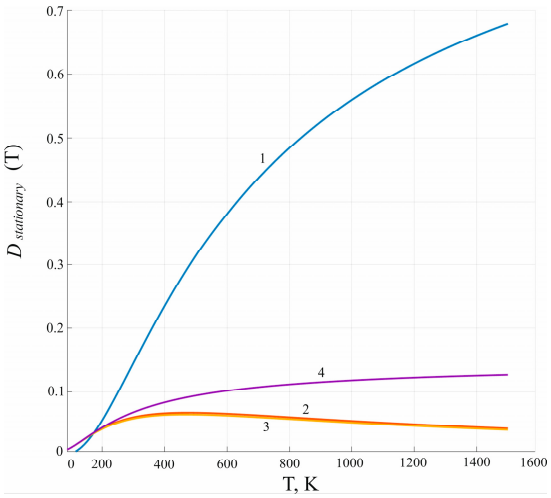

Figure A19. d $= 10^{-5}$ m.

Appendix C.4. For the Activation Energy $U_0 = 0.07$ *eV*

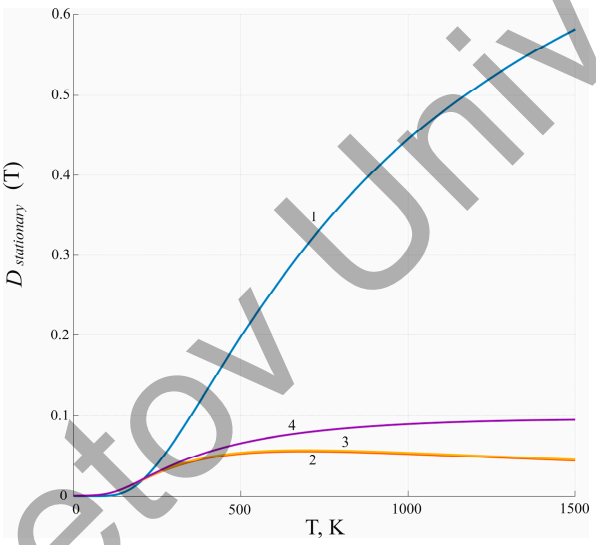

Figure A20. d $= 10^{-9}$ m.

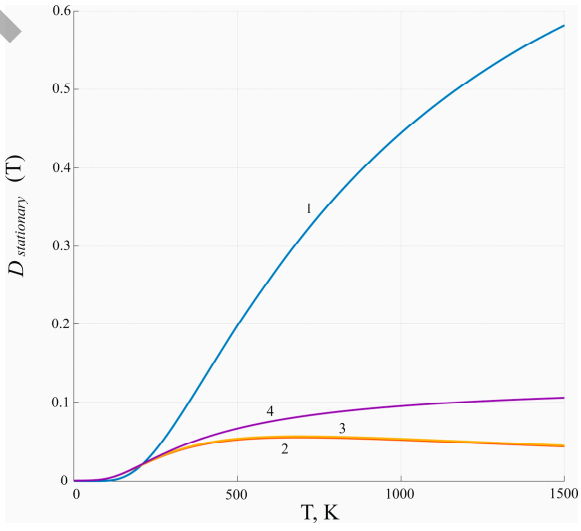

Figure A21. d $= 10^{-8}$ m.

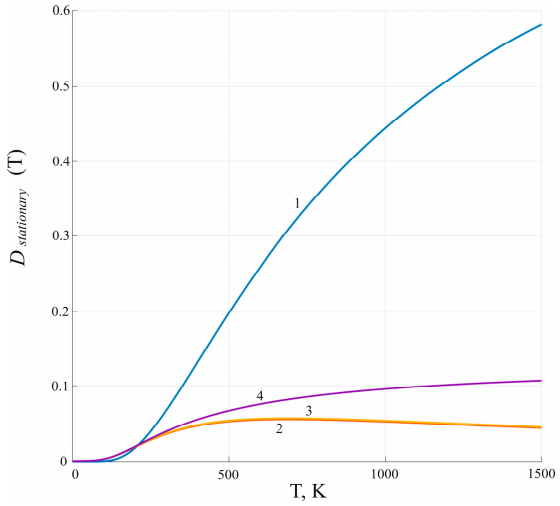

Figure A22. d = 10^{-7} m.

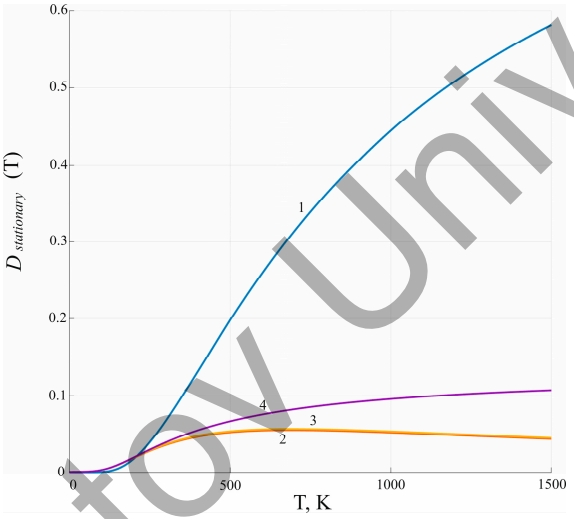

Figure A23. d = 10^{-6} m.

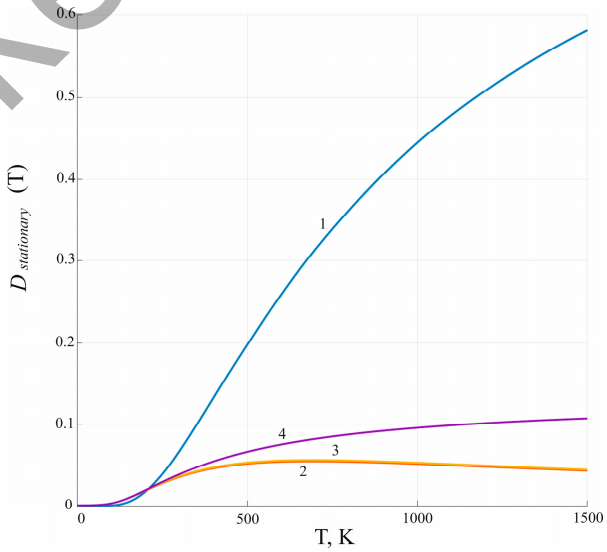

Figure A24. d = 10^{-5} m.

Appendix C.5. For the Activation Energy $U_0 = 0.1\ eV$

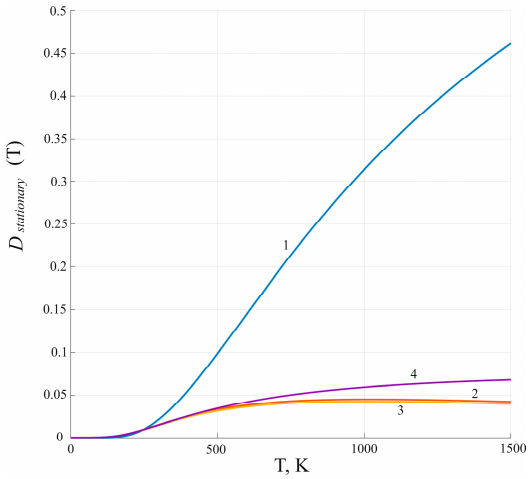

Figure A25. d $= 10^{-9}$ m.

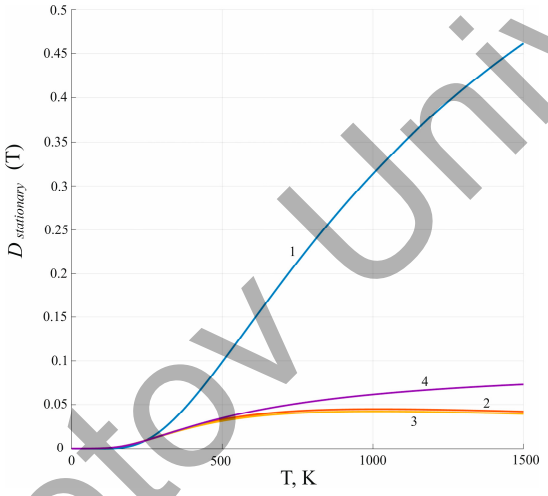

Figure A26. d $= 10^{-8}$ m.

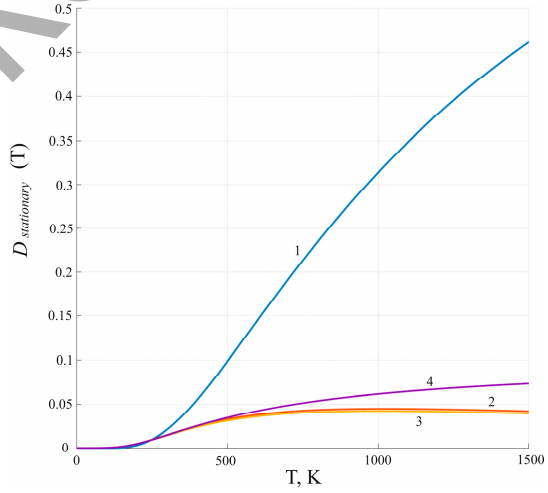

Figure A27. d $= 10^{-7}$ m.

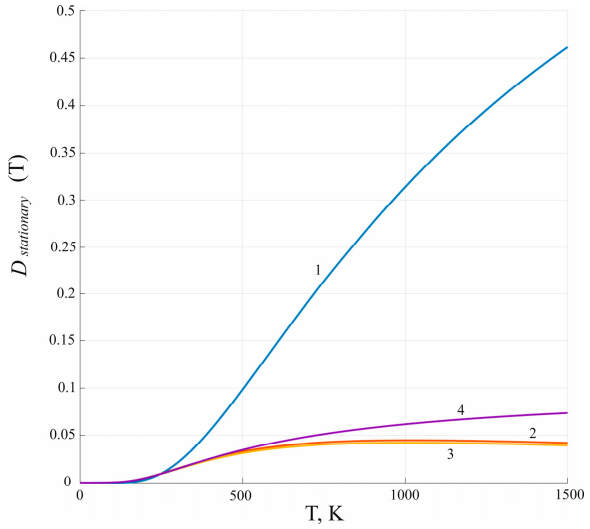

Figure A28. d $= 10^{-6}$ m.

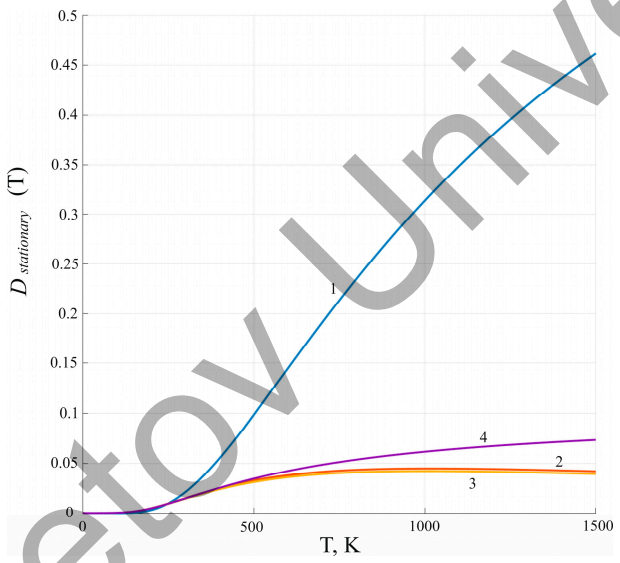

Figure A29. d $= 10^{-5}$ m.

Figures A5, A10, A14, A19 and A24 coincide with Figures 3–7 respectively, and represent the theoretical temperature spectra of stationary quantum transparency $D_{stationary}(\mathrm{T})$ calculated for the different value of the proton activation energy $\mathrm{U}_0 = 0.01$ eV, $\mathrm{U}_0 = 0.03$ eV, $\mathrm{U}_0 = 0.05$ eV, $\mathrm{U}_0 = 0.07$; $\mathrm{U}_0 = 0.1$ eV at the thicknesses of the crystalline layer d $= 10^{-9}$ m.

References

1. Annenkov, Y.M.; Ivashutenko, A.S.; Vlasov, I.V.; Kabyshev, A.V. Electric properties of Coronado-Zirconium ceramics. *Proc. Tomsk Polytech. Univ.* **2005**, *308*, 35–38.
2. Abrikosov, A.A. Resonance tunneling in high-temperature superconductors. *UspekhiFiz. Nauk.* **1998**, *168*, 683–695. [CrossRef]
3. Pozdnyakov, A.A.; Sultanaev, R.M.; Kiselev, V.I. Phenomenological theory of relaxation polarization of dielectrics. *Russ. Phys. J.* **1992**, *35*, 35–39. [CrossRef]
4. Ktitorov, S.A. On the determination of the distribution function of relaxation times in terms of dielectric losses. *Tech. Phys. Lett.* **2003**, *29*, 74–79. [CrossRef]
5. Marichev, V.A. Anomalous electrical conductivity of aqueous solutions in submicron cracks and gaps. *J. Appl. Electrochem.* **2005**, *35*, 17. [CrossRef]
6. Movchikova, A.; Malyshkina, O.V.; Pedko, B.B.; Suchaneck, G.; Gerlach, G. Thermal wave study of piezoelectric coefficient distribution in PMN-PT single crystals. *Adv. Appl. Ceram.* **2010**, *109*, 131–134. [CrossRef]

7. Mukhortov, V.M.; Golovko, Y.I.; Mamatov, A.A.; Zhigalina, O.M.; Kuskova, A.N.; Chuvilin, A.L. Influence of Internal Deformation Fields on the Controllability of Nanosized Ferroelectric Films in a Planar Capacitor. *Tech. Phys. Lett.* **2010**, *80*, 77–82. Available online: https://journals.ioffe.ru/articles/viewPDF/9945 (accessed on 23 July 2023).
8. Movchikova, A.A.; Malyshkina, O.V.; Pedko, B.B.; Lisitsin, V.S.; Burtsev, A.V. Influence of thermocycling on the polarization distribution of doped SBN crystals. *Ferroelectrics* **2010**, *399*, 14–19. [CrossRef]
9. Efremova, P.V.; Ped'ko, B.B.; Kuznecova, Y.V. Structural examination of lithium niobate ferroelectric crystals by combining scanning electron microscopy and atomic force microscopy. *Tech. Phys.* **2016**, *61*, 313–315. [CrossRef]
10. Yaroslavtsev, A.B. Ion Diffusion Throw Interface in Heterogeneous Solid Systems with the Modified Surface. *Defect Diffus. Forum* **2003**, *216–217*, 133–140. [CrossRef]
11. Dadayan, A.K.; Borisov, Y.A.; Zolotarev, Y.A.; Bocharov, E.V.; Nagaev, I.Y.; Myasoedov, N.F. Solid-State Catalytic Hydrogen/Deuterium Exchange in Mexidol Russ. *J. Phys. Chem.* **2021**, *95*, 273–278. [CrossRef]
12. Yaroslavtsev, A.B. Perfluorinated ion-exchange membranes. *Polym. Sci. Ser. A* **2013**, *55*, 674–698. [CrossRef]
13. Yaroslavtsev, A.B. Solid electrolytes: Main prospects of research and development. *Russ. Chem. Rev.* **2016**, *85*, 1255–1276. [CrossRef]
14. Yaroslavtsev, A.B. Proton conductivity of inorganic hydrates. *Russ. Chem. Rev.* **1994**, *63*, 429–435. [CrossRef]
15. Gaffar, M.A.; Al-Fadl, A.A. Effect of Doping and Irradiation on Optical Parameters of TriglycineSulphate Single Crystals. *Cryst. Res. Technol.* **1999**, *34*, 915–923. [CrossRef]
16. Prokopova, L.; Novotny, J.; Micka, Z.; Malina, V. Growth of TriglycineSulphate Single Crystal Doped by Cobalt (II) Phosphate. *Cryst. Res. Technol.* **2001**, *36*, 1189–1195. [CrossRef]
17. Ragahvan, C.M.; Sankar, R.; Mohankumar, R.; Jayavel, R. Effect of Amino Acid Doping on The Growth and Ferroelectric Properties of TriglycineSulphate Single Crystals. *Mater. Res. Bull.* **2008**, *43*, 305–311. [CrossRef]
18. Sun, X.; Wang, M.; Pan, Q.W.; Shi, W.; Fang, C.S. Study on the Growth and Properties of Guanidine Doped Triglycine Sulfate Crystal. *Cryst. Res. Technol.* **1999**, *34*, 1251–1254. [CrossRef]
19. Farhana, K.; Jiban, P. Structural and Optical Properties of Triglycine Sulfate Single Crystals Doped with Potassium Bromide. *J. Crystall. Process Technol.* **2011**, *1*, 26–31. Available online: https://www.scirp.org/html/3-1010007_6553.htm (accessed on 24 July 2023). [CrossRef]
20. Strukov, B.A.; Yakushkin, E.D. Local sound velocity and growth defects in triglycinesulfate crystals. *Phys. Solid State* **1978**, *20*, 1551–1553.
21. Shut, V.N.; Kashevich, I.F.; Syrtsov, S.R. Ferroelectric Properties of Triglycine Sulfate Crystals with a Non-uniform distribution of Chromium Impurities. *Phys. Solid State* **2008**, *50*, 118–121. [CrossRef]
22. Genbo, S.; Youping, H.; Hongshi, Y.; Zikong, S.; Qingin, E. A New Pyroelectric Crystal Lysine-Doped TGS (LLTGS). *J. Cryst. Growth* **2000**, *209*, 220–222. [CrossRef]
23. Aravazhi, S.; Jayavel, R.; Subramanian, C. Growth and Characterization of H-Benzophenone and Urea Doped TriglycineSulphate Crystals. *Ferroelectrics* **1997**, *200*, 279–286. [CrossRef]
24. Belonenko, M.B. Characteristic features of nonlinear dynamics of a laser pulse in a photorefractive ferroelectric with hydrogen bonds. *Quantum Electron.* **1998**, *28*, 247–250. [CrossRef]
25. Volk, T. Ferroelectric phenomena in holographic properties of strontium-barium niobate crystals doped with rare-earth elements. *Ferroelectrics* **1997**, *203*, 457–470. Available online: https://scienceon.kisti.re.kr/srch/selectPORSrchArticle.do?cn=NART06221101 (accessed on 23 July 2023). [CrossRef]
26. Lebedev, N.G.; Litinsky, A.O. Model of an ion-embedded stoichiometric cluster for calculating the electronic structure of ionic crystals. *Phys. Solid State* **1996**, *38*, 959–962. Available online: https://journals.ioffe.ru/articles/viewPDF/17380 (accessed on 23 July 2023).
27. Abrahams, S.C.; Kurtz, S.K.; Jamieson, P.B. Atomic displacement relationship to Curie temperature and spontaneous polarization in displacive ferroelectrics. *Phys. Rev.* **1968**, *172*, 551–553. [CrossRef]
28. Kulagin, I.A. Components of the third-order nonlinear susceptibility tensors in KDP, DKDP and $LiNbO_3$nonlinear optical crystals. *Quantum Electron.* **2004**, *34*, 657. Available online: https://iopscience.iop.org/article/10.1070/QE2004v034n07ABEH002823 (accessed on 23 July 2023). [CrossRef]
29. Park, M.H.; Lee, Y.H.; Kim, H.J.; Kim, Y.J.; Moon, T.; Kim, K.D.; Müller, J.; Kerch, A.; Schroeder, U.; Mikolajick, T.; et al. Ferroelectricity and Antiferroelectricity of Doped Thin HfO2-Based Films. *Adv. Mater.* **2015**, *27*, 1811–1831. [CrossRef] [PubMed]
30. Müller, J.; Böscke, T.S.; Bräuhaus, D.; Schröder, U.; Böttger, U.; Sundqvist, J.; Kücher, P.; Mikolajick, T.; Frey, L. Ferroelectric $Zr_{0.5}Hf_{0.5}O_2$ thin films for nonvolatile memory applications. *Appl. Phys. Lett.* **2011**, *99*, 112901. [CrossRef]
31. Lee, S.-S.; Noh, K.-H.; Kang, H.-B.; Hong, S.-K.; Yeom, S.-J.; Park, Y.-J. Characterization of Hynix 16M FERAM adopted novel sensing scheme. *Integr. Ferroelectr.* **2003**, *53*, 343–351. [CrossRef]
32. Malyshkina, O.V.; Movchikova, A.A.; Pedko, B.B.; Boitsova, K.N.; Kiselev, D.A.; Kholkin, A.L. Influence of Eu and Rh impurities on distribution of polarization of strontium-barium niobate crystals. *Ferroelectrics* **2008**, *373*, 114–120. [CrossRef]
33. Kapphan, S.; Pankrath, R.; Kislova, I.; Pedko, B.; Trepakov, V.; Savinov, M. Variation of doping-dependent properties in photorefractive $Sr_xBa_{(1-x)}Nb_2O_6$: Ce, Cr, Ce + Cr. *Radiat. Eff. Defects Solids* **2002**, *157*, 1033–1037. [CrossRef]
34. Arimoto, Y.; Ishiwara, H. Current status of ferroelectric random-access memory. *MRS Bull.* **2004**, *29*, 823–828. [CrossRef]

35. Moise, T.S.; Summerfelt, S.R.; McAdams, H.; Aggarwal, S.; Udayakumar, K.R.; Celii, F.G.; Martin, J.S.; Xing, G.; Hall, L.; Taylor, K.J.; et al. Demonstration of a 4 Mb, high density ferroelectric memory embedded within a 130 nm, 5 LM Cu/FSG logic process. In Proceedings of the International Electron Devices Meeting (IEDM'02), San Francisco, CA, USA, 8–11 December 2002; pp. 535–538. [CrossRef]
36. Rodriguez, J.A.; Remack, K.; Boku, K.; Udayakumar, K.R.; Aggarwal, S.; Summerfelt, S.R.; Celii, F.G.; Martin, S.; Hall, L.; Taylor, K.; et al. Reliability properties of low voltage ferroelectric capacitors and memory arrays. *IEEE Trans. Device Mater. Reliab.* **2004**, *4*, 436–449. [CrossRef]
37. Kim, K.; Lee, S. Integration of lead zirconium titanate thin films for high density ferroelectric random access memory. *J. Appl. Phys.* **2006**, *100*, 051604. [CrossRef]
38. Park, Y.; Lee, J.H.; Koo, J.M.; Kim, S.P.; Shin, S.; Cho Ch., R.; Lee, J.K. Preparation of $Pb(Zr_xTi_{1-x})O_3$ films on trench structure for high-density ferroelectric random access memory. *Integral Ferroelectr.* **2004**, *66*, 85–95. [CrossRef]
39. Shin, S.; Han, H.; Park, Y.J.; Choi, J.Y.; Park, Y.; Baik, S. Characterization of 3D Trench PZT Capacitors for High Density FRAM Devices by Synchrotron X-ray Micro-diffraction. *AIP Conf. Proc.* **2007**, *879*, 1554–1556. [CrossRef]
40. Zhou, Z.; Bowland, C.C.; Patterson, B.A.; Malakooti, M.H.; Sodano, H.A. Conformal $BaTiO_3$ films with high piezoelectric coupling through an optimized hydrothermal synthesis. *ACS Appl. Mater. Interfaces* **2016**, *8*, 21446–21453. [CrossRef]
41. Schroeder, U.; Yurchuk, E.; Müller, J.; Martin, D.; Schenk, T.; Polakowski, P.; Adelmann, C.; Popovici, M.I.; Kalinin, S.V.; Mikolajick, T. Impact of different dopants on the switching properties of ferroelectric hafnium oxide. *Jpn. J. Appl. Phys.* **2014**, *53*, 08LE02. [CrossRef]
42. Müller, J.; Yurchuk, E.; Schlösser, T.; Paul, J.; Hoffmann, R.; Müller, S.; Martin, D.; Slesazeck, S.; Polakowski, P.; Sundqvist, J.; et al. Ferroelectricity in HfO2 enables nonvolatile data storage in 28 nm HKMG. In Proceedings of the VLSI Technology (VLSIT) Symposium on IEEE, Honolulu, HI, USA, 12–14 June 2012; pp. 25–26. [CrossRef]
43. Pešić, M.; Schroeder, U.; Mikolajick, T. Ferroelectric One Transistor/One Capacitor Memory Cell. In *Ferroelectricity in Doped Hafnium Oxide: Materials, Properties and Devices*; Schroeder, U., Hwang, C., Funakubo, H., Eds.; Woodhead Publishing: Sawston, UK, 2019; pp. 413–424. [CrossRef]
44. Chernikova, A.G.; Kozodaev, M.G.; Negrov, D.V.; Korostylev, E.V.; Park, M.H.; Schroeder, U.; Hwang, C.S.; Markeev, A.M. Improved ferroelectric switching endurance of La-doped $Hf_{0.5}Zr_{0.5}O_2$ thin films. *ACS Appl. Mater. Interfaces* **2018**, *10*, 2701–2708. [CrossRef]
45. Delimova, L.; Guschina, E.; Zaitseva, N.; Pavlov, S.; Seregin, D.; Vorotilov, K.; Sigov, A. Effect of seed layer with low lead content on electrical properties of PZT thin films. *J. Mater. Res.* **2017**, *32*, 1618–1627. [CrossRef]
46. Park, J.H.; Kim, H.Y.; Seok, K.H.; Kiaee, Z.; Lee, S.K.; Joo, S.K. Multibit ferroelectric field-effect transistor with epitaxial-like $Pb(Zr,Ti)O_3$. *J. Appl. Phys.* **2016**, *119*, 124108. [CrossRef]
47. Park, J.H.; Joo, S.K. A Novel Metal-Ferroelectric-Insulator-Silicon FET With Selectively Nucleated Lateral Crystallized Pb $(Zr,Ti)O_3$ and $ZrTiO_4$ Buffer for Long Retention and Good Fatigue. *IEEE Electron. Device Lett.* **2015**, *36*, 1033–1036. [CrossRef]
48. Hu, J.M.; Chen, L.Q.; Nan, C.W. Multiferroicheterostructures integrating ferroelectric and magnetic materials. *Adv. Mater.* **2016**, *28*, 15–39. [CrossRef]
49. Magdău, I.B.; Liu, X.-H.; Kuroda, M.A.; Shaw, T.M.; Crain, J.; Solomon, P.M.; Newns, D.M.; Martyna, G.J. The piezoelectronic stress transduction switch for very large-scale integration, low voltage sensor computation, and radio frequency applications. *Appl. Phys. Lett.* **2015**, *107*, 073505. [CrossRef]
50. Chang, J.B.; Miyazoe, H.; Copel, M.; Solomon, P.M.; Liu, X.-H.; Shaw, T.M.; Schrott, A.G.; Gignac, L.M.; Martyna, G.J.; Newns, D.M. First realization of the piezoelectric stress-based transduction device. *Nanotechnology* **2015**, *26*, 375201. [CrossRef]
51. Newns, D.; Elmegreen, B.; Liu, X.H.; Martyna, G.J. A low-voltage high-speed electronic switch based on piezoelectric transduction. *J. Appl. Phys.* **2012**, *111*, 084509. [CrossRef]
52. Newns, D.M.; Elmegreen, B.G.; Liu, X.H.; Martyna, G.J. High response piezoelectric and piezoresistive materials for fast, low voltage switching: Simulation and theory of transduction physics at the nanometer-scale. *Adv. Mater.* **2012**, *24*, 3672–3677. [CrossRef]
53. Newns, D.M.; Elmegreen, B.G.; Liu, X.H.; Martyna, G.J. The piezoelectronic transistor: A nanoactuator-based post-CMOS digital switch with high speed and low power. *MRS Bull.* **2012**, *37*, 1071–1076. [CrossRef]
54. Doh, Y.J.; Yi, G.C. Nonvolatile memory devices based on few-layer graphene films. *Nanotechnology* **2010**, *21*, 105204. [CrossRef]
55. Xie, L.; Chen, X.; Dong, Z.; Yu, Q.; Zhao, X.; Yuan, G.; Zeng, Z.; Wang, Y.; Zhang, K. Nonvolatile Photoelectric Memory Induced by Interfacial Charge at a Ferroelectric PZT-Gated Black Phosphorus Transistor. *Adv. Electron. Mater.* **2019**, *5*, 1900458. [CrossRef]
56. Shen, P.C.; Lin, C.; Wang, H.; Teo, K.H.; Kong, J. Ferroelectric memory field-effect transistors using CVD monolayer MoS_2 as resistive switching channel. *Appl. Phys. Lett.* **2020**, *116*, 033501. [CrossRef]
57. McGuire, F.A.; Lin, Y.C.; Price, K.; Rayner, G.B.; Khandelwal, S.; Salahuddin, S.; Franklin, A.D. Sustained sub-60 mV/decade switching via the negative capacitance effect in MoS_2 transistors. *Nano Lett.* **2017**, *17*, 4801–4806. [CrossRef] [PubMed]
58. Alam, M.A.; Si, M.; Ye, P.D. A critical review of recent progress on negative capacitance field-effect transistors. *Appl. Phys. Lett.* **2019**, *114*, 090401. [CrossRef]
59. Stadler, H.L. Ferroelectric switching time of $BaTiO_3$ crystals at high voltages. *J. App. Phys.* **1958**, *29*, 1485–1487. [CrossRef]
60. Scott, J.F.; McMillan, L.D.; Araujo, C.A. Switching kinetics of lead zirconate titanate sub-micron thin-film memories. *Ferroelectrics* **1989**, *93*, 31–36. [CrossRef]

61. Li, J.; Nagaraj, B.; Liang, H.; Cao, W.; Lee, C.H.; Ramesh, R. Ultrafast polarization switching in thin-film ferroelectrics. *Appl. Phys. Lett.* **2004**, *84*, 1174–1176. [CrossRef]
62. Ishii, H.; Nakajima, T.; Takahashi, Y.; Furukawa, T. Ultrafast polarization switching in ferroelectric polymer thin films at extremely high electric fields. *Appl. Phys. Express* **2011**, *4*, 031501. [CrossRef]
63. Mulaosmanovic, H.; Ocker, J.; Muller, S.; Schroeder, U.; Muller, J.; Polakowski, P.; Slesazeck, S. Switching kinetics in nanoscale hafnium oxide based ferroelectric field-effect transistors. *ACS Appl. Mater. Interfaces* **2017**, *9*, 3792–3798. [CrossRef] [PubMed]
64. Liu, Z.Q.; Liu, J.H.; Biegalski, M.D.; Hu, J.M.; Shang, S.L.; Ji, Y.; Wang, J.M.; Hsu, S.L.; Wong, A.T.; Cordill, M.J.; et al. Electrically reversible cracks in an intermetallic film controlled by an electric field. *Nat. Commun.* **2018**, *9*, 41. [CrossRef] [PubMed]
65. Oh, S.; Hwang, H.; Yoo, I.K. Ferroelectric materials for neuromorphic computing. *APL Mater.* **2019**, *7*, 091109. [CrossRef]
66. Ishibashi, Y.; Takagi, Y. Note on ferroelectric domain switching. *J. Phys. Soc. Jpn.* **1971**, *31*, 506–510. [CrossRef]
67. Ishiwara, H. Proposal of adaptive-learning neuron circuits with ferroelectric analog-memory weights. *Jpn. J. Appl. Phys.* **1993**, *32*, 442–446. [CrossRef]
68. Jerry, M.; Dutta, S.; Kazemi, A.; Ni, K.; Zhang, J.; Chen, P.Y.; Datta, S. A ferroelectric field effect transistor based synaptic weight cell. *J. Phys. D Appl. Phys.* **2018**, *51*, 434001. [CrossRef]
69. Seo, M.; Kang, M.H.; Jeon, S.B.; Bae, H.; Hur, J.; Jang, B.C.; Hwang, K.M. First demonstration of a logic-process compatible junctionless ferroelectric FinFET synapse for neuromorphic applications. *IEEE Electr. Device Lett.* **2018**, *39*, 1445–1448. [CrossRef]
70. Kim, M.K.; Lee, J.S. Ferroelectric analog synaptic transistors. *Nano Lett.* **2019**, *19*, 2044–2050. [CrossRef]
71. Boyn, S.; Grollier, J.; Lecerf, G.; Xu, B.; Locatelli, N.; Fusil, S.; Girod, S.; Carretero, C.; Garcia, K.; Xavier, S.; et al. Learning through ferroelectric domain dynamics in solid-state synapses. *Nat. Commun.* **2017**, *8*, 14736. [CrossRef]
72. Kalytka, V.A.; Mekhtiev, A.D.; Bashirov, A.V.; Yurchenko, A.V.; Al'Kina, A.D. Nonlinear Electrophysical Phenomena in Ionic Dielectrics with a Complicated Crystal Structure. *Russ. Phys. J.* **2020**, *63*, 282–289. [CrossRef]
73. Kalytka, V.A.; Bashirov, A.V.; Taranov, A.V.; Tatkeyeva, G.G.; Neshina, Y.G.; Sidorina, Y.A. Methods of Theoretical Researches the Properties of Electrotechnical Materials Class of Dielectrics with Hydrogen Bonds. *J. Comput. Theor. Nanosci.* **2019**, *16*, 2799–2804. [CrossRef]
74. Kalytka, V.A.; Bashirov, A.V.; Tatkeyeva, G.G.; Sidorina, Y.A.; Ospanov, B.S.; Ten, T.L. The impact of the nonlinear effects on thermally stimulated depolarization currents in ion dielectrics. *Period. Eng. Nat. Sci.* **2021**, *9*, 195–217. [CrossRef]
75. Kalytka, V.A.; Bulatbayev, F.; Neshina, Y.; Bilichenko, Y.; Bilichenko, A.; Bashirov, A.; Sidorina, Y.; Naboko, Y.; Malikov, N.; Senina, Y. Theoretical Studies of Nonlinear Relaxation Electrophysical Phenomena in Dielectrics with Ionic–Molecular Chemical Bonds in a Wide Range of Fields and Temperatures. *Appl. Sci. Sect. Appl. Phys.* **2022**, *12*, 6555. [CrossRef]
76. Annenkov, Y.M.; Kalytka, V.; Korovkin, M.V. Quantum Effects Under Migratory Polarization in Nanometer Layers of Proton Semiconductors and Dielectrics at Ultralow Temperatures. *Russ. Phys. J.* **2015**, *58*, 35–41. [CrossRef]
77. Kalytka, V.A.; Mekhtiyev, A.D.; Bashirov, A.V.; Madi, P.S. Quantum-mechanical model of dielectric losses in nanometer layers of solid dielectrics with hydrogen bonds at ultra-low temperatures. *IOP Conf. Ser. J. Phys.* **2021**, *2104*, 012028. [CrossRef]
78. Kalytka, V.A.; Neshina, Y.; Baimukhanov, Z.; Mekhtiyev, A.; Dunayev, P.; Galtseva, O.; Senina, Y. Influence of Quantum Effects on Dielectric Relaxation in Functional Electrical and Electric Energy Elements Based on Proton Semiconductors and Dielectrics. *Appl. Sci. Sect. Appl. Phys.* **2023**, *13*, 8755. [CrossRef]
79. Kalytka, V.A.; Neshina, Y.G.; Madi, P.S.; Naboko, Y.P. Methods of theoretical researches the non-linear electrophysical properties of solid dielectrics with compound crystalline structure. *IOP Conf. Ser. Mater. Sci. Eng.* **2019**, *698*, 022002. [CrossRef]
80. Kalytka, V.A. Investigating the scheme of numerical calculation the parameters of non-linear electrophysical processes by minimizing comparison function method. *Space Time Fundam. Interact.* **2018**, *3*, 68–77. Available online: https://stfi.ru/ru/issues/2018/03/STFI_2018_03_Kalytka.html (accessed on 23 July 2023). [CrossRef]
81. Kalytka, V.A.; Korovkin, M.V. Quantum Effects at a Proton Relaxation at Low Temperatures. *Russ. Phys. J.* **2016**, *59*, 994–1001. [CrossRef]
82. Kalytka, V.; Korovkin, M.V.; Madi, P.S.; Magauin, B.K.; Kalinin, A.V.; Sidorina, Y.A. Quantum-mechanical model of thermally stimulated depolarization in layered dielectrics at low temperatures. *IOP Conf. Ser. J. Phys.* **2021**, *1843*, 012011. [CrossRef]
83. Kalytka, V.A. *Electrophysics of Proton Semiconductors and Dielectrics*; Karaganda Technical University, KTU Publishing House: Karaganda, Kazahstan, 2021; p. 133. ISBN 978-601-320-399-7.
84. Kalytka, V.; Korovkin, M.; Tatkeyeva, G.; Bashirov, A.; Bilichenko, Y.; Sidorina, Y.; Senina, Y.; Ospanov, B.; Brazhanova, D.; Baidyussenov, G.; et al. Quantum Kinetic Phenomena in Proton Semiconductors and Dielectrics. In Proceedings of the 3rd International Conference on Functional Materials and Chemical Engineering, City Seasons Suites, Dubai, United Arab Emirates, 9–10 November 2022; pp. 95–97.
85. Kalytka, V.A. The mathematical description of the nonlinear relaxation of polarization in dielectrics with hydrogen bonds. *Bull. Samara Univ. Nat. Sci. Ser.* **2017**, *23*, 71–83. [CrossRef]
86. Kalytka, V.A.; Korovkin, M.V. Dispersion Relations for Proton Relaxation in Solid Dielectrics. *Russ. Phys. J.* **2017**, *59*, 2151–2161. [CrossRef]
87. Kalytka, V.A. Nonlinear Quantum Phenomena During the Polarization of Nanometer Layers of Proton Semiconductors and Dielectrics. *Izv. Altai State Univ.* **2021**, *120*, 35–42. [CrossRef]
88. Kalytka, V.A.; Korovkin, M.V.; Mekhtiyev, A.D.; Yurchenko, A.V. Nonlinear Polarization Effects in Dielectrics with Hydrogen Bonds. *Russ. Phys. J.* **2018**, *61*, 757–769. [CrossRef]

89. Kalytka, V.A.; Korovkin, M.V.; Mekhtiev, A.D.; Alkina, A.D. Detailed analysis the non-linear of dielectric losses in proton semiconductors and dielectrics. *Bull. Mosc. Reg. State Univ. Ser. Phys. Math.* **2017**, *4*, 39–54. [CrossRef]
90. Tonkonogov, M.P. Dielectric spectroscopy of hydrogen-bonded crystals, and proton relaxation. *Phys. Usp.* **1998**, *41*, 25–48. [CrossRef]
91. Kalytka, V.A.; Korovkin, M.V.; Madi, P.S.; Kalacheva, S.A.; Sidorina, Y.A. Universal installation for studying structural defects in electrical and optical fiber materials. *IOP Conf. Ser. J. Phys.* **2020**, *1499*, 012046. [CrossRef]
92. Pereira, L.; Mesquita, E.; Alberto, N.; Melo, J.; Marques, C.; Antunes, P.; André, P.S.; Varum, H. Fiber Bragg Grating Sensors for Reinforcing Bar Slippage Detection and Bond-Slip Gradient Characterization. *Sensors.* **2022**, *22*, 8866. [CrossRef]
93. Panda, P.K.; Sahoo, B. PZT to Lead Free Piezo Ceramics: A Review. *Ferroelectrics* **2015**, *474*, 128–143. [CrossRef]
94. Wang, Y.; Yuan, H.; Liu, X.; Bai, Q.; Zhang, H.; Gao, Y.; Jin, B.A. Comprehensive Study of Optical Fiber Acoustic Sensing. *IEEE Access* **2019**, *7*, 85821–85837. [CrossRef]
95. Udd, E.; Spillman, W.B. The Emergence of Fiber Optic Sensor Technology. In *Fiber Optic Sensors: An Introduction for Engineers and Scientists*; Wiley: Hoboken, NJ, USA, 2011; pp. 1–8. [CrossRef]
96. Mekhtiev, A.D.; Yurchenko, A.V.; Ozhigin, S.G.; Neshina, E.G.; Al, A.D. Quasi-distributed fiber-optic monitoring system for overlying rock mass pressure on roofs of underground excavations. *J. Min. Sci.* **2021**, *57*, 354–360. [CrossRef]
97. Wu, H.; Wan, Y.; Tang, M.; Chen, Y.; Zhao, C.; Liao, R.; Chang, Y.; Fu, S.; Shum, P.P.; Liu, D. Real-Time Denoising of Brillouin Optical Time Domain Analyzer with High Data Fidelity Using Convolutional Neural Networks. *J. Lightwave Technol.* **2019**, *37*, 2648–2653. [CrossRef]
98. Madi, P.S.; Kalytka, V.A.; Alkina, A.D.; Nurmaganbetova, M.T. Development of a model fiber-optic sensor of the external action on the basis of diffraction gratings with variable parameters of the system. *IOP Conf. Ser. J. Phys.* **2019**, *1327*, 012036. [CrossRef]